Fuel-efficient and safe heavy-duty vehicle platooning through look-ahead control

VALERIO TURRI

Abstract

The operation of groups of heavy-duty vehicles at small inter-vehicular distances, known as platoons, lowers the overall aerodynamic drag and, therefore, reduces fuel consumption and greenhouse gas emissions. Experimental tests conducted on a flat road and without traffic have shown that platooning has the potential to reduce the fuel consumption up to 10%. However, platoons are expected to drive on public highways with varying topography and traffic. Due to the large mass and limited engine power of heavy-duty vehicles, road slopes can have a significant impact on feasible and optimal speed profiles. Therefore, maintaining a short inter-vehicular distance without coordination can result in inefficient or even infeasible speed trajectories. Furthermore, external traffic can interfere by affecting fuel-efficiency and threatening the safety of the platooning vehicles.

This thesis addresses the problem of safe and fuel-efficient control for heavy-duty vehicle platooning. We propose a hierarchical control architecture that splits this complex control problem into two layers. The layers are responsible for the fuel-optimal control based on look-ahead information on road topography and the real-time vehicle control, respectively. The top layer, denoted the platoon coordinator, relies on a dynamic programming framework that computes the fuel-optimal speed profile for the entire platoon. The bottom layer, denoted the vehicle control layer, uses a distributed model predictive controller to track the optimal speed profile and the desired inter-vehicular spacing policy. Within this layer, constraints on the vehicles' states guarantee the safety of the platoon. The effectiveness of the proposed controller is analyzed by means of simulations of several realistic scenarios. They suggest a possible fuel saving of up to 12% for the follower vehicles compared to the use of existing platoon controllers. Analysis of the simulation results shows how the majority of the fuel saving comes from a reduced usage of vehicles brakes.

A second problem addressed in the thesis is model predictive control for obstacle avoidance and lane keeping for a passenger car. We propose a control framework that allows to control the nonlinear vehicle dynamics with linear model predictive control. The controller decouples the longitudinal and lateral vehicle dynamics into two successive stages. First, plausible braking and throttle profiles are generated. Second, for each profile, linear time-varying models of the lateral dynamics are derived and used to formulate a collection of linear model predictive control problems. Their solution provides the optimal control input for the steering and braking actuators. The performance of the proposed controller has been evaluated by means of simulations and real experiments.

Acknowledgements

Contents

Introduction

H eavy-duty vehicles are responsible for a significant share of the global greenhouse gas emissions and energy consumption. Due to the strong link between freight transportation and the global economic growth, their environmental impact is expected to grow in the coming years, if no measures are taken.

Platooning has been investigated both by governmental institutions and vehicle manufacturers as a means to significantly reduce fuel consumption and greenhouse gas emissions. By letting heavy-duty vehicles drive at a short inter-vehicular distance, the overall aerodynamic drag can be significantly lowered and the consequent fuel consumption can be reduced up to 10%. However, the control of heavy-duty vehicles aimed at reaching high level of fuel-efficiency, while guaranteeing safety on public roads is still an open problem. Platoons are expected to drive on existing highways, where altitude variations and traffic can have large impact on their behavior. In this thesis we address the fuel-efficient and safe platoon control problem with a particular attention to the impact of slopes and external traffic.

The outline of this chapter is as follows. Section 1.1 provides the motivation for heavy-duty vehicle platooning. In Section 1.2, we present the platoon concept, while in Section 1.3, we highlight the main challenges in designing fuel-efficient and safe platooning control. In Section 1.4, we mathematically formulate the studied problem. Lastly, Section 1.5 provides the thesis outline and contributions.

1.1   Motivation

In order to deal with increasingly stringent limitations on greenhouse gas emissions and the continuous increase of the price of oil, the road transport sector is going through significant modifications. While the emissions due to passenger vehicles start to decrease thanks to recent regulatory measures introduced by various governments, the reduction of emissions from the road freight transport sector appears more challenging due its close link with economic growth.

The transportation of goods is fundamental to the world's economic development. The demand for freight transportation is expected to increase in the coming years.
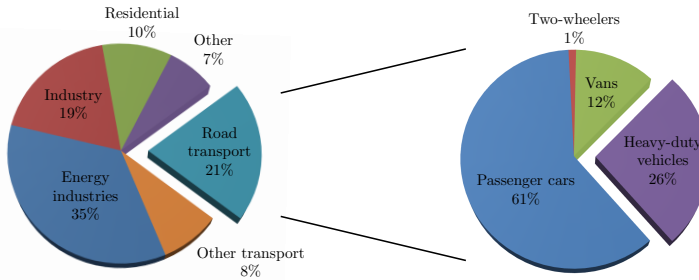
Figure 1.1: Shares of the CO_2 total emissions by sector for the European Union. The CO_2 emissions from the road transport sector have been additionally split between the various vehicle categories (European Commission, 2014; Hill et al., 2011).

Thanks to the flexibility of heavy-duty vehicles, almost half of the transported goods is carried over roads (International Transport Forum, 2015; European Commission, 2014). However, road freight transportation, due to the burning of fossil fuel, is responsible for a large share of the global greenhouse gas emissions. As illustrated in Figure 1.1, a study commissioned by the European Commission has estimated that road freight transportation accounts for 26% of the CO_2 emissions from road transportation which, in turn, is responsible for 21% of the total European CO_2 emissions (Hill et al., 2011; European Commission, 2014). This is in line with statistics on the US transport sector, where heavy-duty vehicles account for 5.4% of the total CO_2 emissions (Frey and Kuo, 2007). Following the predicted growth of the world's GDP at an average annual rate of 3.3%, the freight transport sector is expected to significantly expand. Projections from the International Transport Forum predicts an increase of global CO_2 emissions linked to the surface (road and rail) freight transport sector of up to 247% in 2050 relative to the level of 2010 if no additional measures are taken (International Transport Forum, 2015). Due to the strong connection between greenhouse gas emissions and climate change, these predictions are considered unacceptable and governments all over the world are agreeing in introducing new stringent policies to reduce the greenhouse gas emissions related to road freight transportation (European Commission, 2011; US Enviromental Protection Agency, 2011).

The search for a more sustainable freight transportation system is driven also by other factors, such as the expected increase of the oil price (International Transport Forum, 2015). This increase combined with the need for maintaining competitiveness is requiring heavy-duty vehicle manufactures to develop innovative technologies able to guarantee an increased fuel-efficiency. The fuel cost for a truck fleet owner accounts for more than one third of the total cost of owning and operating a vehicle (Scania AB, 2013; Schittler, 2003). Given an average of 130,000 km driven every year by a heavy-duty vehicle (Hill et al., 2011), the average fuel cost of 1.5 €/l and an efficiency of 3 km/l, the fuel cost for a single vehicle amounts to 65,000 €/year. Considering that a fleet owner usually owns several vehicles, even a reduction of a

Figure 1.2: Four-vehicle platoon driving over an uphill stretch. (Photo provided by courtesy of Scania AB.)

few percent of the fuel consumption translates to significant savings.

1.2 Platooning for a more sustainable freight transportation

Vehicle platooning is an effective method to reduce fuel consumption and, consequently, greenhouse gas emissions. An example of a platoon is displayed in Figure 1.2. By operating groups of vehicles at small inter-vehicular distances, the aerodynamic drag experienced by the follower vehicles is reduced. This phenomenon is caused by a slipstream effect taking place behind a moving vehicle and leads to a reduced pressure on a vehicle moving at a short distance from the first one. Thanks to the proximity between the vehicles, the air vortices behind the first vehicle are reduced and therefore also the first vehicle experiences an aerodynamic drag reduction, albeit smaller than the follower vehicles. In Figure 1.3 we show an estimation of the reduction of the aerodynamic drag as function of the inter-vehicular distance based on the experimental data reported in Hucho (1987). A distance of 10 m in a platoon of two vehicles driving at 80 km/h, for example, produces a reduction of the aerodynamic drag of 40% for the second vehicle and of 4% for the first one. As about a quarter of the heavy-duty vehicle fuel consumption is related to the aerodynamic drag (Hellström, 2010), platooning can have a large effect on the fuel consumption. Indeed, independent studies have shown the potential of truck platooning to save up to 10% of fuel for follower vehicles (Alam et al., 2010; Lammert et al., 2014). However, in order to maintain a short inter-vehicular distance, the control of the longitudinal dynamics is needed.

Besides the reduction of fuel consumption and greenhouse gas emissions, platoon-
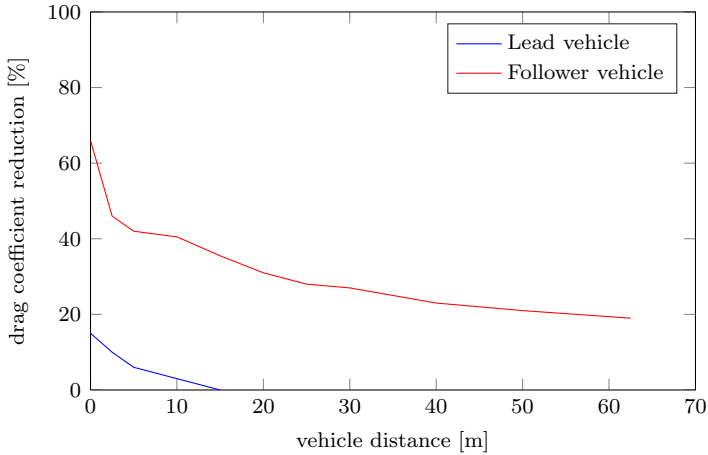
Figure 1.3: Estimation of the reduction of the drag coefficient for two heavy-duty vehicles driving in platoon formation at a speed of 80 km/h for varying inter-vehicular distance. Since the aerodynamic drag is linearly proportional to the drag coefficient a reduction in the drag coefficient reflects a reduction of the aerodynamic drag. The data are adapted from Hucho (1987). Similar results have been obtained in Bonnet and Fritz (2000).

ing carries other advantages, such as an increased safety and a better utilization of the road infrastructure. In Europe, rear-end collisions represent 15% of the serious or fatal road accidents where a heavy-duty vehicle is involved (Almqvist and Heinig, 2013). The automation of the longitudinal dynamics guaranteed by platooning would allow to significantly reduce the number of this type of accidents. Furthermore, platooning can be considered as the first step toward fully-automated vehicles, which are expected to significantly decrease the number of fatalities on our roads. Finally, the short inter-vehicular distance would allow to increase the capacity of the current highways without building extra lanes.

In order to form vehicle platoons, however, coordination is needed. Heavy-duty vehicles represent a small portion of the highway traffic and their location can be sparsely distributed over the road network. Some vehicles will need to change their route or vary their average speed in order to come in the proximity of other heavy-duty vehicles, see the illustration in Figure 1.4. These actions however cannot be naively taken, but also need to be planned based on criteria that incorporate fuel economy. Increasing the speed to catch up with a platoon that is going to split after only a few kilometers can results in a higher total consumption than driving alone with a constant average speed. A more sustainable freight transportation system therefore should cope with the fuel-efficiency problem at different levels, ranging from the coordination and route planning of vehicles to the local control of each vehicle and platoon.
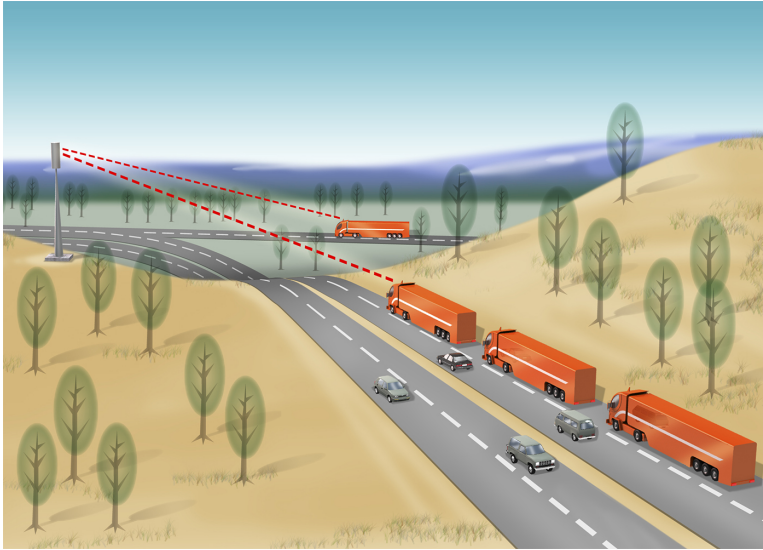
Figure 1.4: Illustration of a coordination maneuver, where the speed of a platoon and a single vehicle are adjusted in order to merge after a road intersection.

1.3 Platooning challenges

Platooning has shown a great potential for reducing vehicle fuel consumption and greenhouse gas emissions. However, the control of a platoon of heavy-duty vehicles able to maintain a high fuel-efficiency while guaranteeing safety is still an open problem. The majority of the experimental tests conducted on heavy-duty vehicle platooning are in fact proofs of concept that have been performed in controlled environments where altitude variations and the interference of traffic have not been included, see Alam et al. (2010), Lammert et al. (2014), Browand et al. (2004) and Bonnet and Fritz (2000). However, slopes and external traffic have a large influence on the fuel consumption and safety of platooning vehicles.

Platoons are expected to drive on public highways where the presence of other vehicles cannot be neglected. The surrounding traffic can interfere with the nominal platoon behavior and thereby affect the fuel-efficiency and threaten the safety. The platoon controller should be able therefore to adapt its speed according to the external vehicles and maintain a fuel-efficient behavior while guaranteeing safety, see Figure 1.5a. In other words, we want that the platoon controller brakes only when needed. It should be able to smoothly and fuel-efficiently decelerate the platoon in the case of a smooth deceleration of the leading vehicle by braking only if necessary and, at the same time, it should be able to react to an emergency braking of the leading vehicle and avoid collisions. Due to the potential heterogeneity of the platooning vehicles, which can significantly differ in mass and braking capability, this is not an easy task. Additionally, the slipstream effect given by platooning

(a) Automatic braking of a platoon due to the interference of an external vehicle.
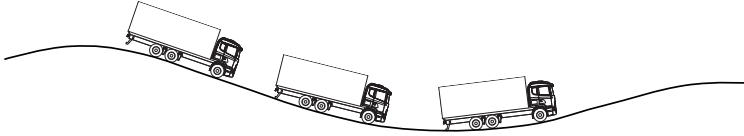
(b) Automatic speed control for a platoon driving over a hilly road.

Figure 1.5: Illustrations of challenging scenarios for heavy-duty vehicle platooning.

generates a reduced aerodynamic force on the follower vehicles that can lead to collision in the platoon in case of harsh braking.

Altitude variations have a large impact on the behaviors of heavy-duty vehicles and their fuel consumption. Figure 1.5b depicts a platoon driving over a hilly road. Because of the large mass and the limited engine power of heavy-duty vehicle, even small slopes produce large longitudinal forces. Hence, they are often not able to keep constant speed during uphill segments (because of limited engine power) and downhill segments (without applying brake, because of the significant inertia). It is common that the vehicles have to brake, and therefore waste energy, in order not to exceed the speed limit during downhill sections. Slopes become even more critical when vehicles are driving in a platoon formation. The additional requirement of keeping a small inter-vehicular distance in fact conflicts with the fact that heavy-duty vehicles experience significantly different longitudinal forces, e.g., gravity force depending on their mass and current road slope and aerodynamic drag depending on the distance from the preceding vehicle. Therefore, in order to guarantee fuel-efficiency while driving over hilly roads, new control strategies based on the cooperation of the platooning vehicles should be investigated.

These problems motivate the need for developing a platoon controller that explicitly takes topography information into account and coordinates acceleration and deceleration of the vehicle platoon in order to reach a high level of efficiency, while guaranteeing safety.

1.4   Problem formulation

The problem studied in this thesis is the control of the longitudinal dynamics of a platoon of N vehicles in order to maximize the fuel-efficiency while guaranteeing safety. As illustrated in Figure 1.3, a short inter-vehicular distance produces a reduced overall aerodynamic drag and therefore a reduced platoon fuel consumption. However, to maintain such short distances while avoiding braking and guaranteeing

safety requires the use of an advanced controller.

Figure 1.6 shows a heterogeneous platoon of $N > 1$ vehicles driving over a hill. The state of each vehicle i is represented by the longitudinal position s_i and speed v_i. Contiguous vehicles are separated by a distance d_i defined as

$$d_i = s_{i-1} - s_i - l_{i-1}, \tag{1.1}$$

where l_i denotes the length of vehicle i. The road is characterized by its road gradient α defined as a function of the longitudinal position. The longitudinal dynamics of each vehicle can be modeled as

$$\begin{aligned}
\dot{v}_i &= \varphi_i(v_i, \alpha(s_i), d_2, ..., d_N, \psi_i, F_{\mathrm{b},i}), \\
\dot{s}_i &= v_i,
\end{aligned} \tag{1.2}$$

where ψ_i and $F_{\mathrm{b},i}$ represent the inputs of vehicle i and denote the fuel flow and the braking force, respectively. The coupling between the vehicles is defined by the aerodynamic drag, which, in general, is a function of the distance between all the vehicles. Each vehicle is characterized by parameters such as mass, roll friction, engine efficiency, etc., included in the model $\varphi_i(\cdot)$. Furthermore, each vehicle has input bounds

$$(\psi_i, F_{\mathrm{b},i}) \in \mathcal{U}_i(v_i), \tag{1.3}$$

representing limits on engine power and braking capability. Given the vehicle dynamics (1.2) and the input constraints (1.3), the the control problem we desire to solve is to minimize the fuel consumption of the entire platoon, defined as

$$\Psi_{\mathrm{platoon}} = \sum_{i=1}^{N} \int \psi_i \, dt, \tag{1.4}$$

while guaranteeing platoon safety. The safety constraint can be formulated as requiring the platoon state to lie in a properly defined set

$$(s_1, v_1, ..., s_N, v_N) \in \mathcal{X}_{\mathrm{safe}}. \tag{1.5}$$

In conclusion the problem that we are studying in this thesis is to design a controller that solves the following optimal control problem:

$$\begin{aligned}
\text{minimize} \quad & \text{platoon fuel consumption (1.4)}, \\
\text{subj. to} \quad & \text{vehicle dynamics (1.2)}, \\
& \text{bounds on inputs (1.3)}, \\
& \text{safety constraint (1.5)}.
\end{aligned} \tag{1.6}$$

1.5   Thesis outline and contribution

In this section, we outline the thesis and its contributions.
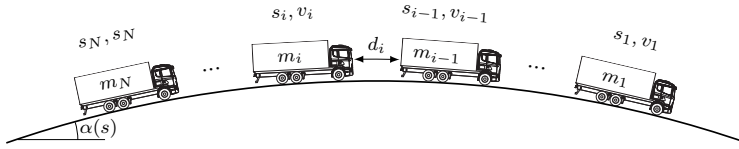
Figure 1.6: Sketch of a platoon of heterogeneous vehicles driving over a hilly road.

Chapter 2: Background

This chapter provides the background on fuel-efficient freight transportation and the role of platooning in such a system. We first introduce the technologies that enable vehicle platooning. Second, we give an overview on the literature related to fuel-efficient heavy-duty vehicle platooning. The majority of these works address the problems of vehicle platooning and look-ahead vehicle control separately. Extremely few works focus instead on the fuel-efficient vehicle platooning by including look-ahead information on the road topography. Third, we present the general problem of creating a fuel-efficient freight transportation system which ranges from how the goods should be dispatched to optimize truck usage to how the actuators of each vehicle should be controlled to reduce fuel consumption. We present a system architecture aimed to divide this complex problem into solvable subproblems and further motivate the control problem studied in this thesis. Lastly, we briefly introduce the mathematical tools that we use to solve this control problem, namely dynamic programming and model predictive control.

Chapter 3: Modeling

In this chapter we present the models of the longitudinal dynamics of a single heavy-duty vehicle and a platoon. Here, we describe the multiple forces that act on the vehicle, putting a particular attention in capturing the dependence of the aerodynamic force on the inter-vehicular distance. Furthermore, a control-oriented model of the powertrain that captures the relation between instantaneous fuel consumption and traction force is included. The chapter ends with the presentation of the control system architecture of a heavy-duty vehicle in which the platoon controller operates.

Chapter 4: Cooperative control for fuel-efficient and safe platooning

In this chapter we present a two-layer control architecture suitable for the longitudinal control of a heavy-duty vehicle platoon that guarantees fuel-efficiency and safety. Each layer is based on an optimal control formulation aimed to optimize the platoon behavior. The higher layer, denoted the platoon coordinator, uses a dynamic programming approach to compute the speed trajectory that should be followed by

each vehicle in the platoon. It ensures the feasibility of the speed trajectory and its fuel-optimality by explicitly taking topography information into account. The lower layer, denoted the vehicle control layer, uses a distributed model predictive control approach to track the computed speed trajectory. This layer ensures the safety of the platoon operation in the case a vehicle starts to be driven manually at any moment.

Chapter 5: Experimental evaluation

In this chapter we evaluate the performance of the platoon controller proposed in Chapter 4 by means of simulations based on realistic scenarios. The two layers are first evaluated separately. The energy and fuel consumption of the platoon obtained through the proposed controller is compared with standard controllers that ignore topography information. Furthermore, the performance of the vehicle controller layer is tested by simulating various braking scenarios. Finally, the functioning of the whole control architecture is analyzed by comparing its performance to the experimental results obtained using a controller based only on local inter-vehicle feedback control.

Chapter 6: Model predictive control for obstacle avoidance

This chapter stands on its own and deals with the obstacle avoidance and lane keeping problems for passengers cars. We propose a novel control framework that combines the simultaneous control of steering and braking actuators with the good performance of linear model predictive control. We first provide a motivation for this work and discuss related control approaches. Second, we describes the control architecture based on the decoupling of longitudinal and lateral dynamics. Lastly, we evaluate the controller by means of simulations and real experiments conducted on a packed-snow surface.

Chapter 7: Conclusion and future work

This chapter contains a summary of the work presented in the thesis and highlights potential future research directions.

Publications by the author

Chapters 2 to 5 are based on the following publications:

> V. Turri, B. Besselink, and K. H. Johansson. Cooperative look-ahead control for fuel-efficient and safe heavy-duty vehicle platooning. Preprint available at *arXiv:1505.00447 [cs.SY]* (2015). Submitted for journal publication.

V. Turri, B. Besselink, J. Mårtensson, and K. H. Johansson. Fuel-efficient heavy-duty vehicle platooning by look-ahead control. In *53rd IEEE Conference on Decision and Control*, 654–660. Los Angeles, CA, USA (2014).

B. Besselink, V. Turri, S. H. van de Hoef, K.-Y. Liang, A. Alam, J. Mårtensson, and K. H. Johansson. Cyber-physical control of road freight transport. Preprint available at *arXiv:1507.03466 [cs.SY]* (2015). Submitted for journal publication.

A. Alam, B. Besselink, V. Turri, J. Mårtensson, and K. H. Johansson. Heavy-duty vehicle platooning towards sustainable freight transportation. *IEEE Control Systems Magazine* (2015). Conditionally accepted.

Chapter 6 is based on the paper:

V. Turri, A. Carvalho, H. E. Tseng, K. H. Johansson, and F. Borrelli. Linear model predictive control for lane keeping and obstacle avoidance on low curvature roads. In *16th International IEEE Annual Conference on Intelligent Transport*, 378–383. The Hague, The Netherlands (2013).

The order of the author names reflects the workload, where the first had the most important contribution. In all the publications the thesis author participated actively in the discussions and derivations of the theory and results, as well as in the paper writings.

Background

Thus chapter establishes the required background to the rest of the thesis. We first introduce the technologies that enable look-ahead vehicle platooning and the existing longitudinal control functionalities that relate to it. Then, we give an overview of the literature related to look-ahead vehicle platooning. There exist only few works that address the fuel-efficient vehicle platooning control by explicitly taking road topography information into account. Such overview, therefore, mainly focuses on the works that deal with the problems of platooning control and look-ahead vehicle control, separately. Afterwards, we give a broader perspective on the potential for increasing fuel-efficiency in the freight transport sector. We propose a system architecture for fuel-efficient freight transportation aimed at maximizing the benefits from platooning. Such architecture deals with problems ranging from how to fuel-optimally route vehicles over the road network exploiting platoon possibilities, to how to efficiently control the vehicle actuators. Lastly, we introduce the concepts of dynamic programming and model predictive control (MPC) that will be exploited in the platoon controller proposed in Chapter 4.

The chapter is organized as follows: in Section 2.1 we present the technologies that enable the safe and fuel-efficient implementation of vehicle platooning. Sections 2.2 and 2.3 provide a literature overview on vehicle platooning control and look-ahead vehicle control, respectively. The fuel-efficiency problem from the whole freight transport sector perspective is discussed in Section 2.4 and a system architecture centered on platooning is presented. Section 2.5 presents a short overview on the concepts of dynamic programming and MPC. Lastly, Section 2.6 summarizes the chapter.

2.1 Enabling technologies for platooning

In order to safely operate heavy-duty vehicles at a short inter-vehicular distance as necessary for a reduced aerodynamic drag, the automation of the longitudinal dynamics is needed.

In the automotive industry, the first step towards this goal has been obtained
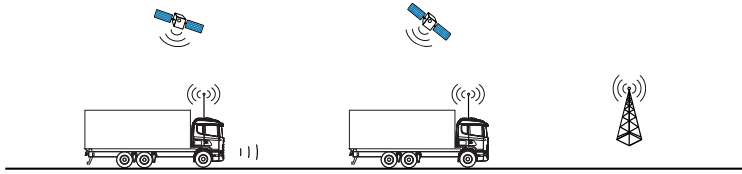
Figure 2.1: Advances in technology provide the tools for realizing safe and fuel-efficient vehicle platooning. Radar measures the distance and relative speed information with respect to the preceding vehicle. GPS data can be fused with speed and acceleration measurements to estimate the vehicle state with a precision of centimeters. Wireless sensor units allow the platooning vehicles to share state information and to communicate with a back-end office or cloud services, thanks to V2V and V2I communications.

with the introduction of the adaptive cruise control (ACC). The ACC typically relies on information collected by a radar placed in the front of the vehicle, namely measurements of the inter-vehicular distance and relative speed with respect to the preceding vehicle. This information, combined with speed measurements of the current vehicle, is used to control the longitudinal dynamics of the vehicle by keeping a certain spacing policy from the preceding one. The limited precision of the radar and the fact that only the relative position and speed are measured, however, results in delays in detecting accelerations and decelerations of the preceding vehicle. As a result, only using radar information does not allow to maintain significantly small inter-vehicular distance without compromising the vehicle safety. Moreover, delays in deceleration detection are critical in the case of more than two vehicles driving at a short inter-vehicular distance, i.e., platoons. Since each vehicle can only estimate the acceleration of the preceding vehicle with a certain delay, the acceleration of the head of the platoon can only be detected with a significant delay by the tail of the platoon. This can produce unwanted behavior such as the amplification of distance errors and control effort along the platoon.

The introduction of wireless sensor units in vehicle enables both the communication between different vehicles, known as vehicle-two-vehicle (V2V) communication, and between vehicles and infrastructure, known as vehicle-two-infrastructure (V2I) communication, see Figure 2.1.

The V2V communication allows each vehicle to have a more complete and accurate knowledge of the platoon state. By fusing GPS data with speed and acceleration measurements each vehicle knows its state with a precision of centimeters (Sahlholm and Johansson, 2010) and thanks to V2V communication this information can be sent to the other platooning vehicles. Furthermore, V2V communication allows vehicles to share parameters that are critical for platooning, such as vehicle mass, braking capability or actuator limitations. V2V communication therefore provides the framework for developing more advanced longitudinal control strategies, known as cooperative adaptive cruise control (CACC) strategies.

On the other hand, the V2I communication allows the platooning vehicles to

receive information on the road ahead, e.g., topography information or traffic status. Topography information can be exploited to improve the fuel-efficiency of vehicles. By including such information in a look-ahead control (LAC) framework the speed of single vehicles can in fact be adjusted to minimize their fuel consumption, for example, by avoiding unnecessary braking during downhills. The same idea, as studied in this thesis, can be extended to vehicles driving in platoon formation for which the speed needs to be coordinated in order to maintain a short inter-vehicular distance. In this case we will talk about cooperative look ahead control (CLAC). The V2I communication can also be exploited to communicate with off-board systems, such as a back-end office or cloud services (Whaiduzzaman et al., 2014). This provides the means for implementing more complex tasks related to platooning, e.g., the coordination of vehicles on a road network in order to create platoons as it will be addressed in Section 2.4.

Extensive research has been conducted on V2V and V2I (V2X) communications, see Sichitiu and Kihl (2008) and Willke et al. (2009). Some of the main challenges faced in these works are related to communication reliability (Ramachandran et al., 2007), the requirement for limited delay (Bilstrup et al., 2008) and communication security (Raya and Hubaux, 2005). These are considered significant problems in V2V communication especially because of the intrinsic decentralized nature and highly dynamic characteristic of vehicle networks. Multiple standards are currently under study by telecommunication companies and institutions in order to implement reliable V2X communication. The IEEE 802.11p (802.11p, 2010) is an amendment to the IEEE 802.11 standard approved in 2010 aimed at adding wireless access in vehicular environments. It defines the wireless medium access control (MAC) and physical layer specifications in order to enable data exchange between (high-speed) vehicles and infrastructure. For the implementation of the IEEE 802.11p standard the United States Federal Communications Commission and the European Telecommunications Standards Institute have allocated part of the 5.9 GHz band, although the frequency range is not exactly the same. The standard IEEE 1609.4 (Chen et al., 2009) is an extension of the MAC layer aimed at providing a time-division scheme to alternately switch within the channels of the 5.9 GHz band to support different applications concurrently. The SAE J2945 (SAE International, 2015) standard defines the message dictionary and the data format for V2X communication and is a topic of ongoing research.

2.2 Vehicle platoon control

Although commercial implementations of platooning are yet to come due to the current lack of a complete communication standard and a favorable legislation, the concept of platooning has a long history. The first public presentation of an automated convoy of vehicles driving at a short inter-vehicular distance dates back to 1939 during the New York World's Fair. At this exposition, General Motors showed a film entitled *To New Horizons* (General Motors, 1939) which presents a

future where cars are able to maintain a safe distance by using automated radio control and where curved road sides help the driver to keep the vehicle within its lane. Early works on the dynamical behavior of a string of (manually driven) vehicles start to appear in the fifties. In Pipes (1953), a simple model of the driver is used to explain the delayed start of a string of vehicles when the light turns green at an intersection.

Only in the sixties, the platoon concept, intended as a string of automatically controlled vehicles, started to gain a certain attention from the control community. An early work (Levine and Athans, 1966) proposed an optimal control approach for the automation of the longitudinal dynamics of a string of vehicles. This controller uses a centralized framework and indirectly assumes that there are no limitations imposed by the communication hardware. In order to deal with limited communication resources and limited computational power, decentralized optimal control approaches for platoon control have also been proposed, see e.g., Chu (1974) and, more recently, Stankovic et al. (2000) and Alam et al. (2015*b*).

An aspect that attracted significant attention and was a mainstream topic in the platooning research for a few decades is the concept of string stability. The notion of string stability was first introduced by Peppard (1974) and refers to the ability of the controlled vehicle string to attenuate disturbances as they propagate through the string. A formal definition of string stability is given in Swaroop and Hedrick (1996) and an overview of its various interpretations existing in literature is given in Ploeg et al. (2014). In order to achieve string stability, Peppard (1974) proposed a PID controller that exploits real-time information from both the preceding and following vehicles in order to track a constant space gap. Sheikholeslamn and Desoer (1990) were able to show that string stability cannot be achieved by only using real-time information from the preceding vehicles (known as the predecessor-following strategy) while tracking a constant space gap. In their work, they propose a different control framework that is able to obtain string stability by exploiting the real-time information from both the preceding and leading vehicle. In Seiler et al. (2004), an explanation for these results is given, based on properties of the transfer function between the position errors of contiguous vehicles. In order to overcome the intrinsic string instability of predecessor-following strategies based on the space gap policy, Chien and Ioannou (1992) proposed the use of a speed-dependent spacing policy. They show that string stability can be achieved in a predecessor-following strategy setup by tracking a gap defined as a constant headway time in addition to the space gap. Although this approach allows to realize string-stable platoons also in an ACC framework (where V2V communication is not available), Naus et al. (2010) and Ploeg et al. (2011) proved that the only use of measurements from the radar cannot guarantee string-stability for small headway times. Furthermore, they show how the additional use in the vehicle control of acceleration information of the preceding vehicle (received through V2V communication) allows to reach string-stability also in the case of a significantly small headway time. While the majority of the studies on string stability considers simple vehicle dynamics, Yanakiev and Kanellakopoulos (1995) propose an adaptive nonlinear controller and prove its string stability for

the more complex dynamics of a string of heavy-duty vehicles. In the recent years, decentralized MPC approaches have been also studied for vehicle platooning (Dunbar and Murray, 2006; Dunbar and Caveney, 2012) and conditions on the controller parameters have been defined in order to guarantee string stability. It is worth to underline that string stability does not translate into safety, but it only guarantees the non-amplification of disturbances along the platoon. For example, if strong braking generates a large deviation equal to the reference distance, collision between vehicles can occur despite string stability.

Until the nineties the research on platooning has been mainly theoretical. The Partners for Advanced Transportation Technology (PATH) project (Shladover, 2007) founded in 1986 in California, USA, brought a new boost to the field. The original aim of the project was the study of the potential of platooning for an increased highway throughput. Within this project, Varaiya (1993) proposed a solution based on platoons of 15 vehicles driving at an inter-vehicular distance of 2 m and platoons separated by 60 m. Due to the short inter-vehicular distance, it is argued that, even if collisions occur, they would have a small impact because of the small relative speed between vehicles. This solution allows to increase the highway throughput up to three times. In Horowitz and Varaiya (2000), a system architecture that splits the described control task in manageable subproblems is proposed. During the project numerous experimental tests involving vehicle platoons of up to eight vehicles using V2V communication have been conducted (Hedrick et al., 2000; Rajamani et al., 2000). Although the environmental aspect was not the focus of the project, noteworthy results on the reduction in fuel consumption for heavy-duty vehicle platooning have been reported (Browand et al., 2004). Furthermore, tests conducted in a wind tunnel with car models suggested an average reduction of 55% of the aerodynamic drag experienced by follower vehicles for a platoon of four vehicles (Zabat et al., 1995).

With the beginning of the PATH project and the related successful experimental results, there was an increased interest of the research community towards more practical aspects of platooning, e.g., traffic impact, safety, user acceptance and fuel-efficiency (Bergenhem and Huang, 2010; Bergenhem et al., 2012; Tsugawa, 2013; Shladover, 2012). In particular, the potential for increased fuel-efficiency has been mostly studied for heavy-duty vehicles, since their particular shape allows for the largest benefits of a reduced aerodynamic drag. Experimental tests (Bonnet and Fritz, 2000; Zhang and Ioannou, 2006; Alam et al., 2010) have shown a reduction of fuel consumption of up to 10% thanks to heavy-duty vehicle platooning. However, tests conducted on public roads, see Shladover (2012) and Alam (2014), have reported the neutralization of the platooning benefits due to traffic interference and road slopes, respectively. The impact of road grade on heavy-duty vehicle platooning is further discussed in the following section.

We conclude this section by giving a brief overview of the safety problem in vehicle platooning. As vehicle platoons are expected to drive on public roads, they need to cope with external vehicles and unexpected events, e.g., an accident ahead. In order to maintain safety, the platoon should be able to react to these scenarios

by guaranteeing that no collisions occur, even in the case of harsh braking of the first vehicle. ACC controllers that guarantee collision avoidance are commercially available (Seiler et al., 1998). Works within the PATH project have studied the safe operation of merging maneuvers between vehicles and platoons (Li et al., 1997; Alvarez and Horowitz, 1997). In Alam et al. (2011) a game-theoretical approach for the safe control of heavy-duty vehicles has been proposed. More recently, an MPC framework has been used to address this problem (Khodayari et al., 2012) and reachability analysis techniques are used to compute the safe state region for ACC and CACC controllers.

2.3   Look-ahead vehicle control

The majority of the works and experimental tests that study the fuel-efficiency aspect of platooning focus on aerodynamic effects due to small inter-vehicular distances, while ignoring the impact of external factors such as altitude variation. Slopes, however, play a significant role on the feasibility and fuel-optimality of speed profiles of heavy-duty vehicles, due to their large mass and limited engine power.

The effect of slopes on a vehicle's fuel consumption has been studied extensively for single vehicles. In the early work by Schwarzkopf and Leipnik (1977), a fuel-optimal problem for a non-linear vehicle model has been formulated and an analytical solution for constant road grade based on the maximum principle was proposed. In Hooker (1988), an approach based on dynamic programming that is able to handle generic road profiles has been proposed. However, due to the complexity of the algorithm, only short road segments could be considered. In order to overcome this limitation, a variation of this technique was proposed in Monastyrsky and Golownykh (1993). In this work, thanks to the reformulation of the problem in the spacial domain and the relaxation of the time constraint, a significant improvement in the computational complexity was reached. In detail, the reduction of the dimension of the state space allowed to consider much more complex scenarios. A similar approach has been taken in Hellström et al. (2006), where a predictive cruise control for heavy-duty vehicles based on topography information and speed limits of the road ahead computes the fuel-optimal speed profile. Experimental tests in Hellström et al. (2009) have shown the ability of such a controller to reduce the fuel consumption of a heavy-duty vehicle driving over a hilly road by up to 3.5%.

There exist very few works that address the inclusion of topography information in order to further improve the fuel-saving potential of platooning. In Alam et al. (2013), multiple strategies for the control of heterogeneous platoons driving over synthetic road topography profiles are analyzed. The authors propose a control strategy that collects the fuel-optimal speed trajectory computed by each vehicle individually and selects the one that is feasible for all the vehicles as a reference for the whole platoon. In Németh and Gáspár (2013), a similar approach is used. In this work, a common reference speed trajectory is also computed by combining the optimal speed trajectories of each vehicle. The combination is done by mini-
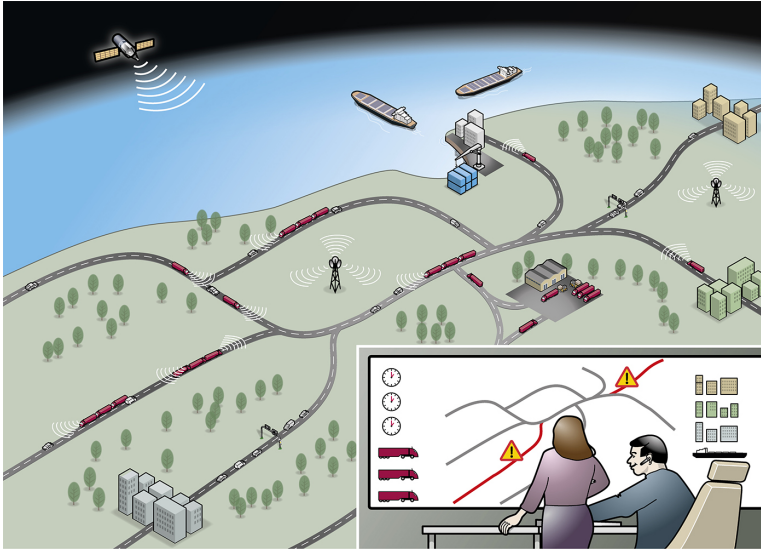
Figure 2.2: Illustration of a heavy-duty vehicles coordination problem. Vehicles with different destinations and time constraints need to be coordinated in order to form platoons. The coordination should be based on fuel-efficiency criteria and platoons should be formed only when favorable.

mizing the deviations of the optimal trajectories of each vehicle from the common speed trajectory of the whole platoon. Both these works, however, do not take the reduction of the aerodynamic drag given by the short inter-vehicular distance into account. This reduction is considered in Kaku et al. (2013), where a nonlinear MPC framework based on a detailed model of the platooning vehicles is proposed. Due to the complexity of the optimization problem resulting from the MPC formulation, however, only a short prediction horizon can be implemented. Such a short horizon does not allow to completely capture the spatial dynamics of realistic topography profiles. Furthermore, in this work the safety of the platoon is not addressed.

In Chapter 4 we present a novel approach to address the cooperative look-ahead problem for fuel efficient and safe heavy-duty vehicle platooning. The large optimization problem aimed at computing fuel-optimal and real-time control inputs for all the vehicles by explicitly taking the topography information into account is split into two manageable subproblems. First, a fuel-optimal speed trajectory for the whole platoon is generated by using a long prediction horizon. Second, such trajectory is distributively and fuel-efficiently tracked by all vehicles, while guaranteeing safety.
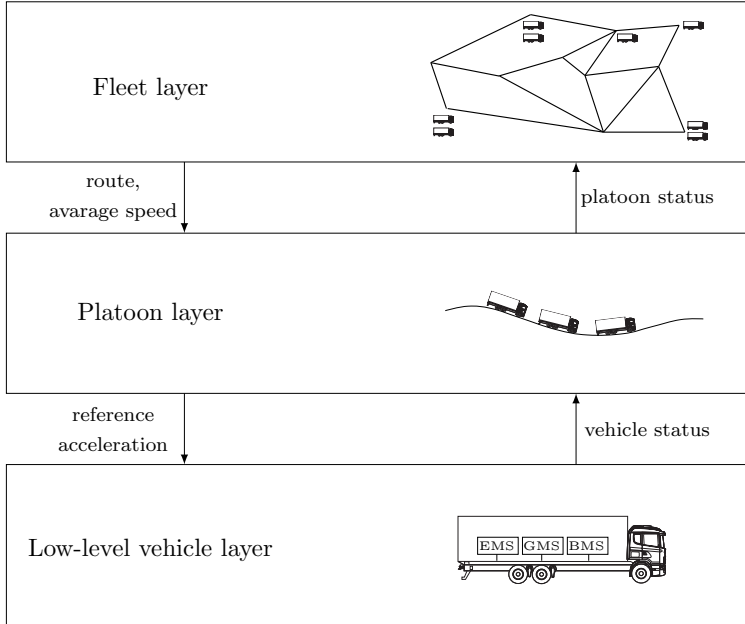
Figure 2.3: Three-layer system architecture for a fuel-efficient freight transport system. The aim of this architecture is to split in solvable subproblems the complex problem of coordinating and controlling heavy-duty vehicles to fully exploit the benefits of platooning.

2.4 Fuel-efficient transportation system

Platooning has a great potential for increasing the fuel-efficiency of heavy-duty vehicles. However, in order to fully exploit the benefits of platooning, the formation of platoons needs to be coordinated, see Figure 2.2. Heavy-duty vehicles represent a small portion of the road traffic and their locations can be sparsely distributed over the road network. In order to form platoons, therefore, the route, departure time and speed profile of each vehicle need to be adjusted. This is not a trivial task. Each vehicle has its own mission defined by a specific starting point, final destination, and a certain time constraint. Therefore, the coordination of heavy-duty vehicles cannot be performed in a naive way. Increasing the average speed to join a platoon that is going to split after only a few kilometers can be less efficient that simply maintaining the original average speed and continue driving alone. Therefore it is evident that the starting time, the route and the speed trajectory of each heavy-duty vehicle need to be planned and coordinated intelligently in order to fully exploit the benefits of platooning.

In order to address the resulting optimization problem aimed at fully exploiting the benefit of platooning, we propose a system architecture inspired by the control

architecture in Alam (2014) and Liang (2014) that splits this large problem in manageable subproblems. This system architecture is depicted in Figure 2.3 and is composed of three layers, namely, the fleet layer, the platoon layer, and the low-level vehicle layer. Each layer is described in the following paragraphs.

The fleet layer is responsible for the coordination of a large fleet of vehicles potentially belonging to multiple fleet owners. Explicitly taking information on destinations and time requirements of all vehicles in the fleet into account, it defines the routes and meeting times and points for the creation of new platoons or the merging of existing ones. Since traffic and slopes have a significant impact on the fuel-consumption of heavy-duty vehicles, topography information and historical and real-time traffic information can be included. In van de Hoef et al. (2015), a centralized approach that addresses this problem is proposed. Their approach is based on the sequential computation of optimal paths for each vehicle and the optimization of each vehicle's average speed in order to enable the formation of platoons. In Larson et al. (2015), instead, a distributed approach over the road network is proposed. A control unit located in each node of the road network decides if it is fuel-efficient for the approaching vehicles to adapt their speed in order to form platoons. The functionality of the fleet layer can also be extended upwards to include the logistics problem, i.e., how the flow of goods needs to be distributed between the available vehicles while taking limitations on size into account, weight and the type of cargo in each vehicle. Alternative approaches aimed at stimulating the formation of platoon have been also studied. For example, Farokhi and Johansson (2013) propose a game-theoretic approach that exploits dynamic congestion fees depending on the vehicle category, i.e., passenger car or heavy-duty vehicle, in order to encourage vehicles belonging to the same category to drive at the same time.

The platoon layer is responsible for the fuel-efficient and safe control of the platoon. It receives requirements on average speed from the cooperation layer and computes the fuel-optimal acceleration of each vehicle. Such computation relies on an optimal control framework that explicitly takes topography information into account and guarantees the safety of platoon operations. The existing few works on the topic have been reviewed in the second part of Section 2.3. A novel approach that addresses this problem is presented in Chapter 4.

The low-level vehicle layer controls the braking and powertrain systems by tracking the reference acceleration defined by the platoon layer. Its implementation relies on management system units typically available in commercial heavy-duty vehicles. These units are the engine management system (EMS), the gear management system (GMS) and the braking management system (BMS). In detail, in the traction phases, the engine and gear management systems (EMS and GMS) control the powertrain in order to deliver the required acceleration. The braking management system (BMS), instead, controls the braking actuators in the braking phases. A more complete treatment of these control units is given in Section 3.3.
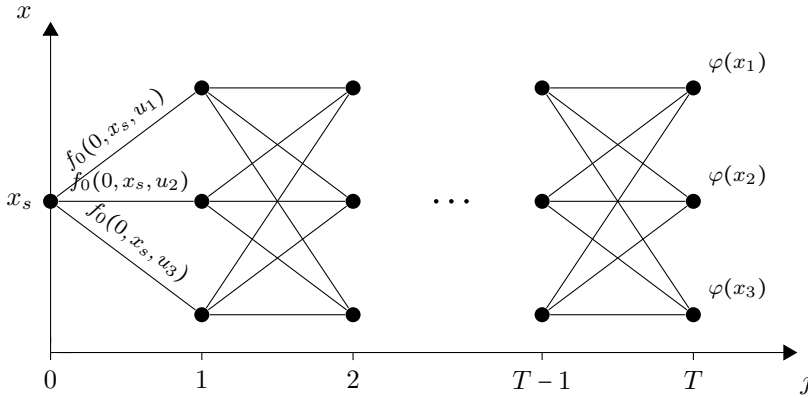
Figure 2.4: Discrete optimal control problem.

2.5   Optimal control

In this section we briefly introduce the two optimal control approaches that will be used in the platoon control formulation of Chapter 4. First, in Section 2.5.1 we present the dynamic programming concept that is used to compute the optimal speed trajectory for the whole platoon, while including topography information of the road ahead. Second, in Section 2.5.2 we present the MPC concept that is used to robustly and safely track this optimal speed trajectory.

2.5.1   Dynamic programming

Dynamic programming is a method to solve an optimal control problem by breaking it down into a collection of simpler optimal control subproblems. By exploiting the overlap of these subproblems, it significantly reduces the number of required arithmetic calculations. The theory of dynamic programming has been formulated in the fifties by Bellman (1957), although it has its origin in the work of Hamilton and Jacobi on calculus of variations. For more recent references see Bertsekas (1995) and Liberzon (2012). In this section we present the dynamic programming concept applied to a discrete system, as it will be used in the platoon controller of Chapter 4.

Consider the optimal control problem of the form

$$J^*(x_s) = \quad \text{minimize} \quad \sum_{j=0}^{T-1} f_0(j, x(j), u(j)) + \varphi(x(T)), \tag{2.1a}$$

$$\text{subj. to} \quad x(j+1) = f(j, x(j), u(j)), \tag{2.1b}$$

$$x(j) \in \mathcal{X} = \{x_1, ..., x_N\}, \tag{2.1c}$$

$$u(j) \in \mathcal{U} = \{u_1, ..., u_M\}, \tag{2.1d}$$

$$x(0) = x_s, \tag{2.1e}$$

where x is the model state that belongs to a finite set $\mathcal{X}$ of N elements (see constraint (2.1c)) and u is the control input that belongs to a finite set $\mathcal{U}$ of M elements (see constraint (2.1d)); the independent variable j represents the enumeration of the stages of the optimal control problem and, in general, may not have anything to do with time (e.g., in the platoon controller of Chapter 4 it represents a space discretization); the variable x_s represents the initial state. Finally, the relation (2.1b) represents the system model, while the cost function (2.1a) weighs functions of the state and the control input. The problem is visualized in Figure 2.4.

The most naive approach to address this problem consists in enumerating all the possible trajectories starting from x_s at stage 0 going forward up to stage T, associating to each trajectory the cost and comparing the costs in order to select the optimal one. The complexity of this approach can be easily computed and results in $\mathcal{O}(M^T T)$ arithmetic operations. In the case of a large number of stages T, this method can result in an extremely long computation time.

The dynamic programming approach relies on the so called "principle of optimality", which can be stated as follows:

Principle of optimality: Let $\{x_j^*\}_{j=0}^T$ and $\{u_j^*\}_{j=0}^{T-1}$ be the optimal state and control trajectories for the problem (2.1), respectively. Then, each control subtrajectory $\{u_j^*\}_{j=k}^{T-1}$ is optimal for the subproblems obtained by the optimization on the form (2.1) but with initial condition $(k, x^*(k))$ (i.e., starting at time k and state $x^*(k)$).

Let $\bar{J}^*(k, x(k))$ be the cost associated to the optimal control trajectory $\{u_j^*\}_{j=k}^{T-1}$ with initial condition $(k, x(k))$ and refer to it as the optimal cost-to-go. Note that the optimal cost-to-go $\bar{J}^*(0, x_s)$ corresponds to the optimal cost $J^*(x_s)$ for the complete problem (2.1).

According to the principle of optimality, given a stage k, one of the N optimal control subtrajectories $\{u_j^*\}_{j=k}^{T-1}$ with initial condition $(k, x(k))$ will belong to the optimal control trajectory $\{u_j^*\}_{j=0}^{T-1}$. Following this observation, the principle of optimality can be exploited by starting from the final stage T and proceeding backwards. At the stage T, the optimal cost-to-go for all the possible initial conditions $(T, x(T))$ is simply defined as the final cost function, i.e., $\bar{J}^*(T, x(T)) = \varphi(x(T))$.

At the generic stage k, the optimal cost-to-go with initial condition $(k, x(k))$ can be defined as the minimum of the costs given by the summation of the cost to reach a certain state at stage $k + 1$ from $x(k)$ and the optimal cost-to-go with the new state as initial condition, i.e.,

$$\bar{J}^*(k, x(k)) = \min_{u(k) \in \mathcal{U}} \left\{ f_0(k, x(k), u(k)) + \bar{J}^*(k + 1, f(k, x(k), u(k))) \right\}. \qquad (2.2)$$

This equation provides a recursive relation between the optimal cost-to-go of contiguous stages. If we apply it to all possible initial conditions $(k, x(k))$ proceeding backwards until stage 0 and we save the corresponding optimal control subtrajectory $\{u_j^*\}_{j=k}^{T-1}$, we will be eventually able to compute the optimal cost $J^*(x_s) = \bar{J}^*(0, x_s)$ and the corresponding optimal control trajectory $\{u_j^*\}_{j=0}^{T-1}$.

As for each stage and each possible state we have to compare M summations, the complexity of the dynamic programming approach can be easily computed and results in $\mathcal{O}(NMT)$ arithmetic operations. Comparing this with the complexity of the naive approach, we can conclude that dynamic programming is significantly more efficient in the case of large T. Furthermore, dynamic programming intrinsically provides a feedback law, as it computes the optimal control trajectory for every stage k and state $x(k)$. Note, however, that, although the complexity is linear in the number of possible states N, N can be an extremely large number, as it grows exponentially with the dimension of the state. This is known as the *curse of dimensionality*.

2.5.2 Model predictive control

Model predictive control (MPC) is a control framework that relies on the iterative solution of optimal control problems based on the predicted state to compute the instantaneous control input. The prediction of the state is based on the system model and this explains the name *model predictive control*. MPC has its origins in the seventies in the process industry, where it was used to control chemical plants and oil refineries (Richalet et al., 1978). The slow dynamics of such systems were favorable to the MPC requirement of solving optimization problems in real-time and the limited computational power of the contemporary hardware. With the increase of the computational power of the last decades, MPC has become attractive for other industries as well, for instance, the automotive industry (Hrovat et al., 2012; Del Re et al., 2010). In this section we introduce the MPC concept. For a more complete treatment of the topic, see Rawlings and Mayne (2009) and Borrelli et al. (2015).
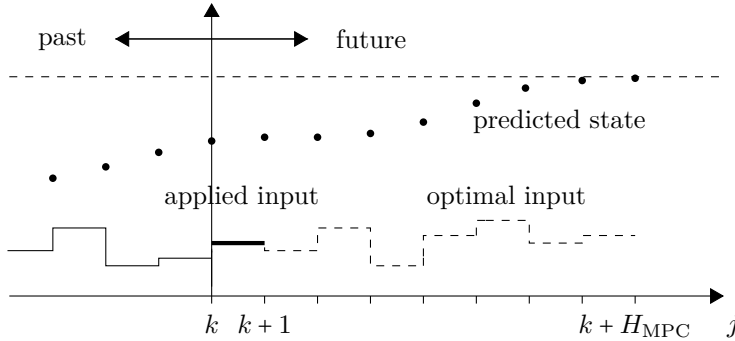
Figure 2.5: Illustration of the MPC concept. At each time instant k, an optimal control problem based on the predicted state is solved. The solving returns the optimal predicted state and the optimal control input trajectories. Of the optimal control input trajectory only the first element is applied to the system. At the time instant $k+1$, a new optimal control problem is formulated and solved.

At each time instant k, the following optimal control problem is solved:

$$\text{minimize} \quad \sum_{j=k}^{k+H_{\text{MPC}}-1} f_0(j, x(j|k), u(j|k)) + \varphi(x(k + H_{\text{MPC}}|k)), \tag{2.3a}$$

$$\text{subj. to} \quad x(j+1|k) = f(j, x(j|k), u(j|k)), \tag{2.3b}$$

$$x(j|k) \in \mathcal{X}, \tag{2.3c}$$

$$u(j|k) \in \mathcal{U}, \tag{2.3d}$$

$$x(k|k) = x(k), \tag{2.3e}$$

where $x(j|k)$ and $u(j|k)$ denote the predicted state and control input at time j computed at time k, respectively, while $x(k)$ denotes current state. The variable H_{MPC} denotes the prediction horizon. The relation (2.3b) represents the prediction model, while the constraints (2.3c) and (2.3d) provide bounds on the predicted state and control input, respectively. The cost function (2.3a) weighs a function of the predicted state and control input from the current time k to time $k + H_{\text{MPC}}$. The solution of the optimal control problem (2.3) returns the optimal state and control input trajectory $\{x^*(\cdot|k)\}_{j=k}^{H_{\text{MPC}}}$ and $\{u^*(\cdot|k)\}_{j=k}^{H_{\text{MPC}}-1}$, respectively, as displayed in Figure 2.5. The MPC algorithm only applies the first element of the optimal control input trajectory $u^*(k|k)$ to the system. At the next time instant $k+1$, a new optimal control problem of the form (2.3) is cast and solved, and this will be repeated for each time instant.

The re-solution at each step of the optimal control problem (2.3), provides feedback in the MPC framework, making it robust to disturbances and model uncertainties. Another significant advantage of the MPC framework is the possibility

to introduce constraints on the future state and control input. This is of a great interest in all the applications where it is convenient that the control system acts in the present for something that will happen in the future. This is the case when a vehicle needs to adapt its speed in order to fuel-efficiently drive over a hilly road (see Chapter 4) or needs to steer in order to avoid a coming obstacle (see Chapter 6).

Due to the non-linearities in the formulation (2.3), the presented framework is typically referred as nonlinear MPC. In the case of a linear prediction model, polytopic constraints on state and control input, and quadratic cost function, we will talk instead of linear MPC. In this case the optimal control problem (2.3) can be recast as a quadratic program for which efficient numerical algorithms are available.

A distributed version of MPC has been successfully used to control vehicle platoons, see Dunbar and Murray (2006) and Dunbar and Caveney (2012). In these works, the platooning vehicles share their optimal state trajectory with the following vehicle. Each following vehicle exploits the received information by including it in its MPC formulation. The authors also provide conditions on the controller parameters that guarantee string stability.

2.6   Summary

Although only the recent advances in technology provide the basis for the commercial implementation of vehicle platooning, the literature on the topic is extensive. The first works on vehicle platooning date back to the sixties and focus more on purely theoretical aspects such as string stability. Only in the nineties, with the beginning of the PATH project, researchers started to study more practical aspects of platooning. Among these aspects, the fuel-efficient control of heavy-duty vehicle platoons gained a certain attention. Thanks to the shape of these vehicles, the short inter-vehicular distance results in a significant reduction of the overall aerodynamic drag and the fuel consumption. Although the large impact of slopes on the fuel consumption of heavy-duty vehicles is well known (as proved by the large number of works on look-ahead control for single vehicles), few works address the inclusion of topography information in the design of fuel-efficient heavy-duty vehicle platooning.

In this chapter we have first presented the technologies that enable vehicle platooning. Second, we have provided an overview of the works that address vehicle platooning and look-ahead vehicle control. Third, the fuel-efficiency problem for the overall good transportation problem has been discussed and a system architecture that maximizes the benefits of platooning has been proposed. Lastly, we have introduced the concepts of dynamic programming and MPC that will be used in the platoon controller formulation of Chapter 4.

Modeling

Heavy-duty vehicles are complex systems with a large number of interacting dynamics. For example, due to the large weight, their braking and powertrain systems have to generate and transfer extremely high torques. This requires the coordination of multiple braking actuators and the damping of oscillations arising in the powertrain. The control system architecture of heavy-duty vehicles is therefore highly distributed and hierarchical. Since the aim of this thesis is the design of a fuel-efficient and safe control of vehicle platoons, we focus on deriving a high-level model of the vehicle in this chapter. With such model we want to capture the longitudinal vehicle dynamics, paying particular attention in correctly modeling the components that play a significant role in the fuel consumption. Low-level vehicle dynamics, i.e., actuator dynamics, are assumed to be controlled by auxiliary management units typically existing in commercial vehicles.

The chapter is organized as follows. In Section 3.1 we introduce the longitudinal models of a single vehicle and of a platoon. A simple fuel model that captures the intrinsic relation between instantaneous fuel consumption and traction force is proposed in Section 3.2. In Section 3.3, we describe the vehicle system architecture in which the platoon controller is expected to operate. Lastly, Section 3.4 provides a summary of the chapter.

3.1 Vehicle and platoon model

In this section we present the models of the longitudinal dynamics of a vehicle and a platoon as will be used in the control formulation in Chapter 4. An overview of the (longitudinal) forces acting on a heavy-duty vehicle is given in Figure 3.1. Using Newton's second law, the dynamics of vehicle i can be expressed as

$$
\begin{aligned}
m_i \dot{v}_i &= F_{\mathrm{e},i} + F_{\mathrm{b},i} + F_{\mathrm{g},i}(\alpha(s_i)) + F_{\mathrm{r},i} + F_{\mathrm{d},i}(v_i, d_i), \\
\dot{s}_i &= v_i,
\end{aligned}
\tag{3.1}
$$

where $v_i \geq 0$ and s_i form the state of the vehicle and denote its speed and longitudinal position, respectively. We collect them in the state vector $x_i = [v_i \; s_i]^{\mathrm{T}}$. $F_{\mathrm{e},i}$ and
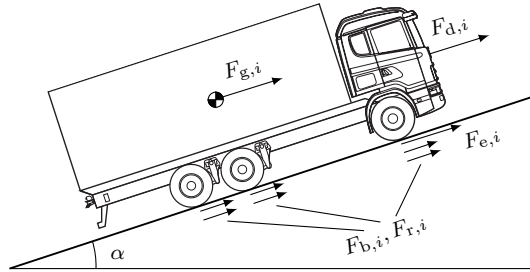
Figure 3.1: Illustration of the forces acting on the heavy-duty vehicle along the longitudinal direction. The sign convention for all forces is according to the direction of travel.

$F_{b,i}$ denote the forces generated by the actuators, i.e., the traction and braking forces, whereas $F_{d,i}$ and $F_{r,i}$ denote the resistive forces acting on the vehicle, i.e., the drag and rolling resistances; $F_{g,i}$ represents the gravitational force defined as the component of the gravity vector in the vehicle longitudinal direction. The parameter m_i represents the mass of vehicle i, while the variable $\alpha(s_i)$ is the road grade and is defined as a function of the vehicle's longitudinal position. Finally d_i denotes the distance of vehicle i to the preceding one.

The model of a platoon of N_v vehicles can be obtained by combining the vehicle model (3.1) for $i = 1, ..., N_v$ and the distance definition

$$d_i = \begin{cases} \infty, & \text{if } i = 1, \\ s_{i-1} - s_i - l_{i-1}, & \text{if } i \geq 2, \end{cases} \tag{3.2}$$

where l_i denotes the length of vehicle i.

In the remainder of this section, we describe each of the forces acting on the vehicle.

Powertrain force

The powertrain is constituted by different components, i.e., the engine, the clutch, the gearbox and the final drive, that transform the fuel into traction energy. Such components are not included in the vehicle model since this is not necessary for our control purpose. The traction force $F_{e,i}$ is therefore treated as a control input. The acceleration corresponding to the required traction force is tracked by a low-level vehicle controller, as in more detail described in Section 3.3. In order to use the model for fuel-efficiency control purpose we derive a fuel model that relates the instantaneous fuel consumption to the traction force and defines the limits for such force in Section 3.2.

Braking force

The braking system of a heavy-duty vehicle is composed of several actuators. Following the same reasoning as for the powertrain, here we assume that the braking force is a control input and the corresponding acceleration is tracked by a low-level controller. The braking actuators acting on each axle can generate a maximum torque $\tau_{a,max}$ (Alam, 2014). This torque is transferred to the road surface through the wheels and the tires. The minimum (according to the sign convention) potential braking force is therefore equal to $-\tau_{a,max}n_ar_w$, where n_a and r_w denote the number of axles and the radius of the wheels, respectively. Due to the limited friction between the tires and the road surface, there is however a threshold on the minimum braking force that can be transferred to the ground. Assuming an equal distribution of the vehicle mass on the axles, this threshold can be approximated as $-\mu m_i g$, where μ and g denote the (positive) road friction coefficient and the gravitational acceleration, respectively (Pacejka, 2005). Therefore, depending on the mass of the vehicle, the minimum braking force can be limited by either the maximum torque that the braking actuators can generate or the minimum force that the wheels are able to transfer on the ground. This constraint can be modeled as follows:

$$F_{b,min,i} \le F_{b,i} \le 0, \tag{3.3}$$

where $F_{b,min,i}$ is defined as

$$F_{b,min,i} = \max\{-\tau_{a,max}n_ar_w, -\mu m_i g\}.$$

Depending on the vehicle parameters, the braking capability of the vehicles in the platoon can vary significantly. Therefore, in order to guarantee safety, a framework that is able to handle heterogeneous platoons is needed.

Gravitational force

Here, we denote the gravitational force with the component of the gravity vector in the vehicle longitudinal direction. Depending on the road grade, such force can be either a resistive or assistive force and its expression can be formulated as

$$F_{g,i}(\alpha(s_i)) = -m_i g \sin(\alpha(s_i)). \tag{3.4}$$

Due the large mass of heavy-duty vehicle, even small road grade generates a significant gravitational force. Therefore, it is common that these vehicles are not able to keep constant speed during an uphill or downhill road stretch without exceeding the engine power limits and without braking.

Rolling resistance

The rolling resistance is generated by the interaction between tires and the road surface. It is a resistive force and is mainly due to the asymmetric deformation of
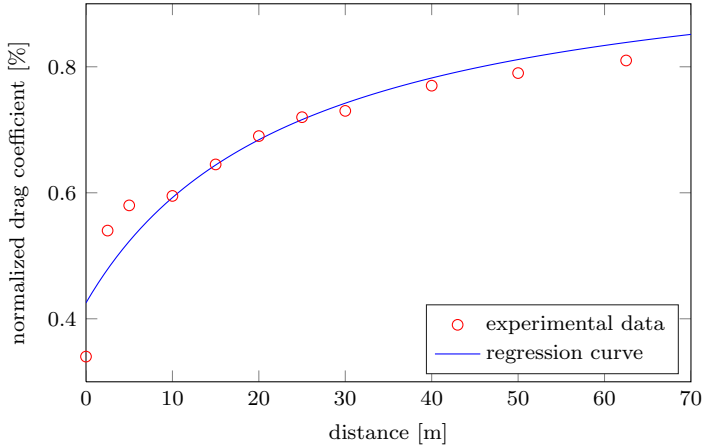
Figure 3.2: Experimental data from Hucho (1987) and regression curve of the normalized drag coefficient experienced by a heavy-duty vehicle as function of the distance to the preceding vehicle.

the tires during compression and expansion (Pacejka, 2005). It is approximately proportional to the vertical load on the tires and is typically modeled as

$$F_{\mathrm{r},i} = -c_r m_i g, \tag{3.5}$$

where c_r denotes the rolling resistance coefficient. This parameter can be influenced by different factors, such as the pressure, temperature and width of the tires.

Aerodynamic drag

The aerodynamic drag is a resistive force due to the interaction between the vehicle and the surrounding air. It grows quadratically with the vehicle speed and gets reduced when driving at a short distance to a preceding vehicle. This phenomenon is due to a slipstream effect between the vehicles that results in a reduced pressure on the second vehicle and reduced air vortices behind the first one. Thanks to the slipstream effect the aerodynamic drag experienced by both vehicles decreases as the inter-vehicular distance shrinks, although such reduction is more significant for follower vehicles. The reduction in the aerodynamic drag is the reason why race bikers or migratory birds try to keep a compact formation while moving and provides a strong motivation for heavy-duty vehicle platooning. The aerodynamic drag can be modeled as

$$F_{\mathrm{d},i}(v_i, d_i) = -\tfrac{1}{2}\rho A_v C_D(d_i) v_i^2, \tag{3.6}$$

where ρ is the air density, A_v is the cross-sectional area of the vehicle and C_D is the aerodynamic drag coefficient (here assumed as vehicle-independent). In order to

capture the reduction of the aerodynamic drag with the inter-vehicular distance, the drag coefficient C_D is defined as a function of the distance to the preceding vehicle d_i. The effect of the short inter-vehicular distance on the preceding vehicles has been neglected since it is significantly smaller than that one on the follower vehicles (see the experimental data in Figure 1.3). The literature reports measurements on air drag coefficient and fuel consumption based on both real experiments (Hucho, 1987; Bonnet and Fritz, 2000; Lammert et al., 2014) and fluid dynamics simulation (Norrby, 2014). All these works show a reduction of the air drag coefficient for short inter-vehicular distances. However, how the reduction relates to the inter-vehicular distance varies. This variability has been attributed to weather conditions (e.g, temperature, humidity or wind) and the shape of the vehicles. In this work we refer to the experimental data presented in Hucho (1987). The dependence of the drag coefficient C_D on the distance d_i is therefore modeled as

$$C_D(d_i) = C_{D,0}\left(1 - \frac{C_{D,1}}{C_{D,2} + d_i}\right), \tag{3.7}$$

where the parameters $C_{D,1}$ and $C_{D,2}$ are obtained by regressing the experimental data presented in Hucho (1987). The experimental data and the regression curve are displayed in Figure 3.2.

3.2   Fuel model

In this section we derive a simple fuel model that captures the intrinsic relation between the instantaneous fuel consumption and the generated traction force. In the model derivation we ignore the transmission engine losses and the rotational inertia of the powertrain components because they are assumed to be negligible when compared to the vehicle mass.

   Engine performance is typically described by the brake specific fuel consumption (BSFC), that defines the ratio between instantaneous fuel consumption and power output for various operation points (i.e., engine speed and generated torque). In Figure 3.3 we show the BSFC map for a heavy-duty vehicle engine of 400 hp (Sandberg, 2001), where the dotted lines represent the collection of operation points with equal generated power. The presented map can be easily converted in a new one that defines the fuel flow ψ_i as function of the engine speed ω_i and the generated engine power P_i, i.e., $\psi_i = \varphi_i(\omega_i, P_i)$. By assumption, the engine power P_i, passing through the clutch, the gearbox and the final gear is completely transferred to the wheels (i.e., $P_i = F_{e,i}v_i$). The rotational speed, instead, changes between the transmission components and is finally transformed into longitudinal speed by the wheels. Ultimately, under the assumption of no longitudinal slip, the vehicle speed v_i can be defined as

$$v_i = k_i g_i \omega_i,$$

where k_i is a constant gain and g_i is the gear ratio of the gearbox. As a result, the fuel flow can be expressed as a function of the speed v_i, the traction force $F_{e,i}$ and
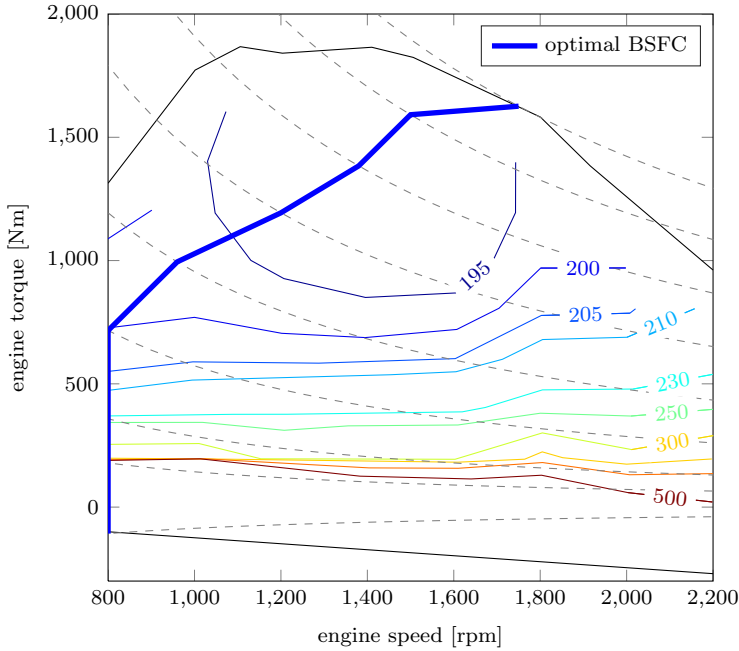
Figure 3.3: BSFC map for a 400 hp engine regenerated from Sandberg (2001). The plot shows the BSFC expressed in g/kWh as function of the engine speed and torque. The dotted lines represent equal power curves, while the blue thick line represents the collection of the fuel-optimal operation points for various generated powers. The thin black lines represent the engine torque lower and upper limits.

the gear ratio g_i as

$$\psi_i = \varphi_i\left(\frac{v_i}{k_i g_i}, F_{e,i} v_i\right). \tag{3.8}$$

In order to be efficiently used in the control design, the fuel model is further simplified by removing the dependence of the fuel flow ψ_i on the gear ratio g_i through the introduction of an additional assumption: the gear ratio can be changed continuously on an unlimited span and the gear management system chooses the most efficient gear ratio. Hence, we redefine the fuel model as

$$\psi_i = \min_{\omega_i} \varphi_i\left(\omega_i, F_{e,i} v_i\right) = \varphi_{\text{opt},i}(F_{e,i} v_i). \tag{3.9}$$

The resulting curve $\varphi_{\text{opt},i}(\cdot)$ is finally linearly regressed in order to obtain the fuel model used in the controller design defined by

$$\psi_i = p_{1,i} F_{e,i} v_i + p_{0,i}. \tag{3.10}$$
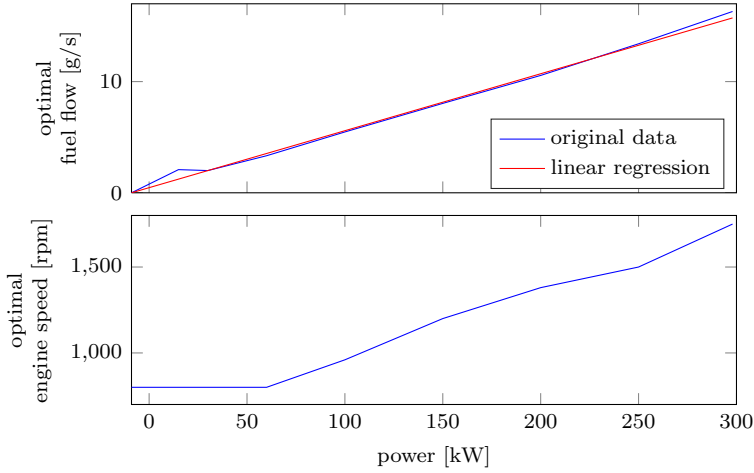
Figure 3.4: The plots show the optimal fuel flow and engine speed as function of the generated power. In the first plot we also display the fuel model expressed in (3.10) obtained by the regression of the raw data.

From this analysis we can obtain bounds on the generated power that are independent from the engine speed and the gear ratio:

$$P_{\min,i} \le F_{e,i} v_i \le P_{\max,i}. \tag{3.11}$$

In Figure 3.4, the two fuel models in (3.9) and (3.10), and the correspondent optimal engine speed are displayed. We note that the approximation error is negligible.

3.3 Vehicle system architecture

The correct functioning of a heavy-duty vehicle is guaranteed by a large number of system units that communicate between each other through the controller area network (CAN) bus. In this section, we present an abstraction of such network that enables the correct functioning of the platoon controller presented in Chapter 4, as displayed in Figure 3.5 (Alam, 2014).

The units at the top of Figure 3.5 represent the interfaces of the vehicle to the outside world. In detail, the global positioning system (GPS) returns the absolute position of the vehicle. The radar measures the distance and relative speed between the current and the preceding vehicles. The wireless sensor unit (WSU) shares real-time information with the other platooning vehicles and allows the communication with external vehicles and off-board systems, such as a back-end office or cloud services. While the GPS and radar are consolidated technologies in vehicles, the WSU is still uncommon and the focus of ongoing research. In particular, governmental institutions and telecommunication companies are collaborating in defining a standard for inter-vehicular communication. The strong interest in their
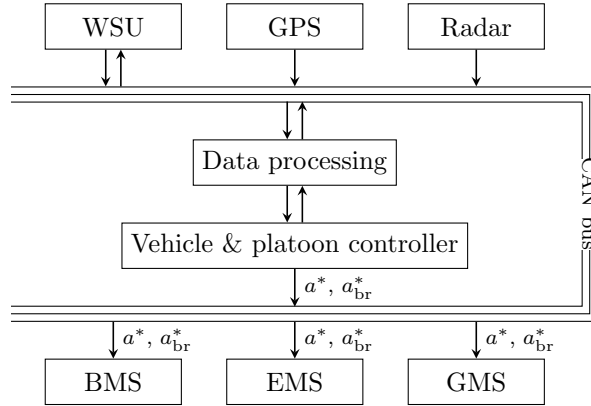
Figure 3.5: Simplified system vehicle architecture.

development is not only driven by vehicle platooning, but also by other intelligent transport system technologies aimed at improving safety and road utilization.

The blocks at the bottom of the figure represent the units controlling the vehicle longitudinal actuators. They receive as input the requested acceleration and a boolean variable representing if this acceleration should be tracked by braking or by injecting fuel. The brake management system (BMS) tracks the required acceleration by coordinating the different braking actuators. In addition to the standard brake discs the BMS for redundancy purpose can also rely on an exhaust brake and a retarder brake. Furthermore, in case of harsh braking, the BMS is responsible for correctly distributing the braking force between the brake discs and guaranteeing that the wheels do not lock. The engine and gear management systems (EMS and GMS) control the vehicle powertrain in the case traction force is required. Because of the significant power the powertrain is expected to generate, the control of the engine, the gearbox and the clutch is not trivial. In particular, the EMS controls the fuel flow in order to track the desired acceleration and ensures that no excessive oscillations are generated in the powertrain. The GMS monitors the engine speed and the requested torque in order to manage the gear shifts. It typically answers to fuel-efficiency criteria, but if needed (e.g., in case of a steep uphill), it engages the gear that can provide the maximum power.

The real-time information from the WSU, GPS and radar are fused in the data processing block and transferred to the vehicle & platoon controller. In this block the functionalities that control the longitudinal dynamics are implemented. These functionalities do not only include the cooperative look-ahead control (CLAC), as proposed in Chapter 4, but also other fuctionalities that control the vehicle in the case it is driving alone or communication is not available. An overview of such control strategies is given in Table 3.1. In particular, the vehicle is controlled by cruise control (CC) when it is driving alone and no information on the road ahead is provided. The availability of topography information allows the vehicle to

improve its fuel-efficiency by adapting its speed profile to the road grade by using look-ahead control (LAC). When the vehicle comes in proximity of a preceding one, information from the radar can be exploited to keep a desired gap policy from it, thanks to the adaptive cruise control (ACC). If the vehicles are able to share their states through vehicle-to-vehicle communication, more advance and reliable controls, known as cooperative adaptive cruise control (CACC), can be implemented. Lastly, the availability of topography information allows the platooning vehicles to fully exploit the fuel-efficiency benefit of platooning by adapting the platoon speed to the road grade thanks to the CLAC. The CC, ACC and LAC are functionalities typically existing in commercial vehicles. In this thesis we focus on the design of a CLAC strategy able to combine the benefits from platooning and loo-ahead control.

Table 3.1: Longitudinal control functionalities.

	alone	platooning w/o communication	platooning with communication
no topography info	CC	ACC	CACC
topography info	LAC	—	CLAC

3.4 Summary

In this chapter we have presented the models of the longitudinal dynamics of a single heavy-duty vehicle and a platoon. This model will form the basis for the design of a fuel-efficient platoon controller in Chapter 4. A particular focus has been put on modeling the aerodynamic drag due to its essential role in vehicle platooning. Furthermore, a simple fuel model that relates the instantaneous fuel consumption to the traction force has been derived under the assumption of a continuously varying gear ratio. Lastly, we have presented an abstraction of the vehicle system architecture that describes the vehicle control units that the platoon controller is expected to interact with and that allow its correct functioning.

Cooperative control for fuel-efficient and safe platooning

I n this chapter we develop a control system for the longitudinal control of a heavy-duty vehicle platoon aimed at reaching a high level fuel-efficiency while guaranteeing safety. The chapter starts with the analysis of the experimental results presented in Alam et al. (2015a), in which a platoon drives over a public highway. The feedback control framework used to control the platoon during the experiments shows its limitation when the road is particularly hilly. This first analysis motivates the development of a cooperative look-ahead control framework and provides some hints on how it should be designed.

The cooperative look-ahead control can be formulated as an optimal control problem that, however, is too complex to be solved in one instance. We therefore propose a two-layer control architecture that splits such problem into manageable subproblems.

The chapter is organized as follows. Section 4.1 presents the analysis of the experimental test in Alam et al. (2015a). Section 4.2 gives a general overview of the two-layer control architecture for the cooperative look-ahead platoon controller. The two layers, namely the platoon coordinator and the vehicle control layer, are lately presented in Sections 4.3 and 4.4, respectively. Finally, Section 4.5 summarizes the chapter.

4.1 Motivating experimental test

In order to obtain a good understanding of the impact of the road gradient on heavy-duty vehicle platooning, in this section we analyze the experimental results presented in Alam et al. (2015a). This analysis will also provide insights in the design of the look-ahead vehicle platooning controller.

In this experiment a platoon of three similar heavy-duty vehicles (the exact vehicle parameters are reported in Table 4.1) is driven over a 45 km highway stretch between the Swedish cities of Mariefred and Eskilstuna. The road map and the
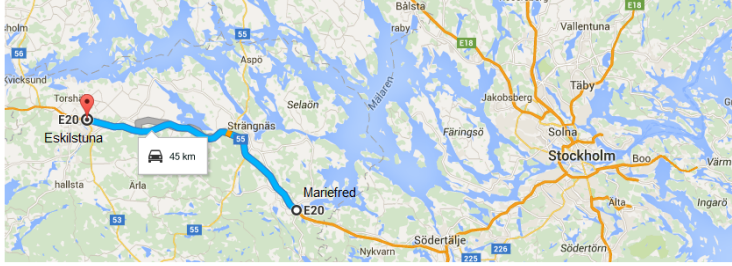
(a) Road map. (Data provided by Google®.)
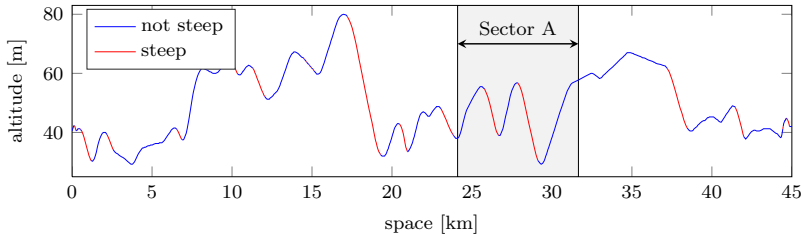
(b) Road topography.

Figure 4.1: The 45 km highway stretch between the Swedish cities of Mariefred and Eskilstuna. The red color highlights the uphill and downhill sections for which the slope is too large for a heavy-duty vehicle of 40 tons and an engine power of 480 hp to maintain a constant speed of 21.5 m/s without exceeding the engine power limit and without braking.

topography for this road is depicted in Figure 4.1. The red color highlights the uphill and downhill sections for which the slope is too large for a heavy-duty vehicle of 40 tons and an engine power of 480 hp to maintain a constant speed of 21.5 m/s without exceeding the engine power limit and without braking. Note that, due to the significant power of the engine there are no uphill stretches highlighted. For the considered road, the steep sections represent 22% of the total length.

Table 4.1: Parameters of the vehicle used in the experimental test in Alam et al. (2015a).

vehicle	mass [tons]	engine power [hp]
1st	37.5	480
2nd	38.4	480
3rd	39.5	480

Overall, the results in Alam et al. (2015a) show that the follower vehicles, by platooning, reduce their fuel consumption by 4.1% and 6.5%, respectively, compared to the case of driving alone. However, the fuel-efficiency drops significantly in the

road sector in which the altitude variation is larger, due to repeated braking actions. In order to understand the impact of slopes on platooning the behavior of the first two vehicles in the platoon is analyzed for the particularly hilly stretch highlighted in Figure 4.1b as Sector A. Over this stretch, the second vehicle manifested an increase of the fuel consumption of 4% compared to the case of driving alone. The vehicles behavior is reported in Figure 4.2. The controller of each vehicle is based on feedback control and is characterized by two modes: a traction mode, where the computed reference acceleration is tracked by the engine management system (EMS), and a braking mode, where instead the reference acceleration is tracked by the braking management system (BMS). In detail, the first vehicle tracks a reference speed of 21.5 m/s using cruise control and it switches to braking mode only when the speed limit of 23.6 m/s is reached. The second vehicle tracks a headway gap (a distance proportional to its speed) from the first vehicle and it switches to braking mode only when the headway gap reaches a certain threshold. In the analyzed sector three critical segments highlighted in Figure 4.2 are identified in which the use of only feedback control shows its limitations. The analysis for the three sectors follows:

Segment 1: due to the steep downhill the first vehicle is not able to maintain the reference speed without braking and therefore it accelerates while coasting (i.e., traveling without injecting any fuel in the engine). The second vehicle, while trying to track the headway gap policy, follows the same behavior. However, due to the reduced experienced air resistance, the second vehicle accelerates more than the first one and, when the critical headway gap is reached, it brakes. The coordination between the accelerations of the two vehicles would have the potential of avoiding this undesired braking.

Segment 2: the headway gap deviates significantly from the reference one, due to a large relative speed at the beginning of the uphill segment and a change of gear during the segment. The second vehicle, in order to reduce the headway gap error, significantly increases its speed. Once the critical headway gap is reached, it strongly brakes. The prediction of the vehicles future behavior would have allowed the second vehicle to reduce the relative speed before reaching the reference headway gap and, therefore, to avoid the undesired braking.

Segment 3: here, the second vehicle shows a more critical behavior compared to the downhill of Segment 1. In fact, during downhills, the vehicles' actuators work close to saturation (small throttling and small braking) which cannot be taken into account by a feedback controller. Therefore, in Segment 3 the control state of the second vehicle continues to switch between traction and braking modes. Additionally, in order not to exceed the speed limit, both vehicles brake at the end of the downhill. The use of a model predictive control (MPC) framework would have allowed to predict correctly the vehicle behavior by taking topography information
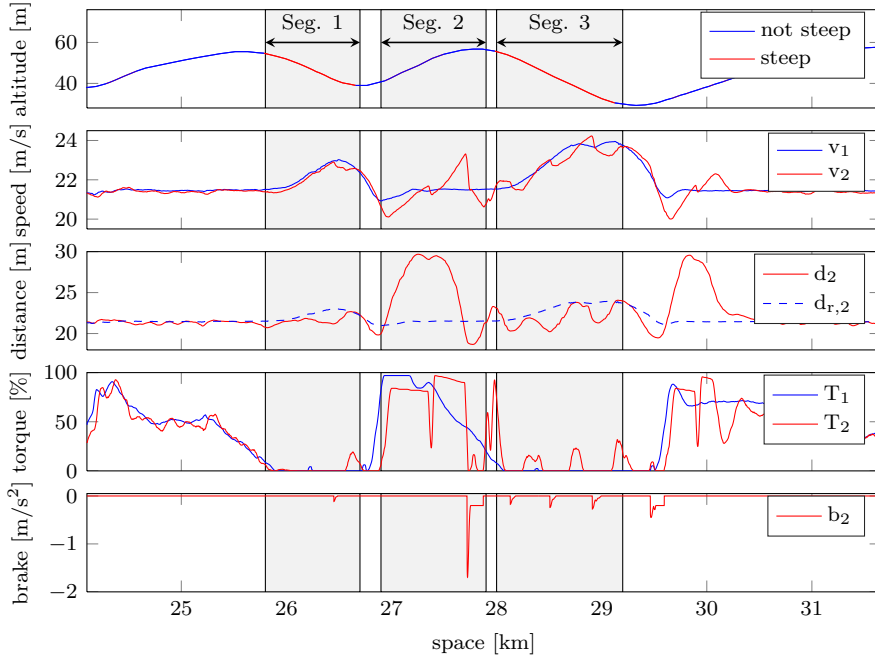
Figure 4.2: Experiment results presented in Alam et al. (2015a) relative to the first two vehicles of a three-vehicle platoon driving over the Sector A highlighted in Figure 4.1b. The first plot shows the road topography, whereas the second plot shows the speed of the two vehicles; the third plot shows the real and reference (according to a headway gap policy) between the vehicles; finally the forth and fifth plots show respectively the normalized engine torque for both vehicles and the normalized braking force for the second vehicle (the braking action of the leading vehicle is not available).

and actuator limits into account, and obtain therefore a smoother behavior of the vehicles. Furthermore, by knowing the entity of the downhill, a look-head control strategy could have allowed to avoid reaching the speed limit and, therefore, braking.

To summarize, the excessive braking of the second vehicle that caused the increase in fuel consumption could have been avoided by cooperatively controlling the vehicles and by predicting their behavior. In detail, in Segments 1 and 3, a coordinated downhill acceleration would have allowed to maintain the gap policy without applying the brakes. In Segments 2 and 3, the prediction of the behavior of the second vehicle would have allowed to avoid the braking phases. Lastly, in Segment 3, the inclusion of topography information in the controller could have been used to decrease the speed of the vehicles before the downhill in order to avoid reaching the speed limits.
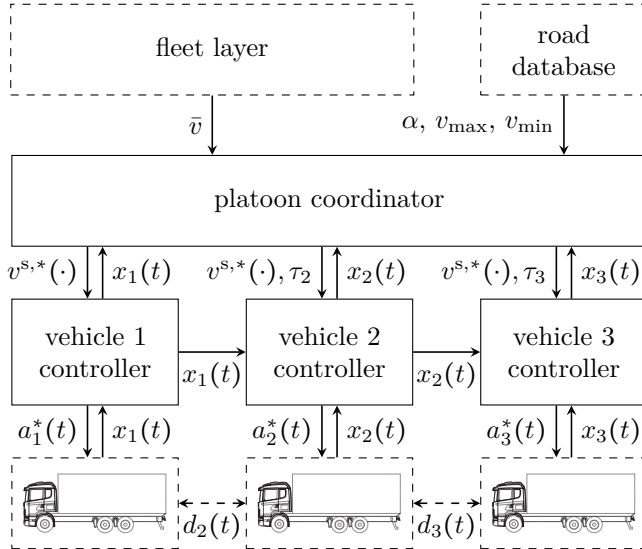
Figure 4.3: Two-layer control architecture for look-ahead heavy-duty vehicle platooning.

4.2   Two-layer platoon control architecture

From the analysis of the previous section we conclude the need of a cooperative look-ahead control strategy for fuel-efficient platooning. In order to capture the topology of the hilly road, the prediction horizon of this controller should be of the order of kilometers, as can be deduced by the example in Figure 4.2. To guarantee fuel-efficiency, the controller should consider a detailed model of each vehicle including actuators. Furthermore, in order to guarantee safety, the controller should admit the possibility that any vehicle in the platoon deviates from the nominal behavior (autonomously or manually) at any moment in order to cope with particular scenarios given by the surrounding traffic. These scenarios include for example the platoon driving in a dense traffic situation, a vehicle cutting in the middle of the platoon or an emergency situation where the maximum braking of the platoon is required. Last but not least, this optimal control problem should run in real-time and generate an input for every vehicle in the platoon.

The optimal control problem that we try to solve is clearly too large to be solved by a single controller. The number of the states of the platoon model grows with the number of vehicles and such states need to be predicted over an extremely long horizon, in order to capture the spatial dynamics of the road topography. In this section, therefore, we propose a control architecture that splits the aforementioned control task into two hierarchical layers aimed to solve smaller optimal control problems, namely the platoon coordinator and vehicle controller layer, as depicted

in Figure 4.3. The proposed platoon control architecture finds its place between the fleet layer and the low-level vehicle layer of the freight transport system architecture shown in Figure 2.3.

The platoon coordinator layer exploits available information on the topography of the planned route to find a fuel-optimal speed profile for the entire platoon, while satisfying an average speed requirement provided by the fleet layer. Hereby, in order to capture the dynamics induced by the road topography, it considers a horizon of several kilometers and takes the constraints (on, e.g., engine power) of all vehicles in the platoon into account. As a result, it can be guaranteed that every vehicle in the platoon is able to track the required speed profile. A single speed trajectory is computed by the platoon coordinator, representing the speed of the platoon. However, when this speed profile is specified as a function of space (i.e., position on the road) and the inter-vehicle spacing is chosen according to a pure time delay, every individual vehicle in the platoon can track this single speed profile. It is remarked that this layer can typically operate in a receding horizon fashion, providing an updated speed profile roughly every 10 seconds or when the recalculation is needed due to a strong deviation from the original speed profile. Finally, as this layer is not safety-critical and not related to a specific vehicle, it can be implemented in any of the platooning vehicles or even in an off-board roadside unit. In Section 4.3, we present a dynamic programming approach to formulate and solve the stated problem.

The vehicle controller is responsible for the real-time control of each vehicle in the platoon and is aimed at tracking the desired speed profile resulting from the platoon coordinator. It also exploits the communication between vehicles of the (predicted) trajectories to ensure the proper spacing strategy. This layer guarantees the safety of platooning operations to, for instance, avoid collisions between trucks. Because of the safety critical aspect, this layer is implemented in a distributed fashion in each vehicle of the platoon. More precisely, each vehicle controller runs in the vehicle & platoon controller block of the system vehicle architecture shown in Figure 3.5. In Section 4.4 a distributed MPC approach for this problem is discussed.

Figure 4.4 shows how the optimization problems in the platoon coordinator and the vehicle controllers interact, and their mathematical structure. Note how the platoon coordinator, in order to have a good prediction of the consumed fuel over the horizon, uses an accurate non-linear model of each vehicle, while the vehicle controller layer, in order to enable the fast computation necessary for the real-time control of the vehicle, uses a linear vehicle model.

4.3   Platoon coordinator

The platoon coordinator is the higher layer of the platoon control architecture in Figure 4.4. It takes as inputs the average speed requirement $\bar{v}$ from the fleet layer and the current vehicles states $x_i(t)$ from their vehicle controllers. By exploiting the available information on the planned route (i.e., slope data α and speed limits $v_{\min}$
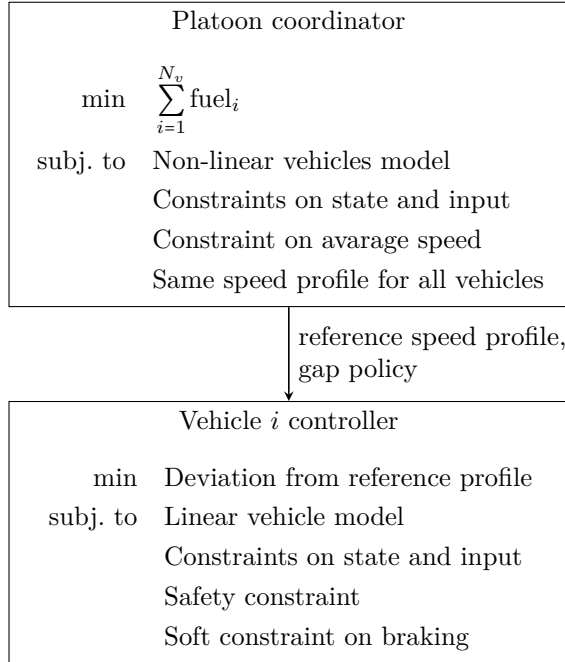
Figure 4.4: Optimal control problems solved in the platoon coordination and vehicle controllers.

and $v_{\max}$), it generates a unique feasible and fuel-optimal speed profile $v^{\mathrm{s},*}(\cdot)$ defined in the spatial domain for all the vehicles within the platoon (i.e., $v_i^{\mathrm{s},*}(z) = v^{\mathrm{s},*}(z)$ for $i = j, ..., N_v$, where z is the spatial variable). Furthermore, according to safety criteria, it specifies the time gaps τ_i, defined as the time delay between two consecutive vehicles passing through the same point, i.e.,

$$s_i(t) = s_{i-1}(t - \tau_i). \tag{4.1}$$

Note that this spacing policy is consistent with the requirement that all vehicles have to follow the same speed profile over space. This can be easily shown by computing the time derivative of the left-hand side of equation (4.1), leading to

$$\frac{ds_i(t)}{dt} = v_i(t) = v_i^{\mathrm{s}}(s_i(t)), \tag{4.2}$$

and the right-hand side of equation (4.1), leading to

$$\begin{aligned}
\frac{ds_{i-1}(t - \tau_i)}{dt} &= v_{i-1}(t - \tau_i) \\
&= v_{i-1}^{\mathrm{s}}(s_{i-1}(t - \tau_i)) = v_{i-1}^{\mathrm{s}}(s_i(t)),
\end{aligned} \tag{4.3}$$

where $v_i^{\mathrm{s}}(s)$ denotes the speed of vehicle i at space s. By combining the time gap definition (4.1) with (4.2) and (4.3), we obtain $v_i^{\mathrm{s}}(s) = v_{i-1}^{\mathrm{s}}(s)$.

The coordinator layer is implemented using a dynamic programming framework, as presented in Section 2.5.1. The parameters that characterize the dynamic programming problem are the discretization interval in space Δs_{DP}, the horizon length H_{DP} and the refresh frequency f_{DP}. We also define the horizon space length as $S_{\mathrm{DP}} = H_{\mathrm{DP}}\Delta s_{\mathrm{DP}}$.

In the coming subsections we introduce all the components of the dynamic programming formulation, i.e., the vehicle model, the constraints on the input and states and finally the cost function.

4.3.1 Platoon model

The platoon coordinator layer uses a discretized version of the vehicle model (3.1), where the discretization is carried out in the spacial domain using the implicit Euler approximation. The discretized vehicle model is:

$$v_i^{\mathrm{s}}(z_k)\frac{v_i^{\mathrm{s}}(z_k) - v_i^{\mathrm{s}}(z_{k-1})}{\Delta s_{\mathrm{DP}}} = F_{\mathrm{e},i}^{\mathrm{s}}(z_k) + F_{\mathrm{b},i}^{\mathrm{s}}(z_k) \tag{4.4a}$$
$$- m_i g[\sin(\alpha(z_k)) + c_r]$$
$$- \tfrac{1}{2}\rho A_v C_D(d_i^{\mathrm{s}}(z_k))(v_i^{\mathrm{s}}(z_k))^2,$$
$$v_i^{\mathrm{s}}(z_k)\frac{t_i^{\mathrm{s}}(z_k) - t_i^{\mathrm{s}}(z_{k-1})}{\Delta s_{\mathrm{DP}}} = 1, \tag{4.4b}$$

where z_k is the discretized space variable, $v_i^{\mathrm{s}}(z_k)$, $F_{\mathrm{e},i}^{\mathrm{s}}(z_k)$, $F_{\mathrm{b},i}^{\mathrm{s}}(z_k)$ and $d_i^{\mathrm{s}}(z_k)$ are the speed, the engine and braking forces and the distance to the preceding vehicle expressed as function of space, respectively.

The advantage of using the space discretization is that, by relaxing the average speed requirement, there is no constraint depending on time. The relaxation is done by removing the average speed constraint and introducing instead the travel time over the horizon in the cost function, as presented in Section 4.3.3. This allows to ignore the time dynamics and therefore reduce significantly the computational complexity.

A drawback of the space discretization is that the distance definition (3.2) cannot be expressed in the spatial domain. Instead, the following approximated expression, as function of the current vehicle speed $v_i^{\mathrm{s}}(z_k)$, is used:

$$d_i^{\mathrm{s}}(z_k) = v_i^{\mathrm{s}}(z_k)\tau_i - l_{i-1}. \tag{4.5}$$

In the dynamic programming formulation we refer to (4.4a) as

$$v_i^{\mathrm{s}}(z_{k-1}) = f_{v,i}^{\mathrm{s}}(v_i^{\mathrm{s}}(z_k), u_i^{\mathrm{s}}(z_k)),$$

where $u_i^{\mathrm{s}}(z_k)$ is the input vector defined as $u_i^{\mathrm{s}}(z_k) = [F_{\mathrm{e},i}^{\mathrm{s}}(z_k), F_{\mathrm{b},i}^{\mathrm{s}}(z_k)]^{\mathrm{T}}$.

4.3.2   Model constraints

The platoon model is constrained by introducing bounds on the input and the speed.

Input constraints

According to (3.3) and (3.11), the engine and braking forces are bounded by the following constraints:

$$P_{\mathrm{min},i} v_i^{\mathrm{s}}(z_k) \le F_{\mathrm{e},i}^{\mathrm{s}}(z_k) \le P_{\mathrm{max},i} v_i^{\mathrm{s}}(z_k),$$
$$F_{\mathrm{b},\mathrm{min},i} \le F_{\mathrm{b},i}^{\mathrm{s}}(z_k) \le 0. \tag{4.6}$$

In the dynamic programming formulation, we refer to these constraints as $u_i^{\mathrm{s}}(z_k) \in \mathcal{U}_i^{\mathrm{s}}(z_k)$.

State constraints

In order to take the road speed limits into account, the speed is bounded by

$$v_{\mathrm{min}}(z_k) \le v_i^{\mathrm{s}}(z_k) \le v_{\mathrm{max}}(z_k). \tag{4.7}$$

We refer to this constraint as $v_i^{\mathrm{s}}(z_k) \in \mathcal{V}^{\mathrm{s}}(z_k)$.

Moreover, in order to require all the vehicle to follow the same speed profile, the constraint

$$v_i^{\mathrm{s}}(z_k) = v^{\mathrm{s}}(z_k), \quad i = 1, ..., N_v. \tag{4.8}$$

is introduced. As we have previously shown in this section, this constraint results in a time gap spacing policy. The practical effect of such constraint is to reduce the search space of the dynamic programming algorithm to one dimension rather then the number of vehicles in the platoon, enabling therefore fast computation.

4.3.3   Cost function

The objective of the platoon coordinator layer is to define the optimal speed profile that minimizes the fuel consumption of the whole platoon, while maintaining a certain average speed. This is done by defining the cost function as the weighted sum of two terms: a first term $J_{\mathrm{f}}(v^{\mathrm{s}}(z_j), u_i^{\mathrm{s}}(z_j))$ for $j = k, ..., k + H_{\mathrm{DP}} - 1$ and $i = 1, ..., N_v$ representing the amount of fuel consumed by the platoon and a second term $J_{\mathrm{t}}(v^{\mathrm{s}}(z_j))$ for $j = k, ..., k + H_{\mathrm{DP}} - 1$ representing the travel time over the horizon, i.e.,

$$J_{\mathrm{DP}}(v^{\mathrm{s}}(z_j)), u^{\mathrm{s}}(z_j)) = J_{\mathrm{f}}(v^{\mathrm{s}}(z_j), u_i^{\mathrm{s}}(z_j)) + \beta J_{\mathrm{t}}(v^{\mathrm{s}}(z_j)), \tag{4.9}$$

where β represents a trade-off weight[1]. A similar approach has been used in Hellström et al. (2006) to compute the optimal speed trajectory for a single heavy-duty vehicle.

---

[1]Instead of the constraint on the average speed of Figure 4.4, the parameter β is tuned to give the desired average time.

The term $J_{\mathrm{f}}(v^{\mathrm{s}}(z_j), u_i^{\mathrm{s}}(z_j))$ is computed by using the fuel model (3.10) and including a final term representing the kinematic energy of the platoon at the end of the horizon:

$$J_{\mathrm{f}}(v^{\mathrm{s}}(z_j), u_i^{\mathrm{s}}(z_j)) = \sum_{i=1}^{N_v} \sum_{j=k}^{k+H_{\mathrm{DP}}-1} \Delta s_{\mathrm{DP}} \left(p_{1,i} F_{\mathrm{e},i}^{\mathrm{s}}(z_j) + \frac{p_{0,i}}{v^{\mathrm{s}}(z_j)} \right)$$
$$- \sum_{i=1}^{N_v} p_{1,i} \frac{m_i (v^{\mathrm{s}}(z_{h+H_{\mathrm{DP}}-1}))^2}{2}.$$

Here, we recall that N_v denotes the number of the vehicles in the platoon, whereas $p_{1,i}$ and $p_{0,i}$ are parameters characterizing the fuel model of vehicle i.

The term $J_{\mathrm{t}}(v^{\mathrm{s}}(z_j))$ is obtained by using the time model (4.4b):

$$J_{\mathrm{t}}(v^{\mathrm{s}}(z_j)) = \sum_{j=k}^{k+H_{\mathrm{DP}}-1} \frac{\Delta s_{\mathrm{DP}}}{v^{\mathrm{s}}(z_j)}.$$

4.3.4   Dynamic programming formulation

We now have all the elements to formulate the dynamic programming problem solved in the platoon coordinator:

$$\underset{u^{\mathrm{s}}(z_j)}{\text{minimize}} \quad J_{\mathrm{DP}}(v^{\mathrm{s}}(z_j), u^{\mathrm{s}}(z_j)) \tag{4.10a}$$

$$\text{subj. to} \quad v_i^{\mathrm{s}}(z_{j-1}) = f_{v,i}^{\mathrm{s}}(v_i^{\mathrm{s}}(z_j), u_i^{\mathrm{s}}(z_j)), \tag{4.10b}$$

$$u_i^{\mathrm{s}}(z_j) \in \mathcal{U}_i^{\mathrm{s}}(z_j), \tag{4.10c}$$

$$v_i^{\mathrm{s}}(z_j) = v^{\mathrm{s}}(z_j) \in \mathcal{V}^{\mathrm{s}}(z_j), \tag{4.10d}$$

$$z_k = s_1(t), \tag{4.10e}$$

$$v^{\mathrm{s}}(z_k) = v_1(t), \tag{4.10f}$$

for $j = k, ..., k + H_{\mathrm{DP}} - 1$, where the equations (4.10e) and (4.10f) represent the initial conditions of the DP formulation.

4.4   Vehicle controller

This section focuses on the distributed MPC-based controllers running in the vehicle control layer of the control architecture depicted in Figure 4.3.

Each vehicle controller runs locally. Vehicle i receives the optimal speed profile $v^{\mathrm{s},*}(\cdot)$ and the time gap τ_i from the platoon coordinator and obtains state information from the preceding vehicle. By tracking the optimal speed profile and gap policy requirement, and satisfying a safety constraint, it generates the optimal state and input trajectories, respectively $x_i^*(\cdot|t)$ and $a_i^*(\cdot|t)$, and the desired instantaneous acceleration $a_i^*(t)$ for the vehicle low-level controllers. The parameters that characterize the MPC formulation are the discretization time Δt_{MPC}, the horizon steps

number H_{MPC}, the refresh frequency f_{MPC} and the length of the horizon defined as $T_{\text{MPC}} = H_{\text{MPC}}\Delta t_{\text{MPC}}$. Here, we assume a maximum delay in the vehicle-to-vehicle (V2V) communication of Δt_{MPC}.

In the coming subsections we introduce all the components of the MPC formulation, i.e., the vehicle model, the constraints on the input and state, the safety constraint, and, finally, the cost function.

4.4.1 Vehicle model

In the MPC formulation the vehicle is described by

$$x_i(t_{j+1}|t_k) = Ax_i(t_j|t_k) + Ba_i(t_j|t_k), \qquad (4.11)$$

where

$$A \triangleq \begin{bmatrix} 1 & 0 \\ \Delta t_{\text{MPC}} & 1 \end{bmatrix}, \quad B \triangleq \begin{bmatrix} \Delta t_{\text{MPC}} \\ 0 \end{bmatrix}.$$

The variables $x_i(t_j|t_k) = [v_i(t_j|t_k)\ s_i(t_j|t_k)]^{\mathrm{T}}$ and $a_i(t_j|t_k)$ denote the predicted state (speed and position) and control input (desired acceleration) trajectories of vehicle i associated to the update time t_k. We also introduce three additional trajectories associated to each update time t_k that will be used later in the MPC formulation:

- the optimal state trajectory $x_i^*(t_j|t_k)$,

- the state reference trajectory $\bar{x}_i(t_j|t_k)$,

- the assumed state trajectory $\hat{x}_i(t_j|t_k)$,

for $j = k, ..., k + H_{\text{MPC}} - 1$ and the corresponding input control trajectories defined likewise. While the predicted and optimal trajectories are functions of the optimization variable, the reference and assumed trajectories are precomputed. More precisely the reference trajectories $\bar{x}_i(t_j|t_k) = [\bar{v}_i(t_j|t_k)\ \bar{s}_i(t_j|t_k)]^{\mathrm{T}}$ and $\bar{a}_i(t_j|t_k)$ are computed from the reference trajectory $v^{\mathrm{s},*}(\cdot)$ and the current position $s(t_k)$ of the vehicle. In particular, $\bar{s}_i(t_j|t_k)$ is defined recursively as

$$\bar{s}_i(t_j|t_k) = \begin{cases} s_i(t_j), & j = k, \\ \bar{s}_i(t_{j-1}|t_k) + \Delta t_{\text{MPC}}\bar{v}^{\mathrm{s},*}(\bar{s}_i(t_{j-1}|t_k)), & j > k, \end{cases}$$

while $\bar{v}_i(t_j|t_k)$ is defined as

$$\bar{v}_i(t_j|t_k) = v^{\mathrm{s},*}(\bar{s}_i(t_j|t_k)).$$

The control input reference trajectory $\bar{a}_i(t_j|t_k)$ is defined as finite differences of $\bar{v}_i(t_j|t_k)$, i.e.,

$$\bar{a}_i(t_j|t_k) = (\bar{v}_i(t_{j+1}|t_k) - \bar{v}_i(t_j|t_k))/\Delta t_{\text{MPC}}.$$

The assumed state and control input trajectories are computed from the optimal and real trajectories of the vehicle as

$$
\hat{x}_i(t_j|t_k) = \begin{cases} x_i(t_j), & j < k, \\ x_i^*(t_j|t_{k-1}), & k \le j < k + H_{\mathrm{MPC}}, \end{cases} \tag{4.12}
$$

and $\hat{a}_i(t_j|t_k)$ likewise. The assumed trajectories represent the most accurate knowledge of the past and future state and control input trajectories of each vehicle. Using a similar framework to that one presented in Dunbar and Murray (2006), such trajectories are communicated by each vehicle to the following one. In this way, the assumed trajectories of the preceding vehicle can be exploited in each vehicle MPC formulation in order to track the required gap policy. Note that the dependence of the assumed trajectories to the optimal trajectories computed the previous step (see definition (4.12)) reflects the assumption of a maximum delay in V2V communication of Δt_{MPC}.

4.4.2 Input and model constraints

In order to take the bounds on the braking force (3.3) and the engine power (3.11) into account, as done in the platoon coordinator layer, the control input a_i is bounded by the following non-linear constraint:

$$
\frac{F_{\mathrm{b,min},i}}{m_i} + \frac{F_{\mathrm{ext}}(x_i, \hat{s}_{i-1})}{m_i} \le a_i \le \frac{P_{i,\mathrm{max}}}{m_i v_i} + \frac{F_{\mathrm{ext}}(x_i, \hat{s}_{i-1})}{m_i}, \tag{4.13}
$$

where $F_{\mathrm{ext}}(x_i, \hat{s}_{i-1})$ denotes the summation of the external forces acting on the vehicle and is defined as

$$
\begin{aligned}
F_{\mathrm{ext}}(x_i, \hat{s}_{i-1}) = & - m_i g(\sin(\alpha(s_i)) + c_r) \\
& - \tfrac{1}{2} \rho A_v C_D (\hat{s}_{i-1} - s_i - l_i) v_i^2.
\end{aligned} \tag{4.14}
$$

The control input is additionally bounded by a soft constraint in order to allow braking only if necessary, i.e., when the safety constraint (see Section 4.4.3) is activated or the braking is required by the platoon coordinator. This is formulated as follows:

$$
a_i + \varepsilon_i \ge \min(a_{\mathrm{c},i}, \bar{a}_i), \; \varepsilon_i \ge 0, \tag{4.15}
$$

where ε_i is the softening variable and $a_{\mathrm{c},i}$ is the coasting acceleration (i.e., no braking and fuel injection) and is defined as:

$$
a_{\mathrm{c},i} = \frac{P_{i,\mathrm{min}}}{m_i v_i} + \frac{F_{\mathrm{ext}}(x_i, \hat{s}_{i-1})}{m_i}. \tag{4.16}
$$

In the MPC formulation we refer to the constraint (4.13), (4.14) as $a_i(t_j|t_k) \in \mathcal{A}_i(x_i(t_j|t_k), \hat{x}_{i-1}(t_j|t_k))$ and to the soft constraint (4.15), (4.16) as $a_i(t_j|t_k) +$

$\varepsilon_i(t_j|t_k) \in \mathcal{A}_{e,i}(x_i(t_j|t_k), \hat{x}_{i-1}(t_j|t_k))$. We remark that the dependence of the input constraints on the assumed trajectory of the preceding vehicle is due to the aerodynamic drag reduction with the inter-vehicular distance reduction.

The speed is bounded according to the constraint (4.7) as

$$v_{\min}(s_i(t_j|t_k)) \le v_i(t_j|t_k) \le v_{\max}(s_i(t_j|t_k)).$$

In the MPC formulation, we refer to this constraint as $v_i(t_j|t_k) \in \mathcal{V}(s_i(t_j|t_k))$.

4.4.3 Safety constraint

The platoon is intended to operate on public highways where other vehicles are present. The designed controller therefore should be able to cope with cases where the platoon behavior deviates from the predicted one because of internal disturbances (e.g., gear shifts) or external events (e.g., high traffic or a vehicle cutting into the platoon). In this section we focus on the safety problem, leaving to further work the study of how such events should be handled (i.e., autonomously or by switching to manual driving).

The platoon is considered safe if, whatever a vehicle in the platoon does, there exists an input for all the follower vehicles such that a collision can be avoided. The safety of the platoon is guaranteed by ensuring that the state of each vehicle lies within a safety set and it is firstly studied by considering two adjacent vehicles and later extended to the entire platoon. In here we consider the following continuous-time vehicle dynamics:

$$\dot{\tilde{x}}_i = \left[\begin{array}{c} \dot{\tilde{v}}_i \\ \dot{\tilde{s}}_i \end{array} \right] = f(\tilde{x}_i, \tilde{a}_i) = \left[\begin{array}{c} \tilde{a}_i \\ \tilde{v}_i \end{array} \right], \tag{4.17}$$

where $\tilde{v}_i$, $\tilde{s}_i$ and $\tilde{a}_i$ are the speed, position and acceleration of vehicle i, respectively.

Let now focus on the dynamics of two adjacent vehicles described by

$$\left[\begin{array}{c} \dot{\tilde{x}}_{i-1} \\ \dot{\tilde{x}}_i \end{array} \right] = F(\tilde{x}_{i-1}, \tilde{x}_i, \tilde{a}_{i-1}, \tilde{a}_i) = \left[\begin{array}{c} f(\tilde{x}_{i-1}, \tilde{a}_{i-1}) \\ f(\tilde{x}_i, \tilde{a}_i) \end{array} \right], \tag{4.18}$$

where the acceleration of the current vehicle $\tilde{a}_i$ is the control input, while the acceleration of the preceding vehicle $\tilde{a}_{i-1}$ is the exogenous input that can be regarded as a disturbance. We also introduce the admissible set

$$\tilde{\mathcal{X}} = \left\{ \left[\tilde{x}_{i-1}^{\mathrm{T}} \ \tilde{x}_i^{\mathrm{T}} \right]^{\mathrm{T}} : \tilde{v}_{i-1} \ge 0, \ \tilde{v}_i \ge 0, \ \tilde{s}_{i-1} - \tilde{s}_i \ge l_{i-1} \right\}$$

as the set of all admissible states, where l_i denotes the length of vehicle i. In order to obtain a closed form of the safety set, the following conservative approximations

of the the exogenous and control inputs are introduced:

$$
\tilde{a}_{i-1} \in \mathcal{A}^{\mathrm{p}}(\tilde{x}_{i-1}) = \begin{cases} [\underline{a}_{\min,i-1}, \overline{a}_{\max,i-1}], & \text{if } \tilde{v}_{i-1} > 0, \\ [0, \overline{a}_{\max,i-1}], & \text{if } \tilde{v}_{i-1} = 0, \end{cases} \tag{4.19a}
$$

$$
\tilde{a}_i \in \mathcal{A}^{\mathrm{f}}(\tilde{x}_i) = \begin{cases} [\overline{a}_{\min,i}, \underline{a}_{\max,i}], & \text{if } \tilde{v}_i > 0, \\ [0, \underline{a}_{\max,i}], & \text{if } \tilde{v}_i = 0, \end{cases} \tag{4.19b}
$$

where $\underline{a}_{\min,i}$, $\overline{a}_{\min,i}$, $\underline{a}_{\max,i}$ and $\overline{a}_{\max,i}$ are lower and upper bounds on the minimum and maximum possible accelerations of vehicle i, respectively. Such bounds are computed under reasonable assumptions on the vehicles and road properties, i.e., the vehicles' speed is limited ($0 \le \tilde{v}_i \le v_{\max}$) and the road slope α is bounded ($|\alpha| \le \alpha_{\max}$). For example, the bounds $\underline{a}_{\min,i}$ and $\overline{a}_{\min,i}$ represent the minimum braking acceleration in the best and worst case environmental conditions. They can be computed as

$$
\underline{a}_{\min,i} = \min_{0 \le v \le v_{\max}, |\alpha| \le \alpha_{\max}, d \ge 0} a_{\min,i}(v, \alpha, d),
$$

$$
\overline{a}_{\min,i} = \max_{0 \le v \le v_{\max}, |\alpha| \le \alpha_{\max}, d \ge 0} a_{\min,i}(v, \alpha, d),
$$

where $a_{\min,i}(v, \alpha, d)$ denotes the minimum braking acceleration and, according to the vehicle model presented in Chapter 3, is defined as

$$
a_{\min,i}(v, \alpha, d) = \frac{F_{\mathrm{b,min},i}}{m_i} - g \sin(\alpha) - c_r g - \frac{\rho A_v C_D(d) v^2}{2 m_i}.
$$

Note that, due to the definition of the bounds and because of the dominance of the $F_{\mathrm{b,min},i}/m_i$ term in the definition of $a_{\min,i}$, the following inequalities hold:

$$
\underline{a}_{\min,i} \le \overline{a}_{\min,i} \le 0, \tag{4.21a}
$$

$$
\underline{a}_{\max,i} \le \overline{a}_{\max,i}. \tag{4.21b}
$$

A similar approach can be taken for computing the bounds on the maximum traction acceleration $\underline{a}_{\max,i}$ and $\overline{a}_{\max,i}$.

In order to guarantee the safety of the subsystem (4.18), we should guarantee that the state $[\tilde{x}_{i-1}^{\mathrm{T}} \, \tilde{x}_i^{\mathrm{T}}]^{\mathrm{T}}$ always lies in a safety set $\mathcal{S}_i$ included in $\tilde{\mathcal{X}}$, for any admissible trajectory of the preceding vehicle. We now define the safety set $\mathcal{S}_i \subseteq \tilde{\mathcal{X}}$, displayed in Figure 4.5, as

$$
\mathcal{S}_i = \{[\tilde{x}_{i-1}^{\mathrm{T}} \, \tilde{x}_i^{\mathrm{T}}]^{\mathrm{T}} : g_j(\tilde{x}_{i-1}, \tilde{x}_i) \ge 0, \ j = 1, ..., 4\}, \tag{4.22}
$$

where

$$
\begin{aligned}
g_1(\tilde{x}_{i-1}, \tilde{x}_i) &= \tilde{s}_{i-1} - \tilde{s}_i - l_{i-1} - \frac{\tilde{v}_{i-1}^2}{2\underline{a}_{\min,i-1}} + \frac{\tilde{v}_i^2}{2\overline{a}_{\min,i}}, \\
g_2(\tilde{x}_{i-1}, \tilde{x}_i) &= \tilde{s}_{i-1} - \tilde{s}_i - l_{i-1}, \\
g_3(\tilde{x}_{i-1}, \tilde{x}_i) &= \tilde{v}_{i-1}, \\
g_4(\tilde{x}_{i-1}, \tilde{x}_i) &= \tilde{v}_i
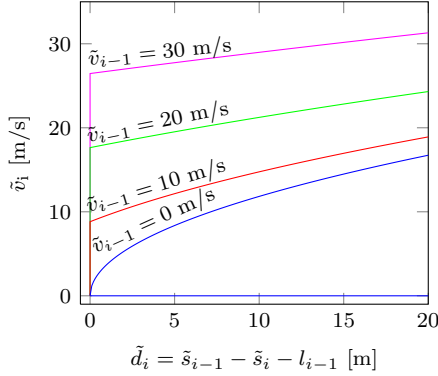\end{aligned} \tag{4.23}
$$

Figure 4.5: Projection of the boundary $\partial\mathcal{S}_i$ of the safety set $\mathcal{S}_i \subseteq \tilde{\mathcal{X}}$ on the $(\tilde{d}_i, \tilde{v}_i)$ plane for $\tilde{v}_{i-1} = 0, 10, 20, 30$ m/s. The variable $\tilde{d}_i$ denotes the distance between the two adjacent vehicles. The bounds on the minimum braking acceleration has been chosen such that $\underline{a}_{\min,i-1} < \overline{a}_{\min,i}$.

and we state the following result:

Lemma 1. Given the dynamical system (4.18) and the constraints (4.19a) and (4.19b) on the exogenous and control inputs respectively, there exists a control law $\tilde{a}_i = \varphi([\tilde{x}_{i-1}^{\mathrm{T}}\, \tilde{x}_i^{\mathrm{T}}]^{\mathrm{T}}) \in \mathcal{A}^{\mathrm{f}}(\tilde{x}_i)$ such that for all $[\tilde{x}_{i-1}^{\mathrm{T}}(t_0)\, \tilde{x}_i^{\mathrm{T}}(t_0)]^{\mathrm{T}} \in \mathcal{S}_i$ and $\tilde{a}_{i-1} \in \mathcal{A}^{\mathrm{p}}(\tilde{x}_{i-1})$, the condition $[\tilde{x}_{i-1}^{\mathrm{T}}(t)\, \tilde{x}_i^{\mathrm{T}}(t)]^{\mathrm{T}} \in \mathcal{S}_i$ holds for all $t \geq t_0$.

In other words, $\mathcal{S}_i$ is a robust controlled invariant set (Blanchini, 1999).

Proof. By using Nagumo's theorem for robust controlled invariant sets (Blanchini, 1999), the lemma can be proven by showing that for all $[\tilde{x}_{i-1}^{\mathrm{T}}\, \tilde{x}_i^{\mathrm{T}}]^{\mathrm{T}} \in \partial\mathcal{S}_i$ (defined as the boundary of $\mathcal{S}_i$), there exists an $\tilde{a}_i \in \mathcal{A}^{\mathrm{f}}$ such that, for all $\tilde{a}_{i-1} \in \mathcal{A}^{\mathrm{p}}$, the relation

$$\nabla g_j(\tilde{x}_{i-1}, \tilde{x}_i)^{\mathrm{T}} F(\tilde{x}_i, \tilde{x}_{i-1}, \tilde{a}_{i-1}, \tilde{a}_i) \geq 0 \tag{4.24}$$

holds for all j such that $g_j(\tilde{x}_{i-1}, \tilde{x}_i) = 0$. Because of the structure of the problem, the control input $\tilde{a}_i$ is chosen as maximum braking, i.e.,

$$\tilde{a}_i = \begin{cases} \overline{a}_{\min,i}, & \text{if } \tilde{v}_i > 0, \\ 0, & \text{if } \tilde{v}_i = 0, \end{cases} \tag{4.25}$$

for any $[\tilde{x}_{i-1}^{\mathrm{T}}\, \tilde{x}_i^{\mathrm{T}}]^{\mathrm{T}} \in \partial\mathcal{S}_i$ and $\tilde{a}_{i-1} \in \mathcal{A}^{\mathrm{p}}(\tilde{x}_{i-1})$. We organize the proof by considering the $[\tilde{x}_{i-1}^{\mathrm{T}}\, \tilde{x}_i^{\mathrm{T}}]^{\mathrm{T}} \in \partial\tilde{\mathcal{S}}_i$ defined by the activation of each $g_j(\tilde{x}_{i-1}, \tilde{x}_i) \geq 0$:

- for $[\tilde{x}_{i-1}^{\mathrm{T}}\,\tilde{x}_i^{\mathrm{T}}]^{\mathrm{T}}$ such that $g_1(\tilde{x}_{i-1},\tilde{x}_i) = 0$, and $g_j(\tilde{x}_{i-1},\tilde{x}_i) \geq 0$, for $j \in \{2,3,4\}$,

$$\nabla g_1(\tilde{x}_{i-1},\tilde{x}_i)^{\mathrm{T}} F(\tilde{x}_{i-1},\tilde{x}_i,\tilde{a}_{i-1},\tilde{a}_i) = \left(1 - \frac{\tilde{a}_{i-1}}{\underline{a}_{\min,i-1}}\right)\tilde{v}_{i-1} - \left(1 - \frac{\tilde{a}_i}{\underline{a}_{\min,i}}\right)\tilde{v}_i,$$

$$= \left(1 - \frac{\tilde{a}_{i-1}}{\underline{a}_{\min,i-1}}\right)\tilde{v}_{i-1} \geq 0,$$

  where the equality and inequality hold because of the definition of $\tilde{a}_i$ in (4.25) and $g_3(\tilde{x}_{i-1},\tilde{x}_i) \geq 0$.

- for $[\tilde{x}_{i-1}^{\mathrm{T}}\,\tilde{x}_i^{\mathrm{T}}]^{\mathrm{T}}$ such that $g_2(\tilde{x}_{i-1},\tilde{x}_i) = 0$, and $g_j(\tilde{x}_{i-1},\tilde{x}_i) \geq 0$, for $j \in \{1,3,4\}$,

$$\nabla g_2(\tilde{x}_{i-1},\tilde{x}_i)^{\mathrm{T}} F(\tilde{x}_{i-1},\tilde{x}_i,\tilde{a}_{i-1},\tilde{a}_i) = \tilde{v}_{i-1} - \tilde{v}_i \geq 0,$$

  where the inequality holds by noticing that the combination of $g_1(\tilde{x}_{i-1},\tilde{x}_i) \geq 0$, $g_2(\tilde{x}_{i-1},\tilde{x}_i) = 0$ and the relation (4.21a) gives $\tilde{v}_{i-1} \geq (\underline{a}_{\min,i}/\overline{a}_{\min,i})\tilde{v}_i$.

- for $[\tilde{x}_{i-1}^{\mathrm{T}}\,\tilde{x}_i^{\mathrm{T}}]^{\mathrm{T}}$ such that $g_3(\tilde{x}_{i-1},\tilde{x}_i) = 0$, and $g_j(\tilde{x}_{i-1},\tilde{x}_i) \geq 0$, for $j \in \{1,2,4\}$,

$$\nabla g_3(\tilde{x}_{i-1},\tilde{x}_i)^{\mathrm{T}} F(\tilde{x}_{i-1},\tilde{x}_i,\tilde{a}_{i-1},\tilde{a}_i) = \tilde{a}_{i-1} \geq 0,$$

  where the inequality holds because of (4.19a). The same can be verified in a similar way for $[\tilde{x}_{i-1}^{\mathrm{T}}\,\tilde{x}_i^{\mathrm{T}}]^{\mathrm{T}}$ such that $g_4(\tilde{x}_{i-1},\tilde{x}_i) = 0$ and $g_j(\tilde{x}_{i-1},\tilde{x}_i) \geq 0$ for $j \in \{1,2,4\}$. □

The choice of the safety set guarantees that the follower vehicle can react to the emergency braking maneuver of its predecessor, such that both vehicles come to a standstill without colliding. We now extend the result in Lemma 1 to the safety of the whole platoon. More precisely, we proof that whatever a vehicle does, there exists an input for all the follower vehicles, such that collision can be avoided. This is formalized by the following theorem:

Theorem 1. Consider a vehicle with index $i_0 < N_{\mathrm{v}}$ and all its follower vehicles $i \in \mathcal{I} = \{i_0 + 1, ..., N_{\mathrm{v}}\}$ satisfying the dynamics in (4.17). Then, there exists a control law $\tilde{a}_i = \varphi(\tilde{x}_i, \tilde{x}_{i-1}) \in \mathcal{A}^{\mathrm{f}}(\tilde{x}_i)$, $i \in \mathcal{I}$ such that for all $[\tilde{x}_{i-1}^{\mathrm{T}}(t_0)\,\tilde{x}_i^{\mathrm{T}}(t_0)]^{\mathrm{T}} \in \mathcal{S}_i$ and $\tilde{a}_{i_0} \in \mathcal{A}^{\mathrm{p}}(\tilde{x}_{i_0})$, the condition $[\tilde{x}_{i-1}^{\mathrm{T}}(t)\,\tilde{x}_i^{\mathrm{T}}(t)]^{\mathrm{T}} \in \mathcal{S}_i$ holds for all $t \geq t_0$ and all $i \in \mathcal{I}$.

Proof. The application of Lemma 1 for $i = i_0 + 1$ proves the existence of an input $\tilde{a}_i \in \mathcal{A}^{\mathrm{f}}(\tilde{x}_i)$ that ensures that $[\tilde{x}_{i-1}^{\mathrm{T}}(t)\,\tilde{x}_i^{\mathrm{T}}(t)]^{\mathrm{T}} \in \mathcal{S}_i$ for all $t \geq t_0$. Then, by noting that $\mathcal{A}^{\mathrm{f}}(\tilde{x}_i) \subseteq \mathcal{A}^{\mathrm{p}}(\tilde{x}_i)$ according to (4.21), it follows that $\tilde{a}_i \in \mathcal{A}^{\mathrm{p}}(\tilde{x}_i)$. The theorem is then proven by induction over the vehicle index, hereby repetitively applying Lemma 1. □

This result is adapted to the MPC formulation in order to guarantee the safety of the platoon. More precisely, each vehicle, knowing the assumed state trajectory of the vehicle ahead, can compute the safety set for its own predicted state. By taking

into account that the real state of the preceding vehicle is known with a one step delay, the safety set $\mathcal{S}_i$ translates to the following safety constraints on each follower vehicle state:

$$s_i(t_{j+1}|t_k) - \frac{v_i^2(t_{j+1}|t_k)}{2\overline{a}_{\min,i}} \leq \hat{s}_{i-1}(t_{j-1}|t_k) - \frac{\hat{v}_{i-1}^2(t_{j-1}|t_k)}{2\underline{a}_{\min,i}} - l_{i-1}, \tag{4.29a}$$

$$s_i(t_{j+1}|t_k) \leq \hat{s}_{i-1}(t_{j-1}|t_k) - l_{i-1}, \tag{4.29b}$$

for $i = 2, ..., N_v$. Note that the use of the predicted state at one step ahead $x_i(t_{j+1}|t_k)$ is due to the discrete nature of MPC; the use of the assumed trajectory of the preceding vehicle at one step behind $\hat{x}_{i-1}(t_{j-1}|t_k)$ is due to the delay in communication (modeled in the assumed trajectory definition (4.12)). The constraints (4.29a) and (4.29b) correspond to the boundaries of $\mathcal{S}_i$ characterized by g_1 and g_2, respectively, as defined in equation (4.23). The constraints corresponding to g_3 and g_4 have been here omitted since they require the vehicles to drive in the forward direction, which is true by assumption. Note that the constraint (4.29b) is not necessary if the bounds on the minimum braking acceleration of contiguous vehicles satisfies the constraint $\underline{a}_{\min,i-1} \leq \overline{a}_{\min,i}$ (this is the case, for example, when the platooning vehicles have the same maximum braking capability, i.e., $F_{\text{b,min},i} = F_{\text{b,min}}$ for all i). In this case, in fact, the vehicle dynamics (4.17) and the definition of the safety set (4.22)–(4.23) prohibit reaching the boundary characterized by g_2 (see Figure 4.5). Finally we remark that, for safety purpose, only the safety constraints for $j = k$ is necessary. In fact it guarantees that, if at the update time t_k the current state of each follower vehicle is safe, then it is going to be safe also at the update time t_{k+1}. However, the safety constraints for $j > k$ gives optimal trajectories that are safe over the whole horizon and therefore produces a smoother and more fuel-efficient behavior of the platoon. In the MPC formulation, we refer to the safety constraints (4.29a)–(4.29b) as $f_{\text{safe}}(x_i(t_{j+1}|t_k), \hat{x}_{i-1}(t_{j-1}|t_k)) \geq 0$.

4.4.4 Cost function

The objective of the vehicle controller layer is to follow the optimal trajectory and the gap policy requirement provided by the platoon coordinator layer. This can be formulated by introducing the following cost function:

$$
\begin{aligned}
J_i^{\text{MPC}}(x_i(\cdot, t_k), a_i(\cdot, t_k), \varepsilon_i(\cdot, t_k)) = \sum_{j=k}^{k+H_{\text{MPC}}-1} & \|x_i(t_j|t_k) - \hat{x}_{i-1}(t_{j-T_i}|t_k)\|_{\zeta_i Q}^2 \\
& + \|x_i(t_j|t_k) - \bar{x}_i(t_j|t_k)\|_{(1-\zeta_i)Q}^2 \\
& + \|a_i(t_j|t_k) - \bar{a}_i(t_j|t_k)\|_R^2 \\
& + \|\varepsilon_i(t_j|t_k)\|_P^2,
\end{aligned}
$$

where

$$\zeta_i = \begin{cases} 0, & \text{if } i = 1, \\ \bar{\zeta} \in [0, 1], & \text{if } i = 2, ..., N_v, \end{cases} \tag{4.30}$$

T_i represents the discretized version of the time gap τ_i (i.e., $T_i = \lfloor \tau_i/\Delta t_{\mathrm{MPC}} \rfloor$) and the notation $\|\cdot\|_S$ is defined as $\|x\|_S^2 = x^{\mathrm{T}} S x$. In detail, the first two terms penalize the deviation of the predicted state from the delayed assumed state trajectory of the preceding vehicle (in order to track the time gap) and the reference state trajectory, respectively; the parameter $\bar{\zeta}$ is chosen to reach a good trade off between these deviations. The third term penalizes the deviation of the predicted control input from the reference input trajectory. Finally, the forth term penalizes the predicted softening-variable of the constraint (4.15) (i.e., undesired braking). The weight Q, R and P are chosen in order to have a good trade-off between the tracking of the state and input reference trajectories and actuators excitation. In particular, P is chosen relatively large such that only the activation of the safety constraint $f_{\mathrm{safe}}(x_i(t_{j+1}|t_k), \hat{x}_{i-1}(t_{j-1}|t_k)) \geq 0$ can require a significant braking force.

4.4.5   Model predictive control formulation

We now have all the elements to formulate the MPC problem:

$$\underset{a_i(\cdot|t_k), \varepsilon_i(\cdot|t_k)}{\text{minimize}} \quad J_i^{\mathrm{MPC}}(x_i(\cdot|t_k), a_i(\cdot|t_k), \varepsilon_i(\cdot|t_k)) \tag{4.31a}$$

$$\text{subj. to} \quad x_i(t_{j+1}|t_k) = A x_i(t_j|t_k) + B a_i(t_j|t_k), \tag{4.31b}$$

$$a_i(t_j|t_k) \in \mathcal{A}_i(x_i(t_j|t_k), \hat{x}_{i-1}(t_j|t_k)), \tag{4.31c}$$

$$a_i(t_j|t_k) + \varepsilon_i(t_j|t_k) \in \mathcal{A}_{\mathrm{e},i}(x_i(t_j|t_k), \hat{x}_{i-1}(t_j|t_k)), \tag{4.31d}$$

$$v_i(t_j|t_k) \in \mathcal{V}(s_i(t_j|t_k)), \tag{4.31e}$$

$$f_{\mathrm{safe}}(x_i(t_{j+1}|t_k), \hat{x}_{i-1}(t_{j-1}|t_k)) \geq 0, \text{ if } i \geq 2, \tag{4.31f}$$

$$\varepsilon_i(t_j|t_k) \geq 0, \tag{4.31g}$$

$$x_i(t_k|t_k) = x_i(t), \tag{4.31h}$$

for $j = k, ..., k + H_{\mathrm{MPC}} - 1$, where equation (4.31h) represents the initial condition of the MPC problem. For implementation purpose the state-dependent constraint set in (4.31c), (4.31d) and (4.31e) will be replaced by $\mathcal{A}_i(\hat{x}_i(t_j|t_k), \hat{x}_{i-1}(t_j|t_k))$, $\mathcal{A}_{\mathrm{e},i}(\hat{x}_i(t_j|t_k)), \hat{x}_{i-1}(t_j|t_k)$ and $\mathcal{V}(\hat{s}_i(t_j|t_k))$, respectively. Taking into account that the safety constraint (4.31f) is quadratic and convex, the MPC problem can be recasted into a quadratic constraint quadratic programming (QCQP) problem for which efficient solvers exist.

The output of the vehicle controller is the desired acceleration $a_i^*(t_k)$ (defined as $a_i^*(t_k) = a_i^*(t_k|t_k)$, where $a_i^*(\cdot|t_k)$ is the optimal input trajectory resulting from the MPC) and a boolean variable $a_{\mathrm{br},i}$ defined as

$$a_{\mathrm{br},i} = \begin{cases} 1, & \text{if } a_i^*(t_k) < a_{\mathrm{c},i}^*(t_k|t_k), \\ 0, & \text{if } a_i^*(t_k) \geq a_{\mathrm{c},i}^*(t_k|t_k), \end{cases} \tag{4.32}$$

that indicates if the desired acceleration defines a traction or braking force. According to such variable, the acceleration will be either tracked by the braking management system or the engine management system, as presented in Section 3.3.

4.5 Summary

In this chapter we have first analyzed the experimental results of a platoon controlled by feedback control driving over a public highway with highly-varying road grade and in the presence of other traffic. This analysis showed the limitation of such controller in this scenario and motivated the development of a cooperative look-ahead control framework that explicitly takes topography information into account. Due to the complexity of the problem we want to solve and the real-time implementation requirement, we propose a control architecture that splits the cooperative look-ahead control problem into two hierarchical layers, namely the platoon coordinator and the vehicle control layer. The platoon coordinator computes a reference speed trajectory that is feasible and optimal for the whole platoon by taking explicitly topography information into account and communicates it to the vehicle control layer. Due to the typically heterogeneous nature of heavy-duty vehicle platoons, this is not a trivial task. The vehicle control layer distributively tracks the speed trajectory and the time gap requirements, while guaranteeing the safety of the platoon. In this chapter we propose a dynamic programming approach to realize the platoon coordinator and a distributed MPC approach to implement the vehicle control layer.

Experimental evaluation

I n this chapter we evaluate the performance of the two-layer control architecture for heavy-duty vehicle platooning proposed in Chapter 4 by means of simulations based on realistic scenarios. First, the higher layer, namely the platoon coordinator, is evaluated by comparing its performance with existing platooning control strategies. Since the focus of this analysis is the fuel-efficiency, we compare the energy and the fuel consumption of the different control strategies. Second, the lower layer, namely the vehicle control layer, is evaluated simulating the behavior of a three-vehicle platoon for different braking profiles of the leading vehicle. Here, we focus on the role of the safety constraint in the model predictive control formulation of this layer. Lastly, the functioning of the whole control architecture is evaluated, by simulating a three-vehicle platoon driving in the same scenario of the analysis of the motivational experiment of Section 4.1.

The chapter is organized as follows. The two layers of the platoon control architecture introduced in Chapter 4, namely the platoon coordinator and vehicle controller layer, are evaluated in Sections 5.1 and 5.2, respectively. In Section 5.3, we evaluate the functioning of the the integrated architecture. Finally, Section 5.4 summarizes the chapter.

5.1 Performance analysis of the platoon coordinator

In this section we analyze the performance of the platoon coordinator, as presented in Section 4.3 and depicted in Figure 4.3, by focusing on fuel-efficiency. We compare its performance with other standard controller setups. To make the analysis independent from the low-level tracking strategy, we assume in this section that the vehicles follow exactly the speed trajectories and spacing policies defined by the high-level controllers.
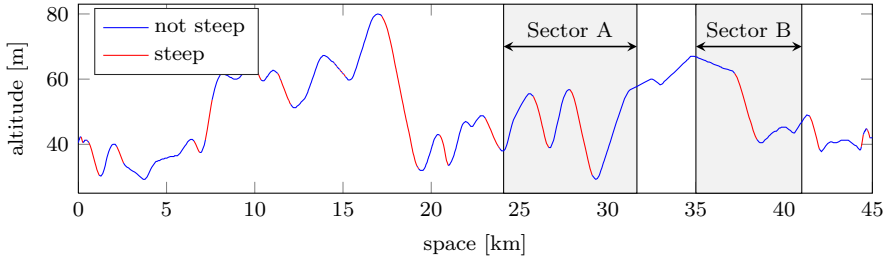
Figure 5.1: Road topography of the 45 km highway stretch between the Swedish cities of Mariefred and Eskilstuna. The red color highlights the uphill and downhill sections where the slope is too large for a heavy-duty vehicle of 40 tons and engine power of 400 hp to maintain a constant speed of 22 m/s without braking or exceeding the engine power limit.

5.1.1 Experiment setup

The comparison is done by using as benchmark the same road scenario introduced in Section 4.1. We therefore consider a platoon of two heavy-duty vehicles driving over the 45 km road stretch between the Swedish cities of Mariefred and Eskilstuna. In Figure 5.1 we repropose the road topography for this road stretch, where the red color highlights the uphill and downhill sections for which the slope is too large for a heavy-duty vehicle of 40 tons and engine power of 400 hp, as used in the simulation, to maintain a constant speed of 22 m/s without exceeding the engine power limit and without braking. Due to the reduced engine power of the vehicles used in the simulation, there are some uphill sections that do not allow the chosen vehicles to maintain the constant reference speed. For the considered road, the steep sections represent 23% of the total length. The controller performance is investigated for both homogeneous and heterogeneous platoons. The performance metrics chosen to compare the different control configurations are the energy and the fuel consumed by the vehicles. In some comparisons the consumed energy is preferred over the consumed fuel because it can be directly related to the energies dissipated by the various forces (i.e., gravitational, rolling, drag and braking forces). The energy consumed by vehicle i is defined as

$$E_i = \sum_{k=0}^{H_{45}-1} \frac{\Delta s_{\mathrm{DP}}}{v_i^{\mathrm{s}}(z_k)} F_{\mathrm{e},i}^{\mathrm{s}}(z_k) v_i^{\mathrm{s}}(z_k) = \Delta s_{\mathrm{DP}} \sum_{k=0}^{k_{45}} F_{\mathrm{e},i}^{\mathrm{s}}(z_k), \qquad (5.1)$$

where H_{45} denotes the number of spacial steps in 45 km. According to the definitions in Chapter 4, $F_{\mathrm{e},i}^{\mathrm{s}}$ and v_i^{s} denote the traction force and speed, respectively, defined in the spatial domain. Δs_{DP} represents the spatial length of the discretization. The consumed fuel instead is defined as

$$\Psi_i = \sum_{k=0}^{H_{45}-1} \left(p_{1,i} F_{\mathrm{e},i}^{\mathrm{s}}(z_k) v_i^{\mathrm{s}}(z_k) + p_{0,i} \right) \frac{\Delta s_{\mathrm{DP}}}{v_i^{\mathrm{s}}(z_k)}. \qquad (5.2)$$

Here, we recall that $p_{1,i}$ and $p_{0,i}$ are parameters characterizing the fuel model of vehicle i as presented in Section 3.2.

The control configurations considered in the comparisons include three control strategies and three gap policies. In detail, the following control strategies are considered:

- cruise control (CC): the first vehicle keeps the constant reference speed v_{CC} on low-grade slopes. If the uphill slope is too large to maintain constant speed, the engine generates the maximum power $P_{\max}$ until the speed reaches v_{CC} again. If the downhill slope is too large to maintain constant speed without braking, the engine coasts (i.e., does not inject any fuel, generating therefore the minimum power $P_{\min}$) until the speed reaches v_{CC} again. However, if the vehicle reaches the speed limit $v_{\max}$, the brakes are activated in order not to overcome it;

- look-ahead control (LAC): the first vehicle exploits the slope information of the road ahead in order to minimize its own fuel consumption.

- cooperative look-ahead control (CLAC): the first vehicle follows the speed profile generated by the platoon coordinator proposed in Chapter 4.

The following gap policies are considered:

- space-gap policy: the second vehicle keeps a constant distance d_{SG} from the first vehicle;

- headway-gap policy: the second vehicle keeps a constant headway time τ_{HG} from the first vehicle, i.e., it keeps a distance proportional to its speed ($d_{\mathrm{HG}}(t) = \tau_{\mathrm{HG}} v_i(t)$);

- time-gap policy: the second vehicle keeps a constant time gap τ_{TG} from the first vehicle according to (4.1).

In order to be able to maintain exactly the desired gap policies as previously assumed, the second vehicle is allowed to overcome the theoretical maximum engine power $P_{\max,i}$ and to brake if necessary. In addition, in order to obtain a fair comparison it is ensured, by tuning the trade-off parameter β of the LAC and CLAC formulations (see definition (4.30)), that the different control strategies have the same average speed $\bar{v}$ and the parameters d_{SG}, τ_{HG} and τ_{TG} are chosen such that the vehicles in the different gap policies have the same distance when driving at constant speed $\bar{v}$ (i.e., $d_{\mathrm{SG}} = \bar{v}\tau_{\mathrm{HG}} = \bar{v}\tau_{\mathrm{TG}} - l_1$). Furthermore, in order to remove the influence of the residual kinematic energy, the initial and final speeds are constrained to be the same in all the controller configurations.

Table 5.1: Vehicle parameters.

Parameter	Value
mass (m_i)	40 t
length (l_i)	18 m
rolling resistance coefficient (c_r)	3×10^{-3}
vehicle cross-sectional area (A_v)	$10\,\mathrm{m}^2$
maximum engine power ($P_{\max,i}$)	298 kW (400 hp)
minimum engine power ($P_{\min,i}$)	−9 kW

5.1.2   Fuel-efficiency analysis for different control strategies

In this section we present the results of the platoon behavior for the three different control strategies, while keeping a time-gap policy (with τ_{TG} = 1.4 s). In the first part, as in the motivational experiment of Section 4.1, we focus on the homogeneous platoon scenario, while in the second part we consider two heterogeneous platoons (i.e., platoons where the second vehicle is respectively heavier and lighter than the leading one).

We now consider a platoon of two identical vehicles, whose parameters values are displayed in Table 5.1. We start the comparison by analyzing the comprehensive bar diagram displayed in Figure 5.2 representing the energy consumed by each vehicle of the platoon for the three control strategies (the corresponding fuel consumption is displayed in the middle column of Table 5.2). This energy is normalized with respect to the energy consumed by a single vehicle driving alone using CC. The consumed energy is additionally split into various components representing the energy dissipated by each force, namely the gravitational, rolling, drag and braking forces. We can first notice how the second vehicle, for all the control strategies, consumes less energy compared to the first one, due to the significant reduction of the energy associated to the drag force. Second, comparing the three control strategies, we can observe how the use of the LAC allows both vehicles to save energy, respectively 3.5% and 6.4% compared to the use of the CC. Instead, by switching from the LAC to the CLAC, the first vehicle consumes 0.1% more energy, while the second one saves 3.7% of energy; therefore the platoon, given by the union of the two vehicles, saves 3.6% of energy. This result is in line with our expectation, since the LAC optimizes the fuel consumption of the first vehicle, while the CLAC targets the reduction of the fuel consumption of the entire platoon. Consequently, the savings of the CLAC strategy with respect to the LAC strategy are expected to increase for platoons of more than two vehicles. Going into the details of the various consumed energy components, first we notice that the gravitational and rolling energy components are the same for both vehicles for all the considered control strategies. This is due to the fact that the energy associated to the gravitational force depends only on the difference of altitude between the initial and final points,
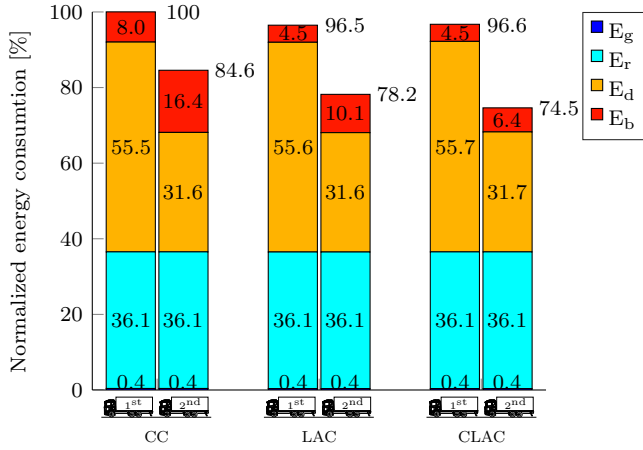
Figure 5.2: Comparison of the energy consumed by each vehicle of a platoon ($m_1 = m_2 = 40$ t), for the three control strategies, namely CC, LAC and CLAC, while keeping a time-gap policy and driving over the 45 km road displayed in Figure 5.1. Each bar represents the consumed energy normalized respect to the the energy consumed by a single vehicle driving alone using CC. The consumed energy is split into various components representing the energy dissipated by each force, namely the gravitational (E_g), rolling (E_r), drag (E_d) and braking (E_b) force.

while the rolling energy only depends on the driven distance, that is the same by experiment design specification. The drag energy, instead, is significantly different for the two vehicles because of its dependence on the distance to the preceding vehicle, while it is approximately the same for the different control strategies. What significantly changes between the different control strategies is the energy dissipated by braking, denoted by E_b in Figure 5.2.

In order to understand the role of the control strategies in the use of brakes in Figure 5.3 we show part of the simulation results corresponding to the road highlighted as segment B in Figure 5.1. In this study we have chosen to focus on a downhill section because this is where the braking action is taking place. The comparison of the platoon behaviors follows:

- CC: during the downhill, starting from speed v_{CC}, the first vehicle accelerates while coasting due to the large road grade. In the meantime the second vehicle has to brake slightly in order to maintain the time gap and compensate the reduced drag force compared to the first vehicle. At 38.1 km, in order not to overcome the speed limit, both vehicles need to brake significantly;

- LAC: by exploiting the topography information of the road ahead, the first vehicle reduces its speed before the downhill by anticipating the coasting phase such that the speed limit is reached only when the slope grade is small enough to stop accelerating while coasting and therefore it avoids braking.

The second vehicle, as in the CC case, has to brake slightly while the first vehicle is coasting but it also avoids the significant braking phase at the end of the downhill;

- CLAC: since in this case the optimization is done considering the fuel consumption of both vehicles, with respect to the LAC case the first vehicle starts to loose speed earlier before the downhill. This allows it to sightly throttle during the downhill, allowing the second vehicle to coast meanwhile and, as in the LAC case, to reach the speed limit only when the slope grade is small enough to stop accelerating while coasting. In this case both vehicles do not need to brake.

Note that, in the case of longer downhill segments, the lower speed bound does not allow the vehicle to decrease the speed enough before the downhill in order not to hit the upper speed limit during the downhill. This is why in some sections of the 45 km benchmark road, in the LAC case, the first vehicle and, in the CLAC case, both vehicles still need to brake.

So far we have considered the case of a homogeneous platoon. What we want to investigate now is the the role of the different control strategies in the case of heterogeneous platoons. To answer this question, in Table 5.2 we have reported the normalized fuel consumption for the cases of two heterogeneous platoons and the same homogeneous platoon previously considered. More in detail, the vehicles have the same powertrain, but their masses vary between 35, 40 and 45 t. Analyzing the table we can notice how in the case of a heavier second vehicle the CLAC allows to save 10.8% of fuel compared to the CC, while, in the case of a lighter second vehicle, it allows to save 5.4%. However if we only analyze the last row we can note how, with the use of the CLAC, the order of the vehicles does not significantly change the normalized fuel consumption. Note that this is not the case in the LAC strategy.

Concluding, the proposed controller (CLAC) has a significant impact on the reduction of the energy and fuel consumption. In detail, the majority of the fuel saving is related to the reduction of energy dissipated by braking during the downhill sections. The impact of such a controller grows in the case of a heavier follower vehicle.

5.1.3   Fuel-efficiency analysis for different gap policies

In the previous analysis we have always considered a time-gap policy. The aim of this section is to compare the platoon performance for different gap policies, namely the space-, headway- and time-gap policies, while keeping the same control strategy (in the analysis we have chosen CC). Note that in order to be able to follow the required gap policy the second vehicle is allowed to exceed the maximum engine power. In this section we only focus on the homogeneous platoon, since the results for a heterogeneous platoon are qualitatively the same. In Figure 5.4 we show the comprehensive bar diagram representing the normalized energy consumed by each vehicle in the platoon for the three gap policies, while using CC as control strategy.
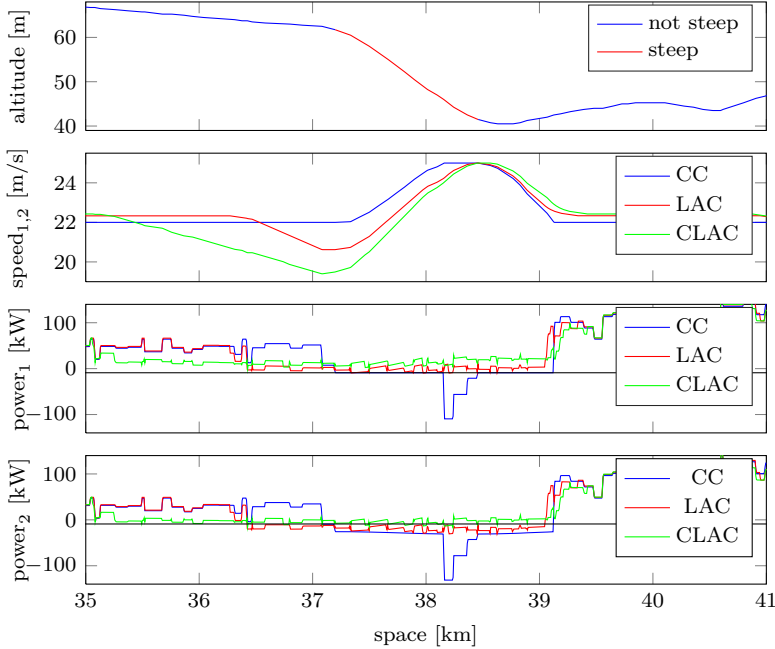
Figure 5.3: Comparison of the behavior of a homogeneous platoon (i.e., $m_1 = m_2 = 40$ t) for three different control strategies, namely CC, LAC and CLAC, while keeping a time-gap policy and driving over the Sector B displayed in Figure 5.1. The first plot shows the road altitude; the second plot shows the speed profiles for the three control strategies followed by both vehicles (because of the time-gap policy, the platooning vehicles follow the same speed profile in the spacial domain); finally the third and forth plots show the summation between the generated power by the engine and the braking systems for the two vehicles and three control strategies; the black lines in such plots define the theoretical minimum and maximum engine power, respectively $P_{\min,i}$ and $P_{\max,i}$ (hence if the power crosses the lower power limit $P_{\min,i}$, the corresponding vehicle is braking).

Table 5.2: Normalized fuel consumption (in %) of the vehicles in the platoon for different control strategies and scenarios (vehicle weights). The fuel is normalized respect to the fuel consumed by the corresponding vehicle driving alone using CC.

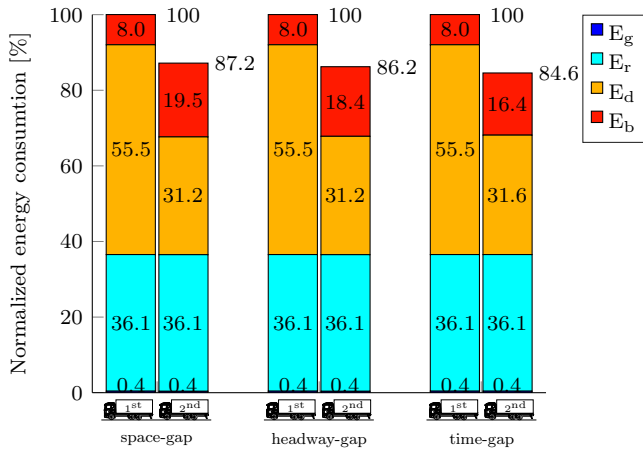|	1st	2nd	1st	2nd	1st	2nd
mass	35 t	45 t	40 t	40 t	45 t	35 t
CC	100.0	90.2	100.0	86.3	100.0	82.1
LAC	97.6	84.9	96.9	80.6	96.3	77.2
CLAC	97.8	78.0	97.0	77.4	96.4	76.7

Figure 5.4: Comparison of the energy consumed by each vehicle of a homogeneous platoon (i.e., $m_1 = m_2 = 40$ t) for three different gap policies, namely space-, headway- and time-gap policies, while using CC as control strategy and driving over the 45 km road displayed in Figure 5.1. For the plots explanation refer to the caption of Figure 5.2.
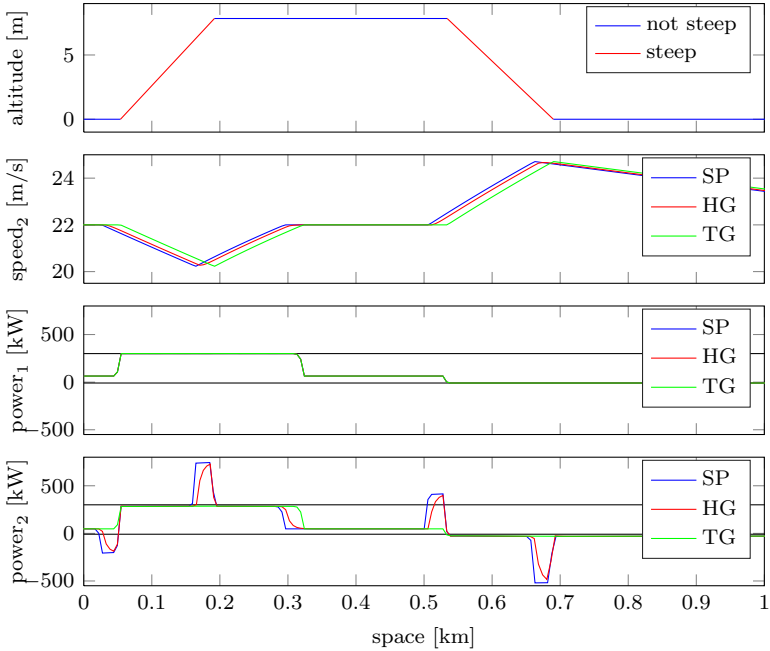
Figure 5.5: Comparison of the behavior of a homogeneous platoon (i.e., $m_1 = m_2 = 40$ t) for three different gap policies, namely space-, headway- and time-gap policies, while using CC as control strategy and driving over a synthetic hill. For the plots explanation refer to the caption of Figure 5.3; note that the second plot shows only the speed trajectories of the second vehicle (the speed trajectory of the first vehicle coincides with that one of the second vehicle in the case of time-gap policy).

Since the first vehicle uses the same control strategy, the energy consumption differs only for the second vehicle. It is interesting to notice that, similar to the comparisons done in the previous section, the main difference between the energy consumption of the second vehicle is related to the energy dissipated by braking. More in detail the headway-gap policy allows the second vehicle to save 1% over the space-gap policy, while the time-gap policy allows to save an additional 1.6% of energy. In order to understand the role of the gap policy on the braking energy, we show the platoon behavior driving over a synthetic hill composed by an uphill section with constant slope grade, a flat section and a downhill section with constant slope grade. The platoon behavior for such a hill is shown in Figure 5.5. Analyzing the second vehicle behavior for each gap policy, the following can be observed:

- time-gap policy: as argued in Section 4.3, the time gap allows the vehicles to follow the same speed profile over space. That means that the generated forces and therefore the generated powers (because of the equal speed result) are equivalent except for a reduction of the air drag component in the second

Table 5.3: Normalized fuel consumption (in %) of the vehicles in the platoon for different control strategies and gap policies. The fuel is normalized respect to the fuel consumed by the corresponding vehicle driving alone using CC.

	space-gap		headway-gap		time-gap	
	1st	2nd	1st	2nd	1st	2nd
CC	100.0	88.6	100.0	87.7	100.0	86.3
LAC	96.9	82.7	96.9	81.9	96.9	80.6
CLAC	97.0	80.4	97.0	79.3	97.0	77.4

vehicle. Therefore the power generated by the second vehicle, as can be observed in Figure 5.5, is approximately a biased equivalent of that one generated by the first vehicle. As a result, the second vehicle complies with the limitation on maximum engine power.

- space-gap policy: the space gap requires the vehicles to follow the same speed profile over time. An interesting consequence can be observed, for example, at the beginning of the uphill section shown in Figure 5.5; as soon as the first vehicle enters the uphill section and decelerates because of limited engine power, the second vehicle, which is still in the flat section, has to brake in order to respect the space gap requirement. In general, excluding the offset given by the drag power, every time the slope increases (in Figure 5.5, entering the uphill and leaving the downhill sections), the second vehicle has to generate less power than the first vehicle, while every time the slope decreases (in Figure 5.5, leaving the uphill and entering the downhill sections) the second vehicle has to generate more power than the first vehicle. As a consequence, the second vehicle has respectively to brake and to exceed the power limit in order to follow the required space-gap policy.

- headway-gap policy: the headway gap can be considered as a trade-off between a time gap and a space gap. In fact, for example, as soon as the first vehicle enters the uphill section and starts to decelerate, the distance between the two vehicles is allowed to decrease, but this decrease is not as fast as in the case of the time gap.

The results obtained by the analysis of the platoon behavior in the case of the synthetic hill are valid also in the case of the original scenario. In conclusion, the time gap allows to save more energy compared to the space and headway gaps. In addition the time gap allows all the vehicles to follow the same speed trajectory in space and, therefore, it scales well with the number of vehicles in the platoon. This is not the case when using a space- or headway-gap policy. The complete results for the normalized fuel consumption are reported in Table 5.3.
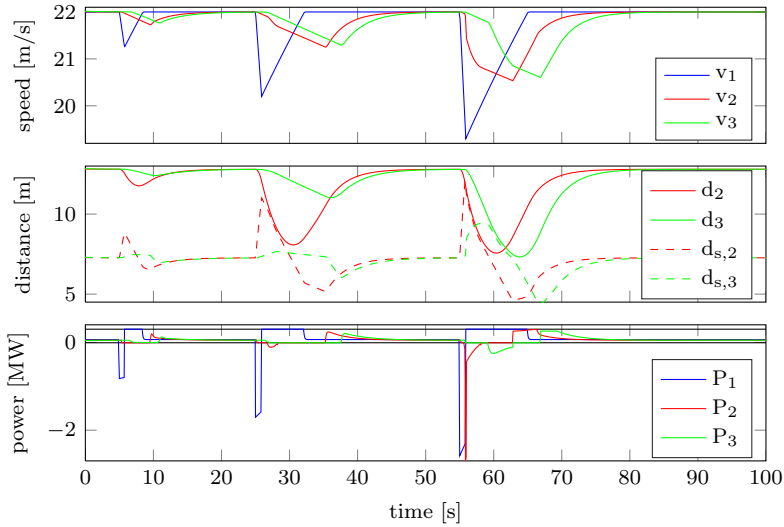
Figure 5.6: Behavior of a three identical vehicles platoon driving on a flat road. The leading vehicle brakes three times at 5, 25 and 55 s, with a braking deceleration of respectively 1, 2 and 3 m/s^2 for 0.9 s. The first plot shows the speed of the three vehicles: the second plot shows the distance between the vehicles and the corresponding safety distance computed using an adaptation of inequality (4.29); the third plot shows the summation between the generated power by the engine and the braking systems of the vehicles.

5.2   Performance analysis of the vehicle control layer

In this section we analyze the performance of the vehicle controller layer (as presented in Section 4.4 and shown in Figures 4.3 and 4.4) by focusing on the safety aspect. The analysis is based on the simulation result displayed in Figure 5.6 and Figure 5.7, where the leading vehicle of a three-vehicle platoon driving on a flat road brakes repeatedly with different braking profiles. Here we assume that the leading vehicle is manually driven in the braking phases and, therefore, the control system does not have a priori knowledge about the braking profile. The considered vehicles are identical with parameters' values defined in Table 5.1. The parameter of the MPC formulation are displayed in the second half of Table 5.4.

5.2.1   Safety analysis

Here, we focus on the safety analysis of the distributed vehicle controller layer and, in particular, we analyze the role of the safety constraint in the MPC formulation, for various situations. In Figure 5.6, the leading vehicle is braking with a deceleration of 1, 2 and 3 m/s^2 for 0.9 s at the time instances 5, 25 and 55 s, respectively. In the second plot of this figure, the effective distances and the ones that would activate the
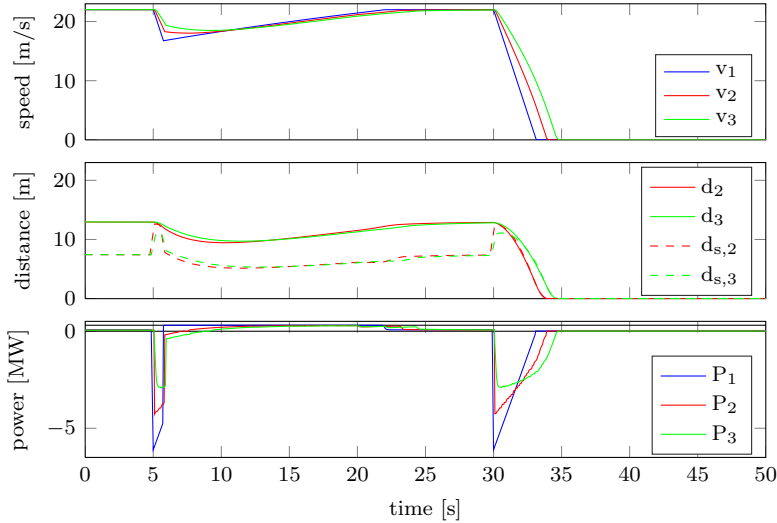
Figure 5.7: Behavior of a three identical vehicles platoon driving on a flat road. The leading vehicle brakes a first time at 5 s for 1 s with a deceleration of 7 m/s^2 and a second time at 25 s with a deceleration of 7 m/s^2 until arriving to full-stop. For the plot explanation refer to the caption of Figure 5.6.

safety constraint (we will refer to it as the safety distance) are shown. First we can notice how, in line with our expectation, the second and third vehicle are braking (see the third plot) only when the effective distance touches the safety distance. In fact here we recall that, according to how the vehicle controller is designed (see Section 4.4.5), only the activation of the safety constraint or a braking request from the platoon coordinator can lead to a significant braking action. Consequently, during the first braking instance of 1 m/s^2, both follower vehicles do not brake, despite the deviation of their states from the reference trajectories. During the second braking of 2 m/s^2, instead, the safety constraint of the second vehicle is activated and therefore it requires a braking action. Finally, during the third braking of 3 m/s^2, the safety constraints of both follower vehicles activate and therefore they both brake. Note that the safety constraint is designed such that fuel-efficiency has priority on driver comfort. In fact, in this case, in order to be fuel-efficient, the braking action is required only when the platoon is in a safety critical situation. However, a priori knowledge of the braking profile of the first vehicle (e.g. by having a model of the driver or handling the braking action autonomously) would have allowed to have a smoother and less intense braking action.

In Figure 5.7, we consider a more challenging scenario in which the first vehicle brakes with higher intensity, simulating an emergency situation. More precisely, it brakes at 5 s with a deceleration of 7 m/s^2 for 1 s and at 30 s with the same deceleration until it arrives to full-stop. We can notice how, also in this scenario,

Table 5.4: Controller parameters.

	Parameter	Value
	Δs_{DP}	6 m
Platoon coordinator	f_{DP}	0.25 Hz
	S_{DP}	$2\,\mathrm{km}$
	Δt_{MPC}	50 ms
Vehicle control	f_{MPC}	20 Hz
	T_{MPC}	8 s

the safety constraint in each vehicle controller activates the braking action and guarantees that no collision occurs between the vehicles.

5.3 Performance analysis of the integrated system

In this section we analyze the simulation results displayed in Figure 5.8 of the platoon under the control of the integrated control architecture, i.e., including both the platoon coordinator and vehicle controller. More precisely, in this analysis we consider a platoon of three identical vehicles (whose parameters are defined in Table 5.1) driving over the Sector A highlighted in Figure 5.1. This is the same sector for which the experimental results in Alam et al. (2015a) are displayed in Figure 4.2 and analyzed in Section 4.1. The controller parameters are depicted in Table 5.4.

At first glance, as expected from the platoon coordinator formulation, we can notice how all the vehicles follow the same speed and distance profiles in the spacial domain. Additionally, in order to follow such profiles, we can observe in the last plot how the second and third vehicle, thanks to the air drag reduction, need to generate less power than the leading vehicle. We now continue the analysis by focusing on the three critical segments highlighted in Figure 5.8:

Segment 1: due to the steep downhill, all vehicles are not able to maintain the constant speed without braking and, therefore, they accelerate. However, the platoon coordinator requires the leading vehicle to throttle slightly such that the follower vehicles can coast. In this case, the coordination role of the platoon coordinator allows to avoid braking action to all vehicles, hereby ensuring a lower overall fuel consumption.

Segment 2: Since no gear shift is taken into account the vehicles are able to maintain the time gap requirement during the uphill. At the end of this section we will show another simulation of the same scenario, where the gear shift is simulated as a drop of engine power for one second.
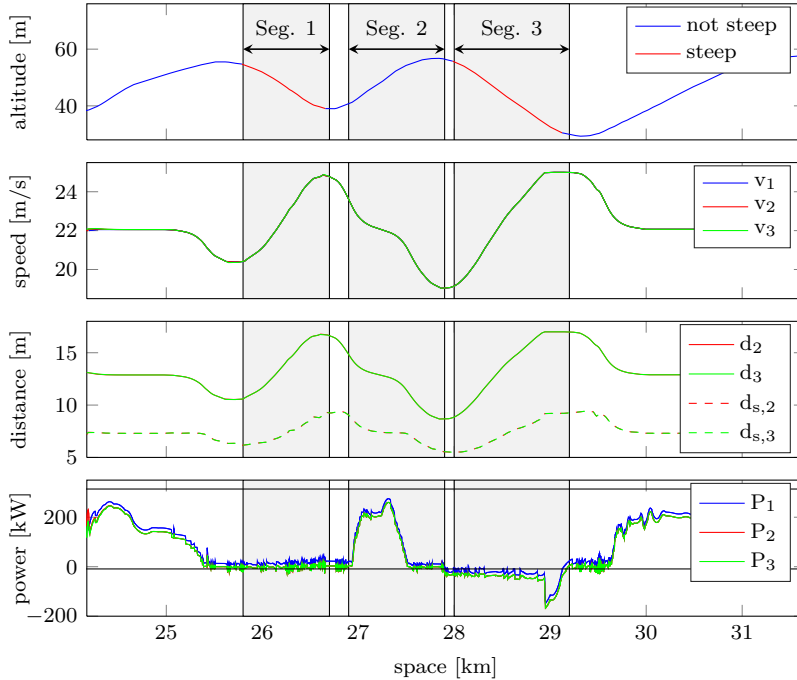
Figure 5.8: Simulation results obtained using the proposed controller for a three-vehicle platoon while driving over the Sector A highlighted in Figure 5.1. The three vehicles are identical with parameters shown in Table 5.1. The first plot shows the road topography. For the explanation of the other plots refer to the caption of Figure 5.6.

Segment 3: due to the longer length of the downhill section compared to the that one of Segment 1, the platoon exhibits a different behavior. First, the platoon coordinator requires all vehicles to decrease the speed to the minimum allowed (in this simulation it is set to 19 m/s) in order to hit the maximum speed limit as late as possible. Second, since the speed limit is reached despite the decrease of speed at the beginning of the downhill, the platoon coordinator requires the first vehicle to coast and the follower vehicles to brake slightly to maximize the efficiency. In fact, in this case, to require the first vehicle to slightly throttle in the first part of the downhill section and brake at its end would be contradictory.

Overall, the platoon shows a fuel-efficient and smooth behavior. We now analyze how the platoon controller behaves in the case of a disturbance acting on one of the vehicles. Here, we consider the same scenario as just analyzed. The disturbance is defined as a drop of the engine power of the second vehicle to 0 kW for 1 s at space 27.22 km, simulating the effect of a gear shift. The behavior of the platoon is displayed in Figure 5.9. The second vehicle, in order to react to the deviation of the
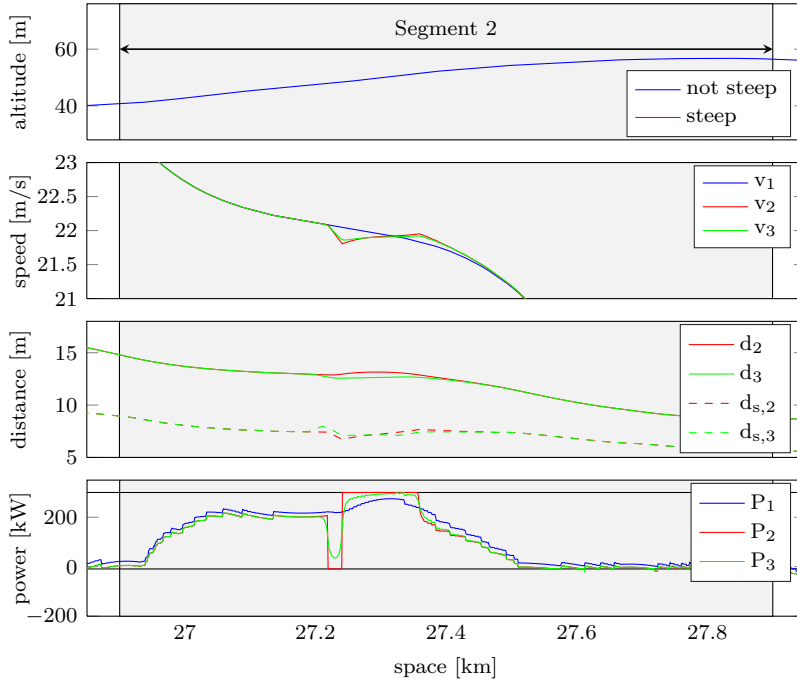
Figure 5.9: Simulation of a similar scenario considered in Figure 5.8, where, instead, a disturbance acts on the input of the second vehicle. In detail, the disturbance is defined as a drop of the engine power to 0 kW for 1 s at space 27.22 km. The figure shows a portion of the simulation corresponding to Segment 2. For the explanation of the plots refer to the caption of Figure 5.8.

state from the reference and the opening of the time gap due to the disturbance, generates the maximum power for 120 m. Thanks to the prediction of the state, the controller stops the full-throttle before reaching the time gap requirement. This gives the time to the second vehicle to reduce its speed while closing the gap. The speed reduction of the second vehicle during the engine power drop is not safety critical as it can be notice in the distance plot of Figure 5.9 (i.e., the distance between the second and third vehicles d_3 does not reach the safety distance $d_{s,3}$). The third vehicle, therefore, by fulfilling the time gap requirement, tracks the delayed trajectory of the second vehicle and starts to reduce its throttling at the same position where the disturbance hit the second vehicle. If the disturbance would have been more intense, the safety constraint could have required the third vehicle to reduce the throttle earlier. In conclusion, the proposed controller exhibited a smooth behavior also in the case of a disturbance acting on the platoon.

5.4   Summary

The performance of the controller proposed in Chapter 4 has been studied.

First, the platoon coordinator has been evaluated by comparing its performance to other standard control strategies, namely CC and LAC. By exploiting the topography information of the road ahead and coordinating the vehicles' acceleration the platoon coordinator avoids unnecessary braking and therefore guarantees a higher level of fuel-efficiency compared to the CC and LAC. The fuel saving becomes more significant in the case the follower vehicle is heavier than the leading one. Furthermore it has been shown how a time-gap policy is superior from a fuel-efficiency point of view compared to headway- and space-gap policies.

Second, the vehicle control layer has been evaluated in two different scenarios. The first one simulates a traffic scenario where the leading vehicle needs to adapt its speed to follow the traffic flow. The vehicle control layer, thanks to a soft constraint, prioritizes the non-use of braking over the time gap and speed tracking, while ensuring safety. In this way, the vehicle control layer is able to handle limited decelerations of the leading vehicle without braking, while it requires braking only when needed. This can be observed in the simulation of the second scenario, where the leading vehicle, by strongly braking, decelerates until reaching full-stop. In this case the follower vehicles brake in order to maintain the vehicles' state in a safety set and also reach full-stop without collision.

Lastly, we evaluate the performance of the integrated control architecture by simulating the same hilly road sector of the experimental test analysis of Section 4.1. The proposed CLAC shows a good behavior in the three critical segments highlighted in the experimental test analysis.

Model predictive control for obstacle avoidance

This chapter presents a novel control framework for lane keeping and obstacle avoidance for a passenger car that combines actions on braking and steering. The controller has been structured such that the nonlinear vehicle dynamics can be robustly controlled by linear model predictive control (MPC) and therefore enable fast and bounded computation. The proposed control design decouples the longitudinal and lateral dynamics into two successive stages. First, plausible braking and throttle profiles are defined over the prediction horizon. Then, based on these profiles, linear time-varying (LTV) models of the vehicle lateral dynamics are derived and used to formulate the associated linear MPC problems. The solutions of the optimization problems are used to determine for every time step, the optimal braking or throttle command and the corresponding steering angle command.

The chapter is organized as follows: Section 6.1 gives the motivation to the problem and provides an overview of related works. Section 6.2 presents the vehicle model used in the control formulation and shows how it can be simplified to obtain an LTV model of the vehicle lateral dynamics. In Section 6.3, we explain how the objectives of lane keeping and obstacle avoidance are formulated as convex constraints on the vehicle's states and inputs. Section 6.4, presents the MPC-based control framework that decouples the longitudinal and lateral dynamics of the vehicle. The effectiveness of the proposed controller is tested in Section 6.5 through hardware-in-the-loop simulations and experiments on a real passenger vehicle. Finally, Section 6.6 summarizes the chapter.

6.1 Introduction

Over the last two decades, the increased presence of electronics and software in vehicles has allowed the introduction of several active safety systems, e.g., anti-lock braking system, electronic stability control and adaptive cruise control. Nevertheless, the number of fatal road traffic incidents due to driver distraction and speeding

is still high (Subramanian, 2012). Recent advances in sensing technologies and 3D environment reconstruction (Bertozzi et al., 2000; Pollefeys et al., 2007; Ferrari et al., 1990) have opened up new possibilities and have provided the basis for the design of advanced autonomous and semi-autonomous guidance systems.

Because of its capability of systematically handling nonlinear time-varying models and constraints, and operating close to the limits of admissible states and inputs, MPC has been widely used to address the autonomous vehicle guidance problem (Anderson et al., 2010; Falcone et al., 2007, 2008; Gao et al., 2010, 2012; Gray et al., 2012). In Anderson et al. (2010), the MPC problem has been formulated as a quadratic program (QP) by limiting the intervention to the steering, and linearizing the vehicle dynamics around a constant vehicle speed and small slip angles. In Gao et al. (2010), Gao et al. (2012) and Gray et al. (2012), the problem of integrated braking and steering control by using a hierarchical control architecture is addressed. A high-level controller generates an obstacle-free trajectory, while a low-level controller tracks this planned trajectory. In order to combine braking and steering, both levels implement a nonlinear MPC formulation which requires the online solution of a non-convex optimization problem. To reduce the real-time computational complexity, Gao et al. (2012) have proposed the use of a spatial vehicle model which simplifies the problem. However, the nonlinear nature of the model used in the MPC problem significantly limits the maximum prediction horizon implementable.

In this chapter we propose a linear MPC-based control architecture suitable for vehicles driving in low curvature roads, such as highways. It addresses the lane-keeping and obstacle avoidance problems by combining steering and braking actions. In particular, the chapter presents two main contributions: first, we derive an LTV model of the vehicle lateral dynamics, as a function of the longitudinal braking or throttle profile; second, we use this model to formulate a linear MPC problem for lane-keeping and obstacle avoidance, accounting for both the longitudinal and lateral dynamics. The linearity of the model allows to recast the MPC problem as a set of convex QPs and, hence, to reduce the overall computational complexity.

6.2 Vehicle model

In this section, we present a modified version of the bicycle model of the vehicle (Falcone et al., 2007) and the corresponding simplified LTV model of the lateral dynamics used in the MPC formulation.

6.2.1 The extended bicycle model

Here we use a modified version of the classical bicycle model, that also accounts for the longitudinal and lateral load transfers while computing the forces acting on the tires. Therefore, this extended bicycle model can be considered as a trade-off between the classical bicycle model and the four wheel vehicle model (Margolis and Asgari, 1991).
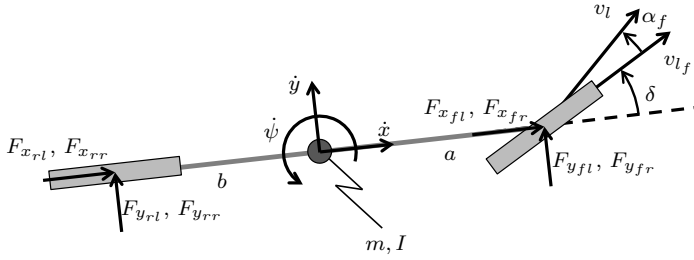
Figure 6.1: Illustration of the bicycle model.

Bicycle model equations

The notation used in the vehicle model is shown in Figure 6.1. The vehicle dynamics are described by the following set of differential equations:

$$m\ddot{x} = F_{x_{fl}} + F_{x_{fr}} + F_{x_{rl}} + F_{x_{rr}} - k_d\dot{x}^2, \tag{6.1a}$$

$$m\ddot{y} = -m\dot{x}\dot{\psi} + F_{y_{fl}} + F_{y_{fr}} + F_{y_{rl}} + F_{y_{rr}}, \tag{6.1b}$$

$$I\ddot{\psi} = a(F_{y_{fl}} + F_{y_{fr}}) - b(F_{y_{rl}} + F_{y_{rr}}), \tag{6.1c}$$

where $\dot{x}$ and $\dot{y}$ denote the longitudinal and the lateral speed of the vehicle, and $\dot{\psi}$ denotes the yaw rate. The constants m and I denote the vehicle's mass and rotational inertia about the yaw axis, respectively, and a and b denote the distances from the center of gravity (CoG) to the front and rear axles, respectively. In Equation (6.1a), $-k_d\dot{x}^2$ represents the aerodynamic longitudinal force with $k_d = \frac{1}{2}\rho C_d A_v$, where ρ is the air density, C_d is the aerodynamic drag coefficient and A_v is the vehicle frontal cross section. $F_{x_{*\bullet}}$ and $F_{y_{*\bullet}}$ (where $* = f, r, \bullet = l, r$) are the tire forces acting along the vehicle longitudinal and lateral axes relative to each wheel. These forces are related to the forces $f_{x_{*\bullet}}$ and $f_{y_{*\bullet}}$ acting along the wheel longitudinal and lateral axes, respectively, through an equality for the rear wheels,

$$F_{x_{r\bullet}} = f_{x_{r\bullet}}, \quad F_{y_{r\bullet}} = f_{y_{r\bullet}},$$

and a rotation depending on the steering angle δ for the front wheels,

$$\begin{aligned} F_{x_{f\bullet}} &= f_{x_{f\bullet}}\cos(\delta) - f_{y_{f\bullet}}\sin(\delta), \\ F_{y_{f\bullet}} &= f_{x_{f\bullet}}\sin(\delta) + f_{y_{f\bullet}}\cos(\delta). \end{aligned} \tag{6.2}$$

Tire forces

In connection to the computation of the longitudinal and lateral load transfers, we introduce the following assumption.

Assumption 1. In the load transfer computation, the effect of the aerodynamic forces acting on the vehicle is negligible.
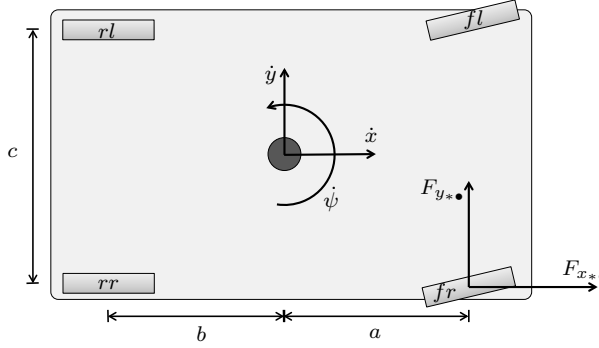
Figure 6.2: Sketch of the vehicle and modeling notation for the computation of the longitudinal and lateral load transfers.

Considering the sketch in Figure 6.2, we can derive the forces acting along the vehicle vertical axis of each wheel $F_{z_{*\bullet}}$ due to the load transfer as,

$$
\begin{aligned}
F_{z_{fl}} &= \frac{bF_z - eF_x}{2(a+b)} - \frac{eF_y}{2c}, & F_{z_{fr}} &= \frac{bF_z - eF_x}{2(a+b)} + \frac{eF_y}{2c}, \\
F_{z_{rl}} &= \frac{aF_z + eF_x}{2(a+b)} - \frac{eF_y}{2c}, & F_{z_{rr}} &= \frac{aF_z + eF_x}{2(a+b)} + \frac{eF_y}{2c}.
\end{aligned}
\tag{6.3}
$$

where $F_x = \sum_{*=f,r;\bullet=l,r} F_{x_{*\bullet}}$, $F_y = \sum_{*=f,r;\bullet=l,r} F_{y_{*\bullet}}$ and $F_z = mg$ are the cumulative forces acting on the wheels along the longitudinal, lateral and vertical vehicle axes, respectively; the constants c and e denote respectively the vehicle width and the height of the CoG and g is the gravitational acceleration.

The second input of the model is the braking ratio, denoted as β, with $\beta = -1$ corresponding to maximum braking and $\beta = 1$ corresponding to maximum throttle. We introduce the following assumptions regarding the longitudinal forces:

Assumption 2. The rotational inertia of the wheels is negligible. The torque $T_{x_{*\bullet}}$ about the wheel's axis produces a longitudinal force $f_{x_{*\bullet}} = T_{x_{*\bullet}}/r$, where r is the wheel's radius.

Assumption 3. The low-level controller of the longitudinal dynamics distributes the forces as

$$
f_{x_{*\bullet}} = F_{z_{*\bullet}}\mu\beta,
\tag{6.4}
$$

where μ denotes the friction coefficient between the tire and the road surface.

Note that $F_{z_{*\bullet}}$ and, consequently $f_{x_{*\bullet}}$, depend on F_x and F_y. The force component $f_{y_{*\bullet}}$ can be computed using a simplified version of the semi-empirical Pacejka formula (Pacejka, 2005) as

$$
f_{y_{*\bullet}} = \sqrt{(\mu F_{z_{*\bullet}})^2 - f_{x_{*\bullet}}^2}\sin(C\arctan(B\alpha_*)),
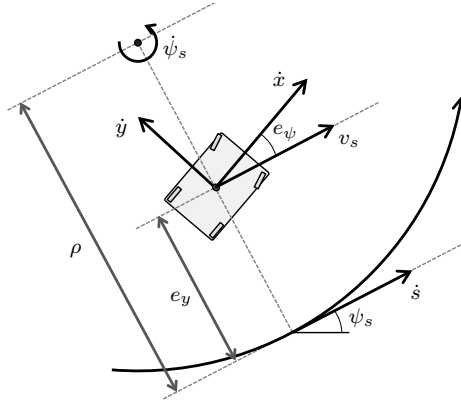\tag{6.5}
$$

Figure 6.3: The curvilinear coordinate system. The dynamics are derived about a curve defining the centerline of a track. The coordinate s defines the arc-length along the track.

where C and B are tire parameters calibrated using experimental data. The variable α_* denotes the slip angles of the front and rear wheels, which can be computed as

$$\alpha_f = \frac{\dot{y} + a\dot{\psi}}{\dot{x}} - \delta, \quad \alpha_r = \frac{\dot{y} - b\dot{\psi}}{\dot{x}}. \tag{6.6}$$

Substituting (6.4) in the expression of $f_{y_{*\bullet}}$, we obtain an alternate representation of the lateral forces which emphasizes the linear relationship between $f_{y_{*\bullet}}$ and $F_{z_{*\bullet}}$:

$$f_{y_{*\bullet}} = \mu F_{z_{*\bullet}} \sqrt{1 - \beta^2} \sin(C \arctan(B\alpha_*)). \tag{6.7}$$

As we will show in the Section 6.2.2, this linear relationship allows to decouple the longitudinal dynamics from the lateral dynamics.

Road curvilinear coordinate system

Figure 6.3 shows the curvilinear coordinate system describing the interaction between the vehicle and the road, which can be used to derive the following kinematic equations:

$$\begin{aligned}
\dot{e}_\psi &= \dot{\psi} - \dot{\psi}_s, \\
\dot{e}_y &= \dot{y}\cos(e_\psi) + \dot{x}\sin(e_\psi), \\
\dot{s} &= \frac{\rho}{\rho - e_y}(\dot{x}\cos(e_\psi) - \dot{y}\sin(e_\psi)),
\end{aligned} \tag{6.8}$$

where e_ψ and e_y denote the heading angle error and the lateral position error relative to the road centerline, respectively, and s denotes the projected vehicle position along the road centerline. ρ and ψ_s are the radius of the curvature and the heading of the road centerline, respectively. $\dot{\psi}_s$ is the time derivative of ψ_s and depends on $\dot{s}$

according to the relation $\dot{\psi}_s = \dot{s}/\rho$. We also define $\psi_r = \frac{d\psi_s}{ds}$ as the derivative of ψ_s with respect to the curvilinear coordinate s. ψ_r is the inverse of ρ and is assumed to be known.

The differential equations (6.1)–(6.8) define the extended bicycle model.

6.2.2 An LTV model for the vehicle lateral dynamics

In this section we present the simplifications required to obtain an LTV model of the lateral dynamics from the extended bicycle model. The discretized version of this model will be used in Section 6.4 to formulate the MPC problem.
The following assumptions are introduced.

Assumption 4. The braking ratio $\beta(t)$ is assumed to be constant over the prediction horizon (i.e., $\beta(t) = \bar{\beta}$).

Assumption 5. The vehicle is driven in a typical highway scenario (i.e. high speed limit and low curvature lane), which implies that:

- the heading angle error is small (i.e., $e_\psi \simeq 0$),

- the steering angle necessary to reach the tire saturation is small (i.e., $\delta \simeq 0$).

Assumption 5 implies that: $\cos \delta \simeq 1$, $\sin \delta \simeq \delta \simeq 0$, $\cos e_\psi \simeq 1$, $\sin e_\psi \simeq e_\psi$, $\frac{\rho}{\rho - e_y} \simeq 1$.
In summary we can rewrite the vehicle model as:

$$m\ddot{x} = mg\mu\bar{\beta} - k_d\dot{x}^2, \tag{6.9a}$$

$$m\ddot{y} = -m\dot{x}\dot{\psi} + F_{y_f} + F_{y_r}, \tag{6.9b}$$

$$I\ddot{\psi} = aF_{y_f} - bF_{y_r}, \tag{6.9c}$$

$$\dot{e}_\psi = \dot{\psi} - \dot{x}\psi_r, \tag{6.9d}$$

$$\dot{e}_y = \dot{y} + \dot{x}e_\psi, \tag{6.9e}$$

$$\dot{s} = \dot{x}, \tag{6.9f}$$

where $F_{y_*} = F_{y_{*l}} + F_{y_{*r}}$. Additionally $F_{x_{*\bullet}} = f_{x_{*\bullet}}$ and $F_{y_{*\bullet}} = f_{y_{*\bullet}}$, where $* = f, r$; $\bullet = r, l$. Note that (6.9a) and (6.9f) completely define the longitudinal dynamics of the vehicle. Therefore, given the input $\bar{\beta}$, the initial speed $\dot{x}(t_0)$ and position $s(t_0)$ of the vehicle, the differential equations (6.9a) and (6.9f) can be integrated to obtain explicit expressions of the speed $\dot{\bar{x}}(t)$ and position $\bar{s}(t)$, respectively.

The only nonlinearity in the remaining differential equations (6.9b)–(6.9e) is contained in the terms $F_{y_f}(\alpha_f)$ and $F_{y_r}(\alpha_r)$, whose expressions can be rewritten by combining (6.3), (6.6) and (6.7) as

$$\begin{aligned}
F_{y_f} &= \mu \frac{(b - e\bar{\beta})mg}{a + b} \sqrt{1 - \bar{\beta}^2} \sin(C \arctan(B\alpha_f)), \\
F_{y_r} &= \mu \frac{(a + e\bar{\beta})mg}{a + b} \sqrt{1 - \bar{\beta}^2} \sin(C \arctan(B\alpha_r)).
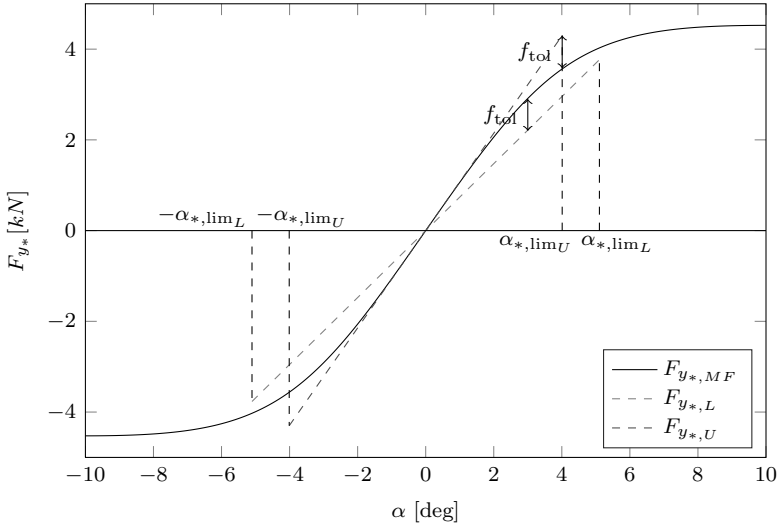\end{aligned} \tag{6.10}$$

Figure 6.4: Plots of the lateral force computed with the simplified Magic Formula ($F_{y_*,MF}$), with the lower ($F_{y_*,L}$) and the upper ($F_{y_*,U}$) linear approximation, for a given value of the vertical force and longitudinal force.

Figure 6.4 displays $F_{y_*}(\alpha_*)$ for a given value of $\bar{\beta}$ and shows how F_{y_*} can be bounded by two linear functions,

$$C_{*_L}\alpha_* \le F_{y_*} \le C_{*_U}\alpha_*,$$

where C_{*_U} and C_{*_L} are functions of the parameters in (6.10). The corresponding slip angle intervals in which the upper and lower approximations are valid are denoted as $[-\alpha_{*,\lim_U}, \alpha_{*,\lim_U}]$ and $[-\alpha_{*,\lim_L}, \alpha_{*,\lim_L}]$, respectively. f_{tol} denotes the maximum acceptable error in the linear approximations of the tire lateral forces. These approximations allow to define the following two LTV models of the lateral vehicle dynamics:

- *Conservative lateral dynamics model:* This model underestimates the cornering ability of the vehicle. In particular, F_{y_f} and F_{y_r} in (6.9b) are approximated by $C_{f_L}(\bar{\beta})\alpha_f$ and $C_{r_L}(\bar{\beta})\alpha_r$, respectively, and F_{y_f} and F_{y_r} in (6.9c) are approximated by $C_{f_L}(\bar{\beta})\alpha_f$ and $C_{r_U}(\bar{\beta})\alpha_r$. Therefore, the resulting conservative lateral dynamics model can be expressed as:

$$
\begin{aligned}
m\ddot{y} &= -m\dot{\bar{x}}\dot{\psi} + C_{f_L}\alpha_f + C_{r_L}\alpha_r, \\
I\ddot{\psi} &= aC_{f_L}\alpha_f - bC_{r_U}\alpha_r, \\
\dot{e}_\psi &= \dot{\psi} - \dot{\bar{x}}\psi_r, \\
\dot{e}_y &= \dot{y} + \dot{\bar{x}}e_\psi, \\
\dot{\delta} &= u,
\end{aligned}
\tag{6.11}
$$

where $\alpha_f = (\frac{\dot{y}+a\dot{\psi}}{\dot{\bar{x}}} - \delta)$ and $\alpha_r = \frac{\dot{y}-b\dot{\psi}}{\dot{\bar{x}}}$. The term *conservative* emphasizes the robustness of the model to the nonlinear tire characteristics. This model plays the main role in the MPC formulation.

Note that the steering angle δ has been added to the state space, while the new input variable is the steering rate, denoted by u. This modification allows to keep the inputs constant over certain time intervals while continuously varying the steering angle. A similar modification has been introduced in the next model.

- *Overreacting lateral dynamics model:* This model overestimates the cornering ability of the vehicle. In particular, F_{y_f} and F_{y_r} in (6.9b) are approximated by $C_{f_U}(\bar{\beta})\alpha_f$ and $C_{r_U}(\bar{\beta})\alpha_r$, respectively, and F_{y_f} and F_{y_r} in (6.9c) are approximated by $C_{f_U}(\bar{\beta})\alpha_f$ and $C_{r_L}(\bar{\beta})\alpha_r$, respectively. The resulting overreacting lateral dynamics model can be written as,

$$
\begin{aligned}
m\ddot{y} &= -m\dot{\bar{x}}\dot{\psi} + C_{f_U}\alpha_f + C_{r_U}\alpha_r, \\
I\ddot{\psi} &= aC_{f_U}\alpha_f - bC_{r_L}\alpha_r, \\
\dot{e}_\psi &= \dot{\psi} - \dot{\bar{x}}\psi_r, \\
\dot{e}_y &= \dot{y} + \dot{\bar{x}}e_\psi, \\
\dot{\delta} &= u,
\end{aligned}
\tag{6.12}
$$

where $\alpha_f = \frac{\dot{y}+a\dot{\psi}}{\dot{\bar{x}}} - \delta$ and $\alpha_r = \frac{\dot{y}-b\dot{\psi}}{\dot{\bar{x}}}$.

Both models hold for slip angles α_f and α_r inside the intervals

$$
|\alpha_f| \leqslant \alpha_{f,\text{lim}}, \qquad |\alpha_r| \leqslant \alpha_{r,\text{lim}},
\tag{6.13}
$$

where $\alpha_{f,\text{lim}} = \min\{\alpha_{f,\text{lim}_U}, \alpha_{f,\text{lim}_L}\}$ and $\alpha_{r,\text{lim}} = \min\{\alpha_{r,\text{lim}_U}, \alpha_{r,\text{lim}_L}\}$. Even if the slip angles do not have the same sign over the horizon, through simulations it has been possible to observe that the vast majority of the trajectories obtained with the nonlinear model are bounded by that ones predicted with the two presented liner models.

6.2.3   Model discretization

Equations (6.9a), (6.9f), (6.11) and (6.12) describe linear continuous-time models. Their discretization is performed in two steps using a forward Euler approximation with a discretization time step Δt. Firstly, given the initial longitudinal position s_k and speed $\dot{x}_k$ at t_k and the braking or throttle effort $\bar{\beta}$, the longitudinal states can be computed over the prediction horizon H_p as

$$
\begin{aligned}
\dot{\bar{x}}_{j+1,k}^{\bar{\beta}} &= \dot{\bar{x}}_{j,k}^{\bar{\beta}} + \Delta t m g \bar{\beta} - \Delta t j_d (\dot{\bar{x}}_{j,k}^{\bar{\beta}})^2, \\
\bar{s}_{j+1,k}^{\bar{\beta}} &= \bar{s}_{j,k}^{\bar{\beta}} + \Delta t \bar{x}_{j,k}^{\bar{\beta}}, \\
\bar{t}_{j+1} &= \bar{t}_j + \Delta t,
\end{aligned}
\tag{6.14}
$$

for $j = k, .., k + H_p - 1$, where $\bar{s}^{\bar{\beta}}_{k,k} = s_k$, $\dot{\bar{x}}^{\bar{\beta}}_{k,k} = \dot{x}_k$ and $\bar{t}_k = t_k$. $\dot{\bar{x}}^{\bar{\beta}}_{j,k}$ and $\bar{s}^{\bar{\beta}}_{j,k}$ represent the longitudinal speed and position, respectively, at time $\bar{t}_j$, predicted at time t_k. Secondly, using the computed sequences $\tilde{s}^{\bar{\beta}}_k = \{\bar{s}^{\bar{\beta}}_{k,k}, .., \bar{s}^{\bar{\beta}}_{k+H_p-1,k}\}$ and $\dot{\tilde{x}}^{\bar{\beta}}_k = \{\dot{\bar{x}}^{\bar{\beta}}_{k,k}, .., \dot{\bar{x}}^{\bar{\beta}}_{k+H_p-1,k}\}$, and a suitable discretization scheme, the models (6.11) and (6.12) can be used to obtain LTV models of the lateral vehicle dynamics to be used in the MPC formulation. We denote the discretized conservative lateral dynamics model by

$$\xi^{\text{cm},\bar{\beta}}_{j+1,k} = A^{\text{cm},\bar{\beta}}_{j,k} \xi^{\text{cm},\bar{\beta}}_{j,k} + B^{\text{cm},\bar{\beta}}_{j,k} u^{\bar{\beta}}_{j,k}, \tag{6.15}$$

and the discretized overreacting lateral dynamics model by

$$\xi^{\text{om},\bar{\beta}}_{j+1,k} = A^{\text{om},\bar{\beta}}_{j,k} \xi^{\text{om},\bar{\beta}}_{j,k} + B^{\text{om},\bar{\beta}}_{j,k} u^{\bar{\beta}}_{j,k}, \tag{6.16}$$

for a given value of $\bar{\beta}$. The state vector of the models is defined as

$$\xi^{*,\bar{\beta}}_{j,k} = \{\dot{y}^{*,\bar{\beta}}_{j,k}, \dot{\psi}^{*,\bar{\beta}}_{j,k}, e_{\psi}{}^{*,\bar{\beta}}_{j,k}, e_y{}^{*,\bar{\beta}}_{j,k}, \delta^{*,\bar{\beta}}_{j,k}\},$$

and the input is the steering rate $u^{\bar{\beta}}_{j,k}$.

6.3 Safety constraints

In this section, we show how the requirements of keeping the vehicle in the lane while avoiding obstacles and operating in a stable region can be expressed as constraints on the vehicle's states and input.

6.3.1 Actuator limits

The use of an Active Front Steering (AFS) unit to drive the steering angle imposes bound on the steering angle and its derivative. These bounds can be represented as linear constraints on the input and the state vector:

$$-\delta_{\lim} \leqslant \delta^{*,\bar{\beta}}_{j,k} \leqslant \delta_{\lim} \tag{6.17a}$$

$$-\dot{\delta}_{\lim} \leqslant u^{\bar{\beta}}_{j,k} \leqslant \dot{\delta}_{\lim}, \tag{6.17b}$$

for $j = k, .., k + H_p - 1$.

6.3.2 Slip angles bounds

The conservative and overreacting lateral dynamics model are valid for values of α_f and α_r satisfying (6.13). This requirement can be expressed as linear constraints on the state vector:

$$\left| \frac{\dot{y}^{*,\bar{\beta}}_{j,k} + a\dot{\psi}^{*,\bar{\beta}}_{j,k}}{\bar{\dot{x}}^{\bar{\beta}}_{j,k}} - \delta^{*,\bar{\beta}}_{j,k} \right| \leqslant \alpha_{f,\lim}, \quad \left| \frac{\dot{y}^{*,\bar{\beta}}_{j,k} - b\dot{\psi}^{*,\bar{\beta}}_{j,k}}{\bar{\dot{x}}^{\bar{\beta}}_{j,k}} \right| \leqslant \alpha_{r,\lim}, \tag{6.18}$$

for $j = k, .., k + H_p - 1$.

6.3.3   Lane boundaries

Lane boundaries can be easily introduced in the model as constraints on the lateral position error $e_{y}{}_{j,k}^{*,\bar{\beta}}$:

$$|e_{y}{}_{j,k}^{*,\bar{\beta}}| \leqslant \frac{1}{2}l_w, \tag{6.19}$$

for $j = k, .., k + H_p - 1$, where l_w denotes the lane width.

6.3.4   Obstacle avoidance constraints

Finally, we show how static and moving obstacles can be expressed as additional linear constraints on the lateral position error $e_{y}{}_{j,k}^{*,\bar{\beta}}$. We introduce the following assumptions:

Assumption 6. The current and the future positions of all obstacles in the proximity of the vehicle are known as function of time.

Assumption 7. The controller knows the side of the obstacle on which it is safe to pass.

These assumptions allow to map the obstacles' positions to a safe region on the road defined by its left and right bounds $e_{y,\text{right}}(t,s)$ and $e_{y,\text{left}}(t,s)$, respectively. Note that these bounds are a function of time t and position s along the road. The pre-computation of $\tilde{s}_k^{\bar{\beta}}$ defines a unique correspondence between $\bar{t}_k$ and $\bar{s}_{j,k}^{\bar{\beta}}$ (i.e. $\bar{s}_{j,k}(\bar{t}_j)$) for a given $\bar{\beta}$, and allows to recast the obstacle avoidance problem as LTV constraints on the lateral position error:

$$e_{y,\text{right}}(\bar{t}_j, \bar{s}_{j,k}) \leqslant e_{y}{}_{j,k}^{*,\bar{\beta}} \leqslant e_{y,\text{left}}(\bar{t}_j, \bar{s}_{j,k}), \tag{6.20}$$

for $j = k, .., k + H_p - 1$.

6.3.5   Summary of constraints

The constraints (6.17a), (6.18), (6.19) and (6.20) can be compactly written as

$$\xi_{j,k}^{*,\bar{\beta}_i} \in \Xi_{j,k}^{\bar{\beta}_i},$$

for $j = k, .., k + H_p - 1$, where $\Xi_{j,k}^{\bar{\beta}_i}$ is time-varying sequence of convex sets. The inequality (6.17b) can be rewritten as $u_{j,k}^{\bar{\beta}_i} \in \mathcal{U}$ for $j = k, .., k + H_p - 1$, where the set $\mathcal{U}$ is convex.
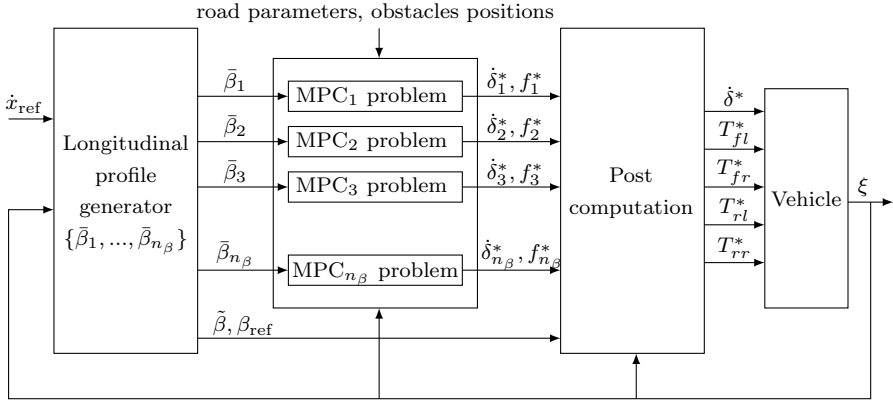
Figure 6.5: Structure of the obstacle avoidance controller.

6.4 Controller design

In this section we describe the MPC architecture used to address the obstacle avoidance problem. As shown in Figure 6.5, we decompose the controller into three sequential blocks: longitudinal profiles generation, MPC problems and post-computation.

6.4.1 Longitudinal profiles generation

The longitudinal profiles generator block is responsible for defining a set of n_β possible braking ratio commands $\tilde{\beta} = \{\bar{\beta}_1, .., \bar{\beta}_{n_\beta}\}$ and a reference braking ratio β_{ref} computed using a PI controller which tracks a given reference speed v_{ref}. In our work, we have investigated two different definitions of the set of braking ratios:

- n_β *braking ratios*: In this approach, we consider the braking ratios to be n_β uniformly spaced points in the interval $[\bar{\beta}_1, \bar{\beta}_{n_\beta}]$. While $\bar{\beta}_1$ is set to -1, $\bar{\beta}_{n_\beta}$ depends on the sign of β_{ref}: if $\beta_{\text{ref}} \leqslant 0$, then $\bar{\beta}_{n_\beta} = 0$; otherwise $\bar{\beta}_{n_\beta} = \beta_{\text{ref}}$.

- 3 *braking ratios*. This definition of the braking ratios set $\tilde{\beta} = \{\bar{\beta}_1, \bar{\beta}_2, \bar{\beta}_{n_\beta}\}$ is a consequence of the observation that the optimal braking ratio β^* changes slowly with time. Hence, given the last two optimal braking ratios β_p^* and β_{pp}^*, $\tilde{\beta}$ is computed as follows:

$$
\tilde{\beta} = \begin{cases} \{\beta_p^* - \Delta\beta, \beta_p^*, \beta_p^* + \Delta\beta\} & \text{if} \quad \beta_p^* = \beta_{pp}^*, \\ \{\beta_p^*, \beta_p^* + \Delta\beta, \beta_p^* + 2\Delta\beta\} & \text{if} \quad \beta_p^* > \beta_{pp}^*, \\ \{\beta_p^* - 2\Delta\beta, \beta_p^* - \Delta\beta, \beta_p^*\} & \text{if} \quad \beta_p^* < \beta_{pp}^*, \end{cases}
$$

where the perturbation $\Delta\beta$ is a parameter to be chosen.

6.4.2 MPC problems

This block formulates and solves the constrained finite-time optimal control problem at each time step. Using (6.14) for every $\bar{\beta}_i$, $i = 1, .., n_\beta$, the sequence of longitudinal positions $\tilde{s}_k^{\bar{\beta}_i}$ and speeds $\dot{\tilde{x}}_k^{\bar{\beta}_i}$ over the prediction horizon H_p is computed. The MPC formulation predicts the vehicle's states using both the conservative and overreacting lateral dynamic models. The states predicted over the horizon H_p using the conservative lateral dynamic model play the main role and they appear both in the cost function and in the constraints. The overreacting lateral dynamic model, instead, has an auxiliary role and it is used with a shorter prediction horizon H_{p_2} in the constraints definition. The MPC problem can be synthesized as follows:

$$\min_{U_k^{\bar{\beta}_i}} \quad f_0(\tilde{\xi}_k^{\mathrm{cm},\bar{\beta}_i}, U_k^{\bar{\beta}_i}), \tag{6.21a}$$

$$\text{subk. to} \quad \xi_{j+1,k}^{\mathrm{cm},\bar{\beta}_i} = A_{j,k}^{\mathrm{cm},\bar{\beta}_i} \xi_{j,k}^{\mathrm{cm},\bar{\beta}_i} + B_{j,k}^{\mathrm{cm},\bar{\beta}_i} u_{j,k}^{\bar{\beta}_i}, \tag{6.21b}$$

$$\xi_{j_2+1,k}^{\mathrm{om},\bar{\beta}_i} = A_{j_2,k}^{\mathrm{om},\bar{\beta}_i} \xi_{j_2,k}^{\mathrm{om},\bar{\beta}_i} + B_{j_2,k}^{\mathrm{om},\bar{\beta}_i} u_{j_2,\bar{\beta}_i}, \tag{6.21c}$$

$$u_{j,k}^{\bar{\beta}_i} \in \mathcal{U}, \tag{6.21d}$$

$$\xi_{j,k}^{\mathrm{cm},\bar{\beta}_i} \in \Xi_{j,k}^{\bar{\beta}_i}, \tag{6.21e}$$

$$\xi_{j_2,k}^{\mathrm{om},\bar{\beta}_i} \in \Xi_{j_2,k}^{\bar{\beta}_i}, \tag{6.21f}$$

$$\xi_{k,k}^{\mathrm{cm},\bar{\beta}_i} = \xi_{k,k}^{\mathrm{om},\bar{\beta}_i} = \xi(t_k), \tag{6.21g}$$

for $j = k, .., k + H_p - 1$ and $j_2 = k, .., k + H_{p_2} - 1$, where $f_0(\tilde{\xi}_k^{\mathrm{cm},\bar{\beta}_i}, U_k^{\bar{\beta}_i})$ is a convex quadratic function depending on the states, the slip angles and the input. $\tilde{\xi}_k^{\mathrm{cm},\bar{\beta}_i} = \{\xi_{k,k}^{\mathrm{cm},\bar{\beta}_i}, \xi_{k+1,k}^{\mathrm{cm},\bar{\beta}_i}, .., \xi_{k+H_p-1,k}^{\mathrm{cm},\bar{\beta}_i}\}$ is the sequence of states over the prediction horizon H_p predicted at time t_k, and updated according to the discretized conservative lateral dynamics model (6.15). $\tilde{\xi}_k^{\mathrm{om},\bar{\beta}_i} = \{\xi_{k,k}^{\mathrm{om},\bar{\beta}_i}, \xi_{k+1,k}^{\mathrm{om},\bar{\beta}_i}, .., \xi_{k+H_{p_2}-1,k}^{\mathrm{cm},\bar{\beta}_i}\}$ is the sequence of states over the prediction horizon H_{p_2} predicted at time t_k, and updated according to the discretized overreacting lateral dynamics model (6.16). $u_{j,k}^{\bar{\beta}_i} \in \mathbb{R}^{m_r}$ is the jth vector of the input sequence $U_k^{\bar{\beta}_i} = \{u_{k,k}^{\bar{\beta}_i}, .., u_{k+H_p-1,k}^{\bar{\beta}_i}\}^T \in \mathbb{R}^{m_r H_p}$. Since the models and the constraints are linear, it is possible to formulate every MPC problem as a QP. Each MPC controller in Figure 6.5 returns the optimal steering rate u_i^* and the optimal value of the cost function $f_{i,\mathrm{lat}}^*$. In order to reduce the computational complexity, the input is kept constant for every H_i time-steps (i.e. $u_{k+iH_i+j,k}^{\bar{\beta}_i} = u_{k+iH_i,k}^{\bar{\beta}_i}$ for $j = 1, ..., H_i - 1$, $i = 0, ..., (H_p/H_i)$). With this simplification the number of optimization variables can be significantly reduced, speeding up the computations.
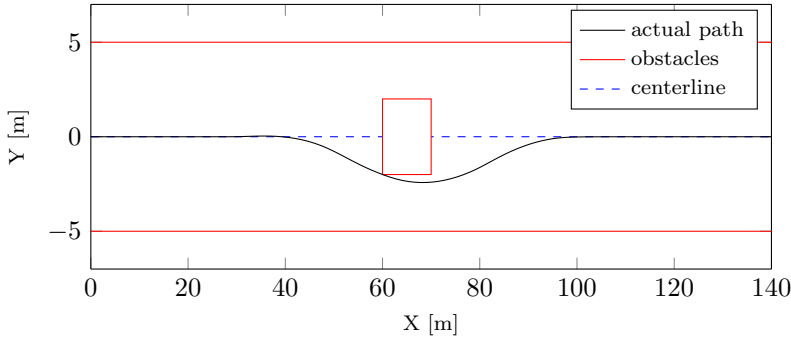
Figure 6.6: Simulation 1: the vehicle avoids one obstacle with an entry speed of 50 km/h.

6.4.3 Post-computation

In the post-computation block, the optimal cost functions $f^*_{i,\text{lat}}$ are augmented by adding a quadratic term representing the deviation of $\bar{\beta}_i$ from β_{ref} as follows,

$$f^*_i = f^*_{i,\text{lat}} + \|\bar{\beta}_i - \beta_{\text{ref}}\|^2_{Q_\beta},$$

The optimal braking ratio β^* and the corresponding steering rate $\dot{\delta}^*$ can be then computed as,

$$(\beta^*, \dot{\delta}^*) = \{(\beta^*_i, \dot{\delta}^*_i) : f^*_i = \min(f^*_1, .., f^*_{n_\beta})\}.$$

6.5 Simulation and experimental results

In this section we present the obtained results through simulations and real experiments.

6.5.1 Simulation setup description and results

Hardware-in-the-loop simulations of the controller are performed on a dSPACE rapid prototyping system consisting of a DS1401 MicroAutoBox (IBM PowerPC 750FX processor, 800 MHz) and a DS1006 processor board (Quad-core AMD Opteron processor, 2.8 GHz). The controller runs on the MicroAutoBox, and the DS1006 board simulates the vehicle dynamics using a nonlinear four wheel vehicle model with a Pacejka tire model. The simulations have been performed using the following parameters: $H_p = 45$, $H_{p2} = 20$ and $H_i = 3$. The considered scenarios consist of a straight slippery road ($\mu = 0.3$) with one or more static obstacles. The edge of each obstacle is at a distance of 2 m from the road centerline. Note that no tolerance has been added to the lane or obstacle bounds to account for the vehicle's width.

Figure 6.6 shows the path of the vehicle while avoiding a single obstacle, while Figure 6.7 shows the path of the vehicle while avoiding two obstacles. The vehicle is
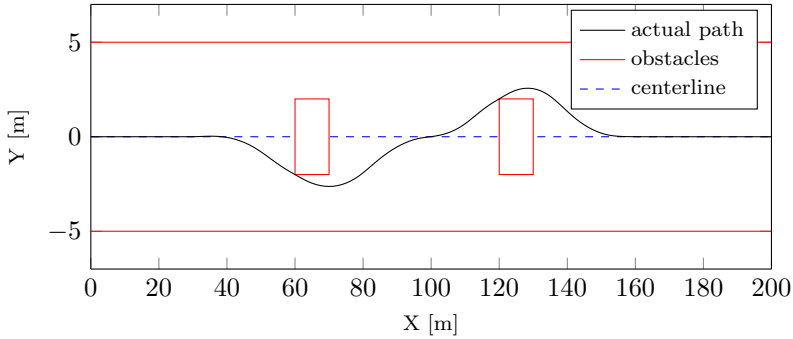
Figure 6.7: Simulation 2: the vehicle avoids two obstacles with an entry speed of 50 km/h.

Figure 6.8: Experimental setup: Jaguar S-Type test vehicle driving on snow.

able to avoid the obstacles and return to the lane centerline in both cases. Moreover, the vehicle travels close to the obstacle while avoiding it.

6.5.2 Experimental setup description and results

The experiments were performed on a Jaguar S–type vehicle (m = 2050 kg, I = 3344 kg-m^2) at the Smithers winter testing center (Raco, MI, U.S.A.) on tracks covered with packed snow ($\mu \approx 0.3$). A picture of the vehicle and the environment is shown in Figure 6.8.

The vehicle is equipped with an Active Front Steering (AFS) system and four wheel independent braking. An Oxford Technical Solutions (OTS) RT3002 sensing system is used to measure the position and orientation in the inertial frame, and the vehicle velocities in the body frame. The OTS RT3002 system comprises of a differential GPS, an IMU and a DSP. The real-time computations are performed on a dSPACE DS1005 Autobox system which consists of a PowerPC 750GX processor running at 933 MHz. The aforementioned hardware components communicate through a CAN bus and the control actions are executed at 10 Hz. The simulations have been performed using the following parameters: H_p = 30, H_{p2} = 20 and H_i = 3.
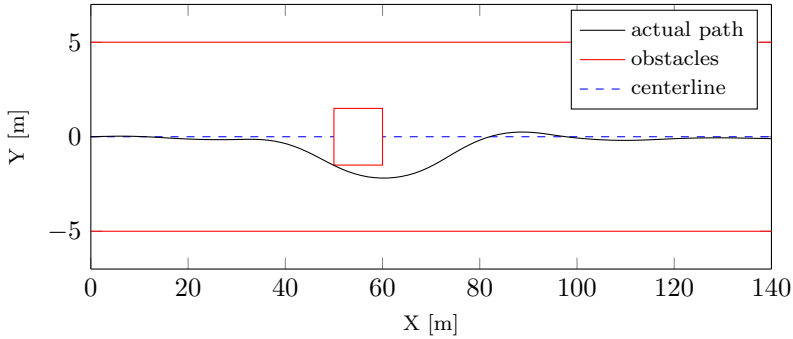
Figure 6.9: Experimental result: the vehicle is able to avoid the obstacle with an entry speed of 50 km/h. The plots show the vehicle trajectory and the vehicle speed, respectively.

The test scenario consists of a straight road with a single obstacle. The edge of the obstacle is at a distance of 1.5 m from the road centerline. The vehicle behavior is shown in Figure 6.9. It is seen that the vehicle avoids the obstacle and returns to the road centerline with a low overshoot. The performance is similar to that seen in simulations. Note that the scenario with two obstacles was not considered in the experiments due to the lack of testing time.

6.6 Summary

We have presented an LTV model of the vehicle dynamics, and used it to formulate an MPC problem for obstacle avoidance and lane keeping. The linearity of the model and convexity of the constraints is used to recast the MPC problem as a set of QP subproblems. The low computational complexity of each subproblem allows to solve the MPC problems in short time while using long prediction horizons, enabling real-time implementation.

Conclusion and future work

Thanks to the recent advances in technology and the strong interest from governmental institutions and industry, vehicle platoons are expected to be soon a reality on our roads. The automatic control of the vehicle longitudinal dynamics aimed at maintaining a short inter-vehicular distance carries numerous benefits, such as an increased safety, a better utilization of the existing roads and a higher fuel-efficiency. In particular, platooning has shown a great potential in reducing the fuel consumption of heavy-duty vehicles. Independent experimental tests have shown the capability to reduce the fuel consumption to up to 10%. In this thesis we have studied the control problem for fuel-efficient and safe heavy-duty vehicle platooning. First, we have derived a control-oriented model of the longitudinal dynamics of a heavy-duty vehicle. Second, we have proposed a two-layer control architecture, based on such a model, that addresses the fuel-efficient and safe platooning problem. Third, we have evaluated the performance of the controller in realistic scenarios. Finally, we have addressed the obstacle avoidance and lane keeping problems for a passenger car by proposing a novel control framework based on model predictive control (MPC).

This chapter concludes the thesis providing a summary of the presented study in Section 7.1 and outlining possible directions for future work in Section 7.2.

7.1 Conclusion

The work presented in the thesis focuses on the control of the longitudinal dynamics of a heavy-duty vehicle platoon in order to maximize the fuel-efficiency, while guaranteeing safety.

First, we have presented the models of the longitudinal dynamics of a heavy-duty vehicle and a platoon as used in the control synthesis. The aim of these models is to capture the behavior of the components that play a significant role in the fuel consumption. In order to explicitly include the effect that platooning has on the fuel consumption, the aerodynamic drag force has been expressed as a function of the distance to the preceding vehicle. Furthermore, by exploiting the simplifying

assumption of a continuous gear ratio, we have proposed a model of the powertrain that captures the intrinsic relation between the instantaneous fuel consumption and the traction force. Lastly, we have presented an abstraction of the system architecture in modern heavy duty-vehicles, highlighting the vehicle control units the platoon controller is interacting with.

Second, we have addressed the problem of designing a control system for heavy-duty vehicle platooning. In order to understand the role that slopes play on heavy-duty vehicle platooning, we have analyzed the experimental results presented in Alam et al. (2015a), in which a platoon is driving on a standard highway. The analysis motivated the necessity for a controller that, by explicitly taking into account road topography information, predicts the behavior of all vehicles in the platoon, coordinates their acceleration, and brakes only if necessary. To address these requirements, we have proposed a control architecture that splits the control task into two layers. The higher layer computes the optimal speed trajectory for the platoon by exploiting topography information of the road ahead. This layer has been implemented using a dynamic programming framework. The vehicles are assumed to be separated by a time gap that offers the advantage of resulting in the same speed profile defined in the spacial domain for all the vehicles, considerably reducing the complexity of the dynamic programming algorithm. The lower layer tracks the optimal speed profile communicated by the platoon coordinator and the time gap requirement. This layer is implemented using a distributed MPC framework. In detail, each vehicle receives from the preceding one its optimal trajectory and, by solving an optimization problem, computes its own optimal trajectory. While the horizon of the higher-layer platoon coordinator is of the order of kilometers, the horizon of the lower-layer vehicle controller is of the order of seconds (that corresponds to tens of meters). This allows for the real-time implementation and the computation of the inputs for the low-level vehicle controllers. Furthermore, thanks to the MPC formulation with a hard constraint on the vehicle state lying in a safety set and a soft constraint that penalizes braking, the vehicles brake only if necessary.

Third, we have evaluated the performance of the proposed platoon control by considering the two layers separately and, finally, combined. First, the platoon coordinator has been evaluated focusing on fuel-efficiency and its performance has been compared to standard controllers, using realistic altitude profiles as benchmark scenario. By exploiting topography information of the road ahead and coordinating the acceleration of the vehicles in a platoon, the platoon coordinator allows to save 3% of fuel for the leading vehicle and 9% for the following vehicles compared to the standard cruise control for a homogeneous platoon. These percentages increase in case of a heterogeneous platoon when the following vehicles are heavier than the leading one. Furthermore, the superiority of a time-gap policy compared to a space- or headway-gap policy has been shown by means of numerical experiments. By studying the energy consumption associated to each force component, we saw that the majority of the fuel saving is due to the reduced use of the brakes. Second, the vehicle control layer has been evaluated by focusing both on safety and fuel-efficiency. Two scenarios have been simulated where the leading vehicle is driven manually.

The vehicle control layer avoids braking for smooth decelerations of the leading vehicle as in the case of some realistic traffic scenarios. On the other hand, when the leading vehicle harshly brakes until reaching full-stop, the vehicle layer avoids collisions in the platoon by properly braking each vehicle. Lastly, we have evaluated the performance of the complete platoon controller, i.e., the combination of the platoon coordinator and the vehicle control layer, by simulating a three-vehicle platoon driving on the topography of a real road. The simulations demonstrated excellent performance of the overall control system.

Finally, in Chapter 6, we have presented an MPC-based control framework for the obstacle avoidance and lane keeping problems for a passenger car, which combines actions on braking and steering. The proposed controller decouples the longitudinal and lateral dynamics of the vehicles into two sequential stages. First, it computes possible braking profiles and associates to each of them two conservative linear time-varying (LTV) models of the lateral vehicle dynamics. Second, the conservative LTV models are used to formulate and solve a linear MPC problem for each braking profile. The solutions to the MPC problems define the optimal braking and steering inputs. This approach allows to robustly control the nonlinear dynamics of a vehicle with a linear MPC framework and, therefore, it enables fast and bounded computation. The controller performance has been evaluated by means of simulations and real experiments. The experiments have been conducted on packed-snow surface and have shown the ability of the proposed controller to avoid an obstacle also in extreme scenarios.

7.2 Future work

In this section we present possible directions for future work on cooperative look-ahead heavy-duty vehicle platooning.

Gearbox management

In the modeling of the heavy-duty vehicle powertrain presented in Chapter 3 we have assumed that the gear ratio can be chosen over a continuous and unbounded interval. Although this assumption is fine for obtaining a vehicle model that can be used in the proposed velocity control framework, it typically does not hold for commercial heavy-duty vehicles where usually the transmission is handled by gearboxes that introduce fixed gear ratios, power losses and delays. Therefore the study of the gearbox control for fuel-efficient platooning requires further investigation. Automatic gearboxes available in commercial vehicles typically rely on hysteresis control with predefined thresholds on engine speed. This approach can result in behavior that is not fuel-efficient, for example, in coasting phases during steep downhills. In this scenario in fact the engine speed of the vehicle tends to be high and, therefore, the engine generates a significant braking force. The optimal engine speed as function of the generated power displayed in Figure 3.4 and the knowledge of the real-time speed can be used to compute the fuel optimal instantaneous gear ratio. However,

the power loss and the delay during the gear shift make the problem of when the vehicles should change gear and which gear they should engage non-trivial. Furthermore, short inter-vehicular distances and the gear shift power loss could require the synchronization of the gear shifts along all vehicles of the platoon.

Automatic handling of external traffic

The only way external traffic is handled in the current framework is by manual driving. In the case of slow traffic, the driver of the leading vehicle is expected to manually adapt the vehicle speed to the traffic flow. In the case of a vehicle cutting in the middle of the platoon, instead, the driver of the vehicle behind the external one is expected to manually widen and maintain a safe gap from the external vehicle until it leaves the platoon. In order to improve the fuel-efficiency during slow traffic and during the cutting in of an external vehicle, the automatic control of such scenarios should be investigated. This can be done by including, for example, the sensing and prediction of other vehicles. However how to best exploit this information is still an open question.

Robustness to model and parameter uncertainties

In this thesis we have assumed that the control system exactly knows the parameter values of all vehicles and that the vehicles behave according to the vehicle model. However, in reality, vehicle parameters, e.g., mass, roll coefficient and engine characteristics, are only partially known or they can be strongly affected by external factors such as engine temperature, tire pressure, condition of the road surface, fuel tank level, etc. Furthermore, the model does not capture certain dynamics as the dependence of the aerodynamic drag force on the wind direction or the loss of power during a gear shift. An interesting direction for future work could be how to extend the current control framework in order to make it robust to parameter variations and model uncertainties. One way to deal with this problem is by including the online estimation of the vehicle parameters. Another interesting way could be to include in the vehicle control layer the tracking of the time gaps with respect to both the preceding and following vehicles. The optimal trajectory and input of each vehicle will be the result of a pushing or pulling effort of the two contiguous vehicles. In this way, during a steep uphill, for example, each vehicle will be concerned with the ability of the following vehicle to keep up the required acceleration. Moreover, during steep downhills, a coasting acceleration higher than the predicted one for a follower vehicle can be handled by the preceding one by increasing its acceleration, avoiding the unnecessary braking.

Real experiments

Finally, the proposed controller needs to be tested, first, in simulations using a more realistic model of the heavy-duty vehicle, and, second, in experiments involving real vehicles. In this phase, it will be crucial to focus on implementation aspects, such as

the real-time requirement. The experimental tests presented in Alam et al. ($2015a$) provided research hints that motivated the work presented in this thesis. We expect that experimental tests based on the proposed platoon control can provide fruitful feedback for future research work.

Acronyms

ACC	Adaptive cruise control
BMS	Braking management system
CAN	Controller area network
CC	Cruise control
CACC	Cooperative adaptive cruise control
CLAC	Cooperative look-ahead control
CoG	Center of gravity
DP	Dynamic programming
EMS	Engine management system
GMS	Gear management system
GPS	Global positioning system
ITS	Intelligent transportation systems
LAC	Look-ahead control
LTV	Linear time-variant
MPC	Model predictive control
PATH	Partners for advanced transportation technology
QP	Quadratic program
WSU	Wireless sensor unit

Bibliography

802.11p. IEEE Standard for information technology – Amendment 6: wireless access in vehicular environments. *IEEE Std 802.11p-2010*, 1–51 (2010).

A. Alam. *Fuel-efficient heavy-duty vehicle platooning.* Ph.D. thesis, KTH Royal Institute of Technology, Stockholm, Sweden (2014).

A. Alam, B. Besselink, V. Turri, J. Mårtensson, and K. Johansson. Heavy-duty vehicle platooning towards sustainable freight transportation. *IEEE Control Systems Magazine* (2015*a*). Conditionally accepted.

A. Alam, A. Gattami, and K. H. Johansson. An experimental study on the fuel reduction potential of heavy duty vehicle platooning. In *13th International IEEE Conference on Intelligent Transportation Systems*, 306–311. Madeira Island, Portugal (2010).

A. Alam, A. Gattami, K. H. Johansson, and C. J. Tomlin. Establishing afety for heavy duty vehicle platooning : a game theoretical approach. In *18th IFAC World Congress*, 2000, 3818–3823. Milano, Italy (2011).

A. Alam, J. Mårtensson, and K. H. Johansson. Look-ahead cruise control for heavy duty vehicle platooning. In *16th International IEEE Conference on Intelligent Transportation Systems*, 928–935. IEEE, The Hague, The Netherlands (2013).

A. Alam, J. Mårtensson, and K. H. Johansson. Experimental evaluation of decentralized cooperative cruise control for heavy-duty vehicle platooning. *Control Engineering Practice*, 38: 11–25 (2015*b*).

C. J. Almqvist and K. Heinig. European accident research and safety report. Technical report, Volvo Trucks (2013). URL `http://www.volvotrucks.com/SiteCollectionDocuments/VTC/Corporate/Values/ARTReport2013.pdf`.

L. Alvarez and R. Horowitz. Safe platooning in automated highway systems. Technical report, California PATH Program (1997).

S. J. Anderson, S. C. Peters, T. E. Pilutti, and K. Iagnemma. An optimal-control-based framework for trajectory planning, threat assessment, and semi-autonomous control of passenger vehicles in hazard avoidance scenarios. *International Journal of Vehicle Autonomous Systems*, 8(2/3/4): 190–216 (2010).

R. Bellman. *Dynamic Programming*. Princeton University Press, Princeton, NJ, USA (1957).

C. Bergenhem and Q. Huang. Challenges of platooning on public motorways. In *17th ITS World Congress*, 1–12. Busan, South Korea (2010).

C. Bergenhem, H. Pettersson, E. Coelingh, C. Englund, S. Shladover, and S. Tsugawa. Overview of platooning system. In *19th ITS World Congress*. Vienna, Austria (2012).

M. Bertozzi, A. Broggi, and A. Fascioli. Vision-based intelligent vehicles : state of the art and perspectives. *Robotics and Autonomous Systems*, 32(1): 1–16 (2000).

D. P. Bertsekas. *Dynamic programming and optimal control*. Athena Scientific, Belmont, MA, USA (1995).

B. Besselink, V. Turri, S. H. van de Hoef, K.-Y. Liang, A. Alam, J. Mårtensson, and K. H. Johansson. Cyber-physical control of road freight transport. *arXiv:1507.03466 [cs.SY]* (2015). Submitted for journal publication.

K. Bilstrup, E. Uhlemann, E. G. Ström, and U. Bilstrup. Evaluation of the IEEE 802.11p MAC method for vehicle-to-vehicle communication. In *IEEE 68th Vehicular Technology Conference*, 1–5. Calgary, Canada (2008).

F. Blanchini. Set invariance in control. *Automatica*, 35: 1747–1767 (1999).

C. Bonnet and H. Fritz. Fuel consumption reduction in a platoon: experimental results with two electronically coupled trucks at close spacing. *SAE Technical Paper*, (724) (2000).

F. Borrelli, A. Bemporad, and M. Morari. *Predictive control for linear and hybrid systems* (2015). In preparation, available online at http://www.mpc.berkeley.edu/mpc-course-material.

F. Browand, J. Mc Arthur, and C. Radovich. Fuel saving achieved in the field test of two tandem trucks. Technical Report June (2004).

Q. Chen, D. Jiang, and L. Delgrossi. IEEE 1609.4 DSRC Multi-channel operations and its implications on vehicle safety communications. In *IEEEE Vehicular Networking Conference*, 1–8 (2009).

C. C. Chien and P. Ioannou. Automatic vehicle-following. In *Proceedings of the IEEE American Control Conference*, 1748–1752. Chicago, IL, USA (1992).

K.-C. Chu. Decentralized control of high-speed vehicular strings. *Transportation Science*, 8(4): 361–384 (1974).

L. Del Re, F. Allgöwer, L. Glielmo, C. Guardiola, and I. Kolmanovsky. *Automotive model predictive control: models, methods and applications*. Springer (2010).

W. B. Dunbar and D. S. Caveney. Distributed receding horizon control of vehicle platoons: stability and string stability. *IEEE Transactions on Automatic Control*, 57(3): 620–633 (2012).

W. B. Dunbar and R. M. Murray. Distributed receding horizon control for multi-vehicle formation stabilization. *Automatica*, 42(4): 549–558 (2006).

European Commission. White paper – Roadmap to a single European transport area: towards a competitive and resource efficient transport system (2011). URL http://ec.europa.eu/transport/themes/strategies/doc/2011_white_paper/white_paper_com(2011)_144\en.pdf.

European Commission. *EU Transport in figures – Statistical pocketbook* (2014). URL http://ec.europa.eu/transport/facts-fundings/statistics/doc/2014/pocketbook2014.pdf.

P. Falcone, F. Borrelli, J. Asgari, H. E. Tseng, and D. Hrovat. Predictive active steering control for autonomous vehicle systems. *IEEE Transactions on Control Systems Technology*, 15(3): 566–580 (2007).

P. Falcone, F. Borrelli, H. E. Tseng, J. Asgari, and D. Hrovat. Low complexity MPC schemes for integrated vehicle dynamics control problems. In *9th International symposium on Advanced Vehicle Control*, volume 1 (2008).

F. Farokhi and K. H. Johansson. A game-theoretic framework for studying truck platooning incentives. In *16th International IEEE Conference on Intelligent Transportation Systems*, 1253–1260. The Hague, The Netherlands (2013).

F. Ferrari, E. Grosso, G. Sandini, and M. Magrassi. A stereo vision system for real time obstacle avoidance in unknown environment. In *IEEE International Workshop on Intelligent Robots and Systems*, 703–708. Genova, Italy (1990).

H. C. Frey and P.-Y. Kuo. Assessment of potential reductions in greenhouse gas emissions in freight transportation. *16th Annual International Emission Inventory Conference* (2007).

Y. Gao, A. Gray, J. V. Frasch, T. Lin, E. Tseng, J. K. Hedrick, and F. Borrelli. Spatial predictive control for agile semi-autonomous ground vehicles. In *11th International Symposium on Advanced Vehicle Control* (2012).

Y. Gao, T. Lin, F. Borrelli, E. Tseng, and D. Hrovat. Predictive control of autonomous ground vehicles with obstacle avoidance on slippery roads. In *ASME 2010 Dynamic Systems and Control Conference*, 265–272 (2010).

General Motors. To New Horizons (1939). URL https://archive.org/details/ToNewHor1940.

A. Gray, M. Ali, Y. Gao, J. K. Hedrick, and F. Borrelli. Integrated threat assessment and control design for roadway departure avoidance. In *2012 15th International IEEE Conference on Intelligent Transportation Systems*, 1714–1719. Alaska, USA (2012).

J. K. Hedrick, M. Tomizuka, and P. Varaiya. Control issues in automated highway systems. *IEEE Control Systems*, (December 1994): 21–32 (2000).

E. Hellström. *Look-ahead control of heavy vehicles*. Ph.D. thesis, Linköping University, Linköping, Sweden (2010).

E. Hellström, A. Fröberg, and L. Nielsen. A real-time fuel-optimal cruise controller for heavy trucks using road topography information. *SAE Technical Paper*, 2006–01–0008 (2006).

E. Hellström, M. Ivarsson, J. Åslund, and L. Nielsen. Look-ahead control for heavy trucks to minimize trip time and fuel consumption. *Control Engineering Practice*, 17(2): 245–254 (2009).

N. Hill, S. Finnegan, J. Norris, C. Brannigan, D. Wynn, H. Baker, and I. Skinner. Reduction and testing of greenhouse gas emissions from heavy duty vehicles. Technical Report 4, AEA Technology (2011). URL http://ec.europa.eu/clima/policies/transport/vehicles/docs/ec_hdv_ghg_strategy_en.pdf.

J. Hooker. Optimal driving for single-vehicle fuel economy. *Transportation Research Part A: General*, 22(3): 183–201 (1988).

R. Horowitz and P. Varaiya. Control design of an automated highway system. *Proceedings of the IEEE*, 88(7): 913–925 (2000).

D. Hrovat, S. Di Cairano, H. Tseng, and I. Kolmanovsky. The development of Model Predictive Control in automotive industry: A survey. In *IEEE International Conference on Control Applications*, 295–302. Dubrovnik, Croatia (2012).

W.-H. Hucho. *Aerodynamics of road vehicles*. Butterworth-Heinemann (1987).

International Transport Forum. ITF Transport Outlook. Technical report (2015). URL http://www.oecd-ilibrary.org/transport/itf-transport-outlook-2015_9789282107782-en.

A. Kaku, A. S. Kamal, M. Mukai, and T. Kawabe. Model predictive control for ecological vehicle synchronized driving considering varying aerodynamic drag and road shape information. *SICE Journal of Control, Measurement, and System Integration*, 6(5): 299–308 (2013).

A. Khodayari, A. Ghaffari, M. Nouri, S. Salehinia, and F. Alimardani. Model predictive control system design for car-following behavior in real traffic flow. In *IEEE International Conference on Vehicular Electronics and Safety*, 87–92. Istanbul, Turkey (2012).

M. P. Lammert, A. Duran, J. Diez, K. Burton, and A. Nicholson. Effect of platooning on fuel consumption of Class 8 vehicles over a range of speeds, following distances, and mass. *SAE International Journal of Commercial Vehicles*, (October): 7–9 (2014).

J. Larson, K.-Y. Liang, and K. H. Johansson. A distributed framework for coordinated heavy-duty vehicle platooning. *IEEE Transactions on Intelligent Transportation Systems*, 16(1): 419–429 (2015).

W. S. Levine and M. Athans. On the optimal error regulation of a string of moving vehicles. *IEEE Transactions on Automatic Control*, 11(3): 355–361 (1966).

P. Li, L. Alvarez, and R. Horowitz. AHS safe control laws for platoon leaders. *IEEE Transactions on Control Systems Technology*, 5(6): 614–628 (1997).

K.-Y. Liang. *Coordination and routing for fuel-efficient heavy-duty vehicle platoon formation.* Licentiate thesis, KTH Royal Institute of Technology, Stockholm, Sweden (2014).

D. Liberzon. *Calculus of variations and optimal control theory: a concise introduction.* Princeton University Press, Princeton, NJ, USA (2012).

D. Margolis and J. Asgari. Multipurpose models of vehicle dynamics for controller design. *SAE Technical Paper* (1991).

V. Monastyrsky and I. Golownykh. Rapid computation of optimal control for vehicles. *Transportation Research Part B: Methodological*, 27(3): 219–227 (1993).

G. Naus, R. Vugts, J. Ploeg, M. van de Molengraft, and M. Steinbuch. String-Stable CACC Design and Experimental Validation : A Frequency-Domain Approach. *IEEE Transactions on Vehicular Technology*, 59(9): 4268–4279 (2010).

B. Németh and P. Gáspár. Optimised speed profile design of a vehicle platoon considering road inclinations. *IET Intelligent Transport Systems*, 8: 200–208 (2013).

D. Norrby. *A CFD study of the aerodynamic effects of platooning.* Master thesis, KTH Royal Institute of Technology, Stockholm, Sweden (2014).

H. Pacejka. *Tire and vehicle dynamics.* Elsevier (2005).

L. E. Peppard. String stability of relative-motion PID vehicle control systems. *IEEE Transactions on Automatic Control*, (October): 579–581 (1974).

L. A. Pipes. An operational analysis of traffic dynamics. *Journal of Applied Physics*, 24(3): 274 (1953).

J. Ploeg, B. T. M. Scheepers, E. van Nunen, N. van de Wouw, and H. Nijmeijer. Design and Experimental Evaluation of Cooperative Adaptive Cruise Control. In *14th International IEEE Conference on Intelligent Transportation Systems*, 14–19. Washington, DC, USA (2011).

J. Ploeg, N. van de Wouw, and H. Nijmeijer. Lp string stability of cascaded systems: application to vehicle platooning. *IEEE Transactions on Control Systems Technology*, 22(2): 786–793 (2014).

M. Pollefeys, D. Nistér, J.-M. Frahm, A. Akbarzadeh, P. Mordohai, B. Clipp, C. Engels, D. Gallup, S.-J. Kim, P. Merrell, C. Salmi, S. Sinha, B. Talton, L. Wang, Q. Yang, H. Stewénius, R. Yang, G. Welch, and H. Towles. Detailed real-time urban 3D reconstruction from video. *International Journal of Computer Vision*, 78(2-3): 143–167 (2007).

R. Rajamani, H.-S. Tan, B. K. Law, and W.-B. Zhang. Demonstration of integrated longitudinal and lateral control for the operation of automated vehicles in platoons. *IEEE Transactions on Control Systems Technology*, 8(4): 695–708 (2000).

K. Ramachandran, M. Gruteser, R. Onishi, and T. Hikita. Experimental analysis of broadcast reliability in dense vehicular networks. *IEEE Vehicular Technology Magazine*, 2(4): 26–32 (2007).

J. B. Rawlings and D. Q. Mayne. *Model Predictive Control: Theory and Design*. Nob Hill Publishing (2009).

M. Raya and J.-P. Hubaux. The security of vehicular ad hoc networks. In *3rd ACM Workshop on Security of Ad Hoc and Sensor Networks*, 11. ACM Press, New York, NY, USA (2005).

J. Richalet, A. Rault, J. L. Testud, and J. Papon. Model Predictive Heuristic Control : Applications to Industrial Processes. *Automatica*, 14: 413–428 (1978).

SAE International. SAE J2735 (2015). URL `http://standards.sae.org/wip/j2945/`.

P. Sahlholm and K. H. Johansson. Road grade estimation for look-ahead vehicle control using multiple measurement runs. *Control Engineering Practice*, 18(11): 1328–1341 (2010).

T. Sandberg. *Heavy truck modeling for fuel consumption simulations and measurements*. Licentiate thesis, KTH Royal institute of technology, Stockholm, Sweden (2001).

Scania AB. Annual report 2013. Technical report, Scania AB (2013). URL `http://www.scania.com/Images/wkr0006_tcm40-362877.pdf`.

M. Schittler. State-of-the-art and merging truck engine technologies for optimized performance, emissions and life cycle costs. Technical report, DaimlerChrysler AG (2003). URL `http://www.osti.gov/scitech/servlets/purl/829810`.

A. Schwarzkopf and R. Leipnik. Control of highway vehicles for minimum fuel consumption over varying terrain. *Transportation Research*, II: 279–286 (1977).

P. Seiler, A. Pant, and J. K. Hedrick. Disturbance propagation in vehicle strings. *IEEE Transactions on Automatic Control*, 49(10): 1835–1841 (2004).

P. Seiler, B. Song, and J. K. Hedrick. Development of a collision avoidance System. In *SAE World Congress*. Detroit, MI, USA (1998).

S. Sheikholeslamn and C. A. Desoer. Longitudinal control of a platoon of vehicles. In *Proceedings of the IEEE American Control Conference*, 1549–1579 (1990).

S. Shladover. PATH at 20–history and major milestones. *IEEE Transactions on Intelligent Transportation Systems*, 8(4): 584–592 (2007).

S. Shladover. Recent international activity in cooperative vehicle-highway automation systems. Technical report, California PATH Program (2012).

M. L. Sichitiu and M. Kihl. Inter-vehicle communication systems: a survey. *IEEE Communications Surveys Tutorials*, 10(2): 88–105 (2008).

S. Stankovic, M. Stanojevic, and D. Siljak. Decentralized overlapping control of a platoon of vehicles. *IEEE Transactions on Control Systems Technology*, 8(5): 816–832 (2000).

R. Subramanian. Motor vehicle traffic crashes as a leading cause Of death in the United States, 2008 and 2009. Technical Report May, U.S. Department of Transportation (2012). URL `http://www-nrd.nhtsa.dot.gov/Pubs/811620.pdf`.

D. Swaroop and J. Hedrick. String stability of interconnected systems. *IEEE Transactions on Automatic Control*, 41(3): 349–357 (1996).

S. Tsugawa. An overview on an automated truck platoon within the energy ITS project. In *7th IFAC Symposium on Advances in Automotive Control*. Tokyo, Japan (2013).

V. Turri, B. Besselink, and K. H. Johansson. Cooperative look-ahead control for fuel-efficient and safe heavy-duty vehicle platooning. *arXiv:1505.00447 [cs.SY]* (2015). Submitted for journal publication.

V. Turri, B. Besselink, J. Mårtensson, and K. H. Johansson. Fuel-efficient heavy-duty vehicle platooning by look-ahead control. In *53rd IEEE Conference on Decision and Control*, 654–660. Los Angeles, CA, USA (2014).

V. Turri, A. Carvalho, H. E. Tseng, K. H. Johansson, and F. Borrelli. Linear model predictive control for lane keeping and obstacle avoidance on low curvature roads. In *16th International IEEE Annual Conference on Intelligent Transport*, 378–383. The Hague, The Netherlands (2013).

US Enviromental Protection Agency. EPA and NHTSA adopt first-ever program to reduce greenhouse gas emissions and improve fuel efficiency of medium- and heavy-duty vehicles. Technical Report August 2011, US Enviromental Protection Agency (2011). URL http://www.epa.gov/otaq/climate/documents/420f11031.pdf.

S. van de Hoef, K. H. Johansson, and D. V. Dimarogonas. Fuel-optimal centralized coordination of truck platooning based on shortest paths. In *Proceedings of the IEEE American Control Conference*, 3740–3745. Chicago, IL, USA (2015).

P. Varaiya. Smart cars on smart roads: problems of control. *IEEE Transactions on Automatic Control*, 38(2): 195–207 (1993).

M. Whaiduzzaman, M. Sookhak, A. Gani, and R. Buyya. A survey on vehicular cloud computing. *Journal of Network and Computer Applications*, 40: 325–344 (2014).

T. Willke, P. Tientrakool, and N. Maxemchuk. A survey of inter-vehicle communication protocols and their applications. *IEEE Communications Surveys & Tutorials*, 11(2): 3–20 (2009).

D. Yanakiev and I. Kanellakopoulos. Longitudinal control of heavy-duty vehicles for automated highway systems. In *Proceedings of IEEE American Control Conference*, June (1995).

M. Zabat, N. Stabile, S. Farascaroli, and F. Browand. The aerodynamic performance of platoons: final report. Technical report, California Partners for Advanced Transit and Highways (PATH) (1995).

J. Zhang and P. Ioannou. Longitudinal control of heavy trucks in mixed traffic: environmental and fuel economy considerations. *IEEE Transactions on Intelligent Transportation Systems*, 7(1): 92–104 (2006).